DEVELOPMENT OF NANOGELS FROM NANOEMULSIONS AND INVESTIGATION OF THEIR RHEOLOGY AND STABILITY

A Thesis Submitted to the

College of Graduate Studies and Research

in Partial Fulfillment of the Requirements for the

Degree of Master of Science in the

Department of Food and Bioproduct Sciences

University of Saskatchewan

Saskatoon, SK

By

Vivek Vardhan Reddy Erramreddy

PERMISSION TO USE

In presenting this thesis in partial fulfillment of the requirements for a Postgraduate degree from the University of Saskatchewan, I agree that the Libraries of this University may make it freely available for inspection. I further agree that permission for copying of this thesis/dissertation in any manner, in whole or in part, for scholarly purposes may be granted by the professor or professors who supervised my thesis work or, in their absence, by the Head of the Department or the Dean of the College in which my thesis work was done. It is understood that any copying or publication or use of this thesis or parts thereof for financial gain shall not be allowed without my written permission. It is also understood that due recognition shall be given to me and to the University of Saskatchewan in any scholarly use which may be made of any material in my thesis.

Requests for permission to copy or to make other uses of materials in this thesis in whole or part should be addressed to:

Head of the Department of Food and Bioproduct Sciences

University of Saskatchewan

Saskatoon, Saskatchewan S7N 5A8

Canada

ABSTRACT

Nanoemulsions with extremely small droplet sizes (<100 nm) have shown several advantages over conventional emulsions. However, almost all nanoemulsions in usage are liquids that restrict their use in many soft materials. The aim of this thesis is to understand the formation and long-term stability of viscoelastic nanogels developed from liquid nanoemulsions.

At first, gelation in 40 wt% canola oil-in-water nanoemulsions were investigated as a function of emulsifier type (anionic sodium dodecyl sulfate (SDS) or nonionic Tween 20) and concentration. Three different regimes of colloidal interactions were observed as a function of SDS concentration. 1) At low SDS concentration (0.5 – 2 times CMC) the counterion shell layer increased the effective volume fraction of the dispersed phase (ϕ_{eff}) close to the random jamming, resulting in repulsive gelation. 2) At SDS concentration between 5 – 15 times CMC, micelle induced depletion attractions led to extensive droplet aggregation and gelation. 3) At very high SDS concentration, however, oscillatory structural forces (OSF) due to layered-structuring of excess micelles in the interdroplet regions led to loss of gelation. In repulsive gelation, reduction in droplet size coupled with the electrical double layer resulted in a linear increase of G′. On the contrary, attractive nanoemulsions showed rapid increase in gel strength below a critical droplet radius, and was explained by transformation of OSF into depletion attraction. No gelation was seen in Tween 20 nanoemulsions, due to lack of repulsive interactions and weak depletion attraction.

Next the influence of the dispersed phase volume fraction (ϕ) on repulsive nanoemulsion gelation was investigated and the G′ values were modeled using empirical scaling law developed by Mason et al. (1995). It was found that an initial liquid regime transformed into glassy phase at a $\phi_{eff} = \phi_g \sim 0.58$, where droplets are entrapped in a cage of neighbouring droplets due to crowding. It was followed by jamming transition at a critical volume fraction (ϕ_j), where droplet deformation led to large increase in elasticity. The model predicted $\phi_j = 0.7$, which is close to the predictions for repulsive polydispersed emulsions found in the literature.

In the final phase long-term stability of the nanogels was evaluated until 90 days, during which the nanogels remained stable to creaming and coalescence. However, repulsive nanogels showed a significant decrease in G′ and the gels converted into flowable liquids over time. For

attractive nanogels decrease in G′ was much less, although given enough time they would also transformed into weak gels. It was hypothesized that surface active compounds generated due to lipid oxidation altered interfacial charge cloud leading to loss of gel strength for repulsive nanogels. For attractive nanogels slippery bonds in the aggregates permitted rotational and translational diffusion of nanodroplets on the surface of each other leading to network compactness and a decrease in gel strength with time.

Overall, it was concluded that it is possible to form nanogels from canola oil nanoemulsions using ionic emulsifiers. The gel strength and stability of the nanogels depends on emulsifier concentration, droplet size, ϕ and the chemical stability of the oil used. More investigation is needed in order to improve the long-term stability of the nanogels. The nanogels possess high potential for use in low-fat foods, pharmaceuticals, and cosmetic products.

ACKNOWLEDGEMENTS

I would like to express my upmost gratitude and special appreciation to my supervisor, Dr. Supratim Ghosh, who have been a tremendous mentor and constructive critique to me. I place on record my sincere gratitude to my graduate chairs, Dr. Takuji Tanaka, Dr. Robert T. Tyler, and Dr. George G. Khachatourians, and my advisory committee member, Dr. Michael Nickerson for the precious support and suggestions. I thank my external examiner, Dr. Richard K. Bowles for his valuable time and inputs. I would like to thank all my colleagues and lab mates (Songshang Bao, Anzhelika Teymurova, Spuritha Yerramilli, Maja Primozic, Chang Chang, Wai Fun Leong, Aakash Patel) for their support and encouragement. Special thanks to Ricky Lam and Andrea Stone for the technical support and training. A special thanks to my family for their love, encouragement, and unconditional support. I also like to show my appreciation to Ann Harley, Patricia Olesiuk, Tanya Napper, and Kendra Panko for their administrative assistance.

Special thanks to Natural Sciences and Engineering Research Council (NSERC), Department of Food and Bioproduct Sciences Devolved Scholarship and New Faculty Graduate Student Support Program (University of Saskatchewan) for the financial assistance towards this research.

TABLE OF CONTENTS

PERMISSION TO USE i

ABSTRACT ii

ACKNOWLDEDGEMENTS iv

TABLE OF CONTENTS v

LIST OF TABLES ix

LIST OF FIGURES x

LIST OF SYMBOLS AND ABBREVIATIONS xix

1 INTRODUCTION 1

1.1 Overview 1

1.2 Objectives 4

1.3 Hypothesis 4

2 LITERATURE REVIEW 6

2.1 Emulsions 6

2.1.1 Types of emulsions 6

2.1.2 Emulsion composition 7

2.1.3 Emulsion preparation 9

2.1.4 Droplet characteristics 10

2.1.5 Droplet interactions in emulsions 11

2.1.6 Emulsion stability and destabilization mechanisms 12

2.1.7 Determination of emulsion stability 15

2.2 Nanoemulsions 16
2.2.1 Definition 16
2.2.2 Nanoemulsion formulation 16
2.2.3 Preparation of nanoemulsions 17
2.2.4 Influence of interfacial layer on nanoemulsion properties 17
2.2.5 Stability and destabilization mechanisms 18
2.2.6 Applications 18
2.3 Rheological behaviour of materials 19
2.3.1 Theory of rheology 19
2.3.2 Measurement techniques 24
2.3.3 Rheology of emulsions 26
2.4 Gelation 30
2.4.1 Types of gels 31
2.4.2 Gelation mechanism 34
2.4.3 Application of gels 36
2.5 Gelation of emulsions and nanoemulsions 36
2.5.1 Gelation influenced by microstructure 37
2.5.2 Attractive gelation 39
2.5.3 Repulsive gelation 43
2.5.4 Applications 47

3 MATERIALS AND METHODS 48
3.1 Materials 48
3.2 Preparation of nanoemulsions 48
3.3 Droplet size distribution 50

3.4 Viscosity 51
3.5 Viscoelasticity 51
3.6 Visual observation 51
3.7 Accelerated shelf-life study 52
3.8 Statistics 52

4 RESULTS AND DISCUSSIONS 54
4.1 Influence of emulsifier concentrations on the gelation of nanoemulsions 54
4.1.1 Droplet size distribution 54
4.1.2 Visual observation of flow behaviour 55
4.1.3 Nanoemulsion viscosity 56
4.1.4 Viscoelastic behaviour of nanoemulsions 59
4.1.5 Mechanism of nanocolloidal gelation 63
4.1.6 Calculation of κ^{-1} and ϕ_{eff} 64
4.1.7 Calculation of depletion interactions 67
4.1.8 Calculation of oscillatory structural forces 71
4.1.9 Summary 74
4.2 Influence of droplet size on nanoemulsion gelation 75
4.2.1 Average droplet size 75
4.2.2 Nanoemulsion viscosity 76
4.2.3 Nanoemulsion viscoelasticity 78
4.2.4 Mechanism of gelation 81
4.2.5 Summary 89
4.3 Effect of oil concentration on repulsive gelation 90
4.3.1 Average droplet size 90

4.3.2 Viscosity of repulsive nanogels 90
4.3.3 Viscoelasticity of repulsive nanogels 94
4.3.4 Modelling the G′ of repulsive nanogels 96
4.3.5 Summary 99
4.4 Long-term storage stability of nanogels 99
4.4.1 Coalescence and accelerated creaming stability of nanogels 99
4.4.2 Rheology as a function of time 103
4.4.3 Effect of aging on gel strength 108
4.4.4 Summary 112

5 CONCLUSIONS 114

6 FUTURE STUDIES 118

7 REFERENCES 121

LIST OF TABLES

Table 3.2.1 Emulsifier concentrations for all nanoemulsions calculated on the basis of 40 wt% nanoemulsions with 1 CMC (8.3 mM) and 2 CMC (16.6 mM). The emulsifier concentration (mM) to oil volume fraction (ϕ) ratio was kept constant in all systems 50

Table 4.1.1 Interfacial shell layer thickness (δ, effective oil phase volume fraction (ϕ_{eff}), effective micelle volume fraction ($\phi_{m\text{-}eff}$) and depletion interaction energy (W_D/k_BT at $h=\delta$) for SDS nanoemulsions calculated at counterion dissociation factor, f = 0.1. ϕ_m and W_D/k_BT (at $h=\delta$) for Tween 20 nanoemulsions are shown. For SDS aqueous phase micelle appears at 41.4 mM concentration, while for Tween 20 it was at 16.6 mM 68

LIST OF FIGURES

Figure 2.1.1 Stabilization by different types of surface active agents. (a) small molecule emulsifier, (b) flexible proteins (caseins), (c) globular proteins (whey proteins) and (d) particles (triglyceride crystals)..... 9

Figure 2.1.2 DLVO interdroplet pair potential between two droplets (adapted from: Ghosh and Rousseau, 2010) 12

Figure 2.1.3 Mechanisms of emulsion destabilization (a) kinetically stabilized O/W emulsion, (b) phase inversion into W/O emulsion, (c) creaming of oil droplets (d) sedimentation of water droplets, (e) flocculation, (f) coalescence, (g) phase separation, (h) Ostwald ripening (adapted with modification from McClements 2007)..... 13

Figure 2.3.1 (A) Hookean solid which is deformed by a length of ΔL by the application of shear stress τ. (B) Shear flow between parallel planes of area A, separated by a distance h. Liquid filling the space between them is sheared by the upper plane moving whole relative velocity is U. The local velocity of fluid is proportional to the lengths of arrows between the two layers..... 20

Figure 2.3.2 Comparision between ideal and nonideal liquids (a) Shear stress vs. rate of strain and (b) apparent viscosity vs. rate of strain for ideal, dilatant and pseudoplastic liquids 21

Figure 2.3.3 Shear stress vs. strain graphs of (A) perfect elastic material which has a linear relationship and (B) a viscoelastic material in which histeresis loop is observed whose area is equal to the energy lost 22

Figure 2.3.4 Viscoelastic response of the material subjected to oscillatory strain with frequency ω 24

Figure 2.3.5 Rheological behavior of emulsions containing various amounts of soft oil droplets (ϕ). (modified image adapted from Mason 1999) 26

Figure 2.3.6 Typical behavior of viscoelastic moduli of O/W emulsion (ϕ = 0.83) as a function of % strain as observed by Knowlton et al. (2014). Left axis represent the elastic and loss moduli (■, ▲) as a function of % strain amplitude given in the x-axis. γ_f represents the fluidization strain at which the cross-over of G′ and G″ occur. Axis on the right represents the shear stress (τ) vs. % strain amplitude. $\gamma_{y,r}$ represent the rheological yield strain, which is the intersection of two lines describing the behavior of shear stress at small and large strain. Figure obtained from Knowlton et al., 2014. 29

Figure 2.5.1 Schematic diagrams of (A) active particle filled gel in which the network structure is caused by crosslinking the biopolymers/hydrocolloids in the continuous phase, and biopolymer/hydrocolloid stabilized droplets served as active fillers. (B) inactive particle filled gel in which the network structure is caused by crosslinking the biopolymers/hydrocolloids in the continuous phase, and droplets served as inactive fillers. (C) Particulate gels in which network structure is caused by aggregation of dispersed droplets in the continuous phase 38

Figure 2.5.2 Schematic representation of aggregation of colloidal particles induced by depletion forces 41

Figure 2.5.3 Schematic representation of the mechanism of nanogel formation. (a) conventional emulsion with large droplets and insignificant effect of shell layer lead to liquid-

like behaviour; (b) random jamming of nanodroplets in repulsive nanogels with similar droplet volume fraction as in the conventional emulsion but with increased effective volume fraction due to the influence of interfacial shell layer thickness 45

Figure 2.5.4 Schematic representation of increase in ϕ_{eff} with the decrease in droplet size at a different thickness of shell layer..... 46

Figure 3.7.1 Schematic representation of the droplet creaming under centrifugal force and transmission profiles of light with time 'n' obtained using a LUMiSizer..... 53

Figure 3.7.2 Model graph of the position of the cream layer with time obtained using LUMiSizer..... 53

Figure 4.1.1 Effect of emulsifier concentration on the average droplet size (d_{32}) of SDS (●) and Tween 20 (○) nanoemulsions. The line represents a power law model fit to the experimental data (r^2 0.8 and 0.97 for SDS and Tween 20, respectively)..... 55

Figure 4.1.2 Pictures from the visual observation experiment of SDS and Tween 20 nanoemulsions. Vials containing nanoemulsions were tilted at a certain angle to record their flow behavior and waited for 30 seconds after which the pictures were taken..... 56

Figure 4.1.3 Change in viscosities of nanoemulsions as a function of shear rate at different emulsifier concentrations. (A) 0.5, 1, 2, 5, 10 and 15 times CMC SDS nanoemulsions, (B) 20, 25, 30 times CMC SDS nanoemulsions, (C) All Tween 20 emulsions. Error bars were not shown for clarity..... 57

Figure 4.1.4 Average values calculated from Herschel-Bulkley and power law model for SDS and Tween 20 emulsions. (A) viscosity of SDS (●) and Tween 20 (○) nanoemulsions at 10 s^{-1} shear rate, (B) yield stress of SDS nanoemulsions. Error

bars represents ± one standard deviation (n=3). 59

Figure 4.1.5 Average Strain dependent storage (G′) (●) and loss moduli (G″) (○) of different SDS nanoemulsions. SDS concentration is expressed as multiples of its critical micelle concentration (CMC) 60

Figure 4.1.6 Characterization of the viscoelastic behavior of SDS (triangle) and Tween 20 (square) nanoemulsions. Values of storage (G′) (closed symbols) and loss (G″) (open symbols) moduli of nanoemulsions (at a frequency of 6.28 rad/sec and 0.1% strain) were plotted from strain sweep measurements data against emulsifier concentration. Lines are used to guide the eye. Error bars represents ± one standard deviation (n=3) 61

Figure 4.1.7 Frequency dependent storage (G′) and loss moduli (G″) of different SDS nanoemulsions. (A) G′, (B) G″ until 15 CMC SDS nanoemulsions; (C) G′ and (D) G″ for 20 – 30 CMC SDS nanoemulsions 63

Figure 4.1.8 Storage modulus (G′) of SDS nanoemulsions in (A) repulsive and (B) attractive regimes expressed as a function of (A) ϕ_{eff} scaled by span of droplet size distribution and (B) depletion interaction energy. The G′ values were obtained from strain sweep measurements at 0.1% strain. In B data for Tween 20 nanoemulsions (○) were also plotted alongside SDS nanoemulsions (●). Lines are used to guide eyes. The difference in the scale of the y-axes between A and B is required for clarity 71

Figure 4.1.9 Calculated oscillatory interaction energy from eq 12 for 40 wt% O/W nanoemulsions stabilized with different concentration of (A) SDS and (B) Tween 20. The oscillating interaction potential is shown until the interdroplet distance equal to effective micelle diameter ($d_{m\text{-}eff}$) for SDS and original micelle diameter (d_m) for Tween 20. It was assumed that at high micelle concentrations (20 – 30 CMC) the shaded area will be inaccessible by the approaching droplet and will be

filled with a layer of micelles. As $d_{m\text{-}eff}$ changes with micelle concentration for SDS, the curves begin at different distances 73

Figure 4.2.1 Effect of number of homogenization passes on the reduction in droplet size of 2 CMC (●) and 15 CMC (○) nanoemulsions. The lines represent the empirical model (eq 4.2.1) fit to the experimental data. Error bars represents ± one standard deviation (n=3). 77

Figure 4.2.2 Change in viscosities of 2 CMC SDS (●) and 15 CMC SDS (○) nanoemulsions as a function of average droplet diameter (d_{32}) obtained after each pass through the homogenizer. Error bars represents ± one standard deviation (n=3). The horizontal error bars are because the average viscosity data were plotted at average d_{32} of the three replicates. The numbers in the graph represent the homogenization passes at each viscosity..... 77

Figure 4.2.3 Yield stress values of 2 CMC (▒) and 15 CMC (▓) emulsions calculated from Hershel-Bulkley model as a function of a number of passes of homogenization. Error bars represents ± one standard deviation (n=3)..... 78

Figure 4.2.4 Average of oscillatory strain dependent storage (G′) and loss moduli (G″) of SDS nanoemulsions after different homogenization passes. (A) G′, (B) G″ of 2 CMC nanoemulsions; (C) G′ and (D) G″ of 15 CMC nanoemulsions. Note the difference in Y-axis scale between 2 and 15 CMC nanoemulsions. Standard deviations of the moduli are not shown for the same. For 15 CMC nanoemulsion data before the third pass (C3) are not shown, as the samples were too weak to show any gelation behaviour within the instrument limits..... 80

Figure 4.2.5 Characterization of the viscoelastic behavior of (A) 2 CMC and (B) 15 CMC nanoemulsions as a function of average droplet size (d_{32}). Values of storage (G′) (closed symbols) and loss (G″) (open symbols) moduli of emulsions (at a

frequency of 6.28 rad/sec and 0.1% strain) were plotted from strain sweep measurements data. The inset shows a zoomed view of G′ and G″ of 15 CMC nanoemulsions from fifth to eighth passes. Note the difference in axis ranges for A and B..... 81

Figure 4.2.6 Average ϕ_{eff} as a function of the number of homogenization pass for (A) 2 CMC and (B) 15 CMC nanoemulsions. Note the scale difference on the y-axis between both A and B. Error bars represents ± one standard deviation (n=3)..... 82

Figure 4.2.7 Characterization of the viscoelastic behavior of (A) 2 CMC and (B) 15 CMC emulsions as a function of ϕ_{eff}. Values of storage (G′) (closed symbols) and loss moduli (G″) (open symbols) of nanoemulsions (at a frequency of 6.28 rad/sec and 0.1% strain) were plotted from strain sweep measurements data against ϕ_{eff}. The inset shows a zoomed view of G′ and G″ of 15 CMC nanoemulsions from fifth to eighth passes. Note the difference in the x-axis for between both the graphs, which was needed to represent the data points more clearly and depict the differences in gelation mechanisms..... 84

Figure 4.2.8 Storage (G′) (●) and loss moduli (G″) (○) of 15 CMC nanoemulsions as a function of ϕ_{eff}. Secondary axis has average W_d/k_BT values calculated for nanoemulsions after each homogenization pass 86

Figure 4.3.1 Average droplet diameter (d_{32}) as a function of number of homogenization passes for (A) LER and (B) HER nanoemulsions with dispersed oil phase volume fractions: 0.30(●), 0.35(○), 0.40(▼), 0.45 (Δ), 0.50(■), 0.60(□). Difference in the ranges omitted on y-axes to accommodate all the data points with clarity in the respective plots. Error bars represents ± one standard deviation (n=3)..... 90

Figure 4.3.2 Apparent viscosities (at a shear rate of 10 s^{-1}) as a function of actual ϕ and average

droplet diameter of repulsive SDS emulsions. Data for both LER (○) and HER (●) nanoemulsions are shown 91

Figure 4.3.3 ϕ_{eff} as a function of average droplet diameter (d_{32}) at different dispersed phase oil concentrations: 0.3(♦), 0.35(■), 0.4(▲), 0.45 (x), 0.5(+), 0.6(●) at SDS emulsifier concentrations of (a) 1 CMC and (b) 2 CMC 92

Figure 4.3.4 Viscosity as a function of the effective oil phase volume fraction (ϕ_{eff}) of repulsive (A) LER and (B) HER nanoemulsions 93

Figure 4.3.5 Storage (G′) (closed symbol) and loss moduli (G″) (open symbol) as a function of % strain obtained from strain sweep measurements at a constant frequency (1Hz) for LER (A and B) and HER (C and D) nanoemulsions at different dispersed phase oil concentrations: 0.3(♦), 0.35(■), 0.4(▲), 0.45 (x), 0.5(+), 0.6(●). The arrow indicates the deviation of G′ from LVR at similar % strain 95

Figure 4.3.6 Plateau storage moduli (G'_p) of all individual nanoemulsions at 0.1% strain obtained from strain sweep measurements as a function of $\phi_{eff.}$ Filled symbols represent LER nanoemulsions while open symbols represent HER nanoemulsions... 96

Figure 4.3.7 Elastic moduli (G′ from Figure 4.3.6) scaled with Laplace pressure as a function of ϕ_{eff} obtained from strain sweep measurements at different dispersed phase oil concentrations: 0.3(♦), 0.35(■), 0.4(▲), 0.45 (x), 0.5(+), 0.6(●) for (A) LER and (b) HER nanoemulsions. r^2 values are 0.35 and 0.47 for the LER and HER nanoemulsions respectively 98

Figure 4.4.1 Sauter mean of droplet diameter (d_{32}) for all six nanogels as a function of storage time in days. Standard deviation is not shown for clarity 100

Figure 4.4.2 Average volume distribution of droplets as a function of droplet size for (A) 0.5 CMC and (B) 15 CMC SDS nanogel 101

Figure 4.4.3 Creaming velocities of nanogels at different RCFs obtained from accelerated shelf-life study using the LUMiSizer 101

Figure 4.4.4. Creaming velocities as a function of time (on day 1 and day 200) of (A) 5 CMC and (B) 10 CMC nanogels at different RCFs obtained from accelerated shelf-life study using LUMiSizer..... 103

Figure 4.4.5 Storage (G′, filled symbol) and loss (G″, open symbol) moduli of repulsive (A) 0.5 CMC (B) 1 and (C) 2 CMC SDS nanogels obtained from strain sweep measurements (at a constant frequency of 9.8 rad/sec) on day 1 (●) and day 90 (▲) of their storage period..... 104

Figure 4.4.6 G′ (filled symbol) and G″ (open symbol) of attractive (A) 5 CMC (B) 10 CMC and (C) 15 CMC SDS nanogels obtained from strain sweep measurements (at a constant frequency of 9.8 rad/sec) on day 1 (●) and day 90 (▲) of their storage period..... 105

Figure 4.4.7 Plateau G′ at 0.1% strain of repulsive (0.5, 1 and 2 CMC SDS) and attractive nanogels (5, 10 and 15 CMC SDS) obtained from strain sweep measurements (at a constant frequency of 9.8 rad/sec) plotted against storage time in days. Error bars represents ± one standard deviation (n=3)..... 106

Figure 4.4.8 Visual observation experiment of SDS nanogels. Vials containing nanogels were tilted at a certain angle to record their flow behavior and waited for 30 seconds after which the pictures were taken. This was done on day 1 and day 90 of their storage period 107

Figure 4.4.9 Yield stress values of nanogels on day 1 (▒) and day 90 (▓) calculated from the Hershel-Bulkley model as a function of emulsifier concentration. The viscosity data used for the model was obtained from rotational rheology experiments. Error bars represents ± one standard deviation (n=3) 108

LIST OF SYMBOLS AND ABBREVIATIONS

$\|G^*\|$	Complex modulus
AFM	Atomic force microscopy
AV	*p*-anisidine value
C_e	Concentration of emulsifier
C_M	Number density of micelles in the continuous phase
CMC	Critical micelle concentration
$C_{monolayer}$	Monolayer concentration of emulsifier
d_{32}	Sauter mean droplet size
d_{43}	Volume mean droplet size
D_f	Fractal dimension
DLA	Diffusion limited aggregation
DLVO	Derjaguin, Landau, Verwey and Overweek
d_m	Diameter of emulsifier micelles
EDL	Electrical double layer
f	Counterion dissociation factor
FF-SEM	Freeze-fracture scanning electron microscopy
g	Gravitational acceleration
G'	Storage modulus
G''	Loss modulus
G'_p	Plateau storage moduli
h	Interdroplet distance
HER	High emulsifier ratio
HIPE	High internal phase emulsions
Hz	Hertz
J	Joules
K	Kelvin
k_B	Boltzmann constant

LER	Low emulsifier ratio
LVR	linear viscoelastic region
mM	Milli moles
N_A	Avogadro number
N_{agg}	Micelle aggregation number
nm	Nanometer
O/W	Oil-in-water
OSF	Oscillatory structural force
Pa	Pascal
P_L	Laplace pressure
P_o	Osmotic pressure created by micelles
psi	Pound force per square inch
PV	peroxide Peroxide value
RLA	Reaction limited aggregation
RT	Room temperature
s	Second
SDLA	Slippery diffusion limited aggregation
SDS	Sodium dodecyl sulphate
SFA	Surface force apparatus
T	Temperature
TEM	Transmission electron microscopy
V_E	Volume of the continuous phase confined between droplets
W/O	Water-in-oil
W_D	Depletion interaction energy
W_{OSF}	Oscillatory structural forces interaction energy
WPI	Whey protein isolate
γ	Strain
δ	Phase angle
ζ	Zeta-potential
τ	Shear stress

τ_{HB}	Hershel-Bulkley yield stress
Γ	Emulsifier surface load at the interface
δ	Electrical double layer thickness
ϕ	Dispersed phase volume fraction
ϕ_{eff}	Effective dispersed phase volume fraction
ϕ_{m}	Micellar volume fraction
$\phi_{\text{m-eff}}$	Effective volume fraction of emulsifier micelles
ϕ_{MRJ}	Dispersed phase volume fraction at maximal random jamming
$\phi_{\text{MRJ monodispersed}}$	Dispersed phase volume fraction at maximal random jamming for monodispersed emulsions
$\phi_{\text{MRJ polydispersed}}$	Dispersed phase volume fraction at maximal random jamming for polydispersed emulsions
γ	Interfacial tension
η	Coefficient of viscosity
κ^{-1}	Debye screening length
μS	Microsiemens
ρ	densityDensity
$\dot{\gamma}$	Shear rate
τ_{HB}	Hershel-Bulkley yield stress
K	Consistency coefficient
n	Flow behaviour indice
σ	Interdroplet distance between depletes

1 INTRODUCTION

1.1 Overview

Controlling and manipulating the nanometer (10^{-9} m) scale particles of food systems may lead to the modification of many macro-scale characteristics, such as texture, sensory attributes and shelf life (Huang et al., 2010). Many products in the food industry are emulsions or produced from emulsions, for example, butter, margarine, salad dressing, sauces, coffee creamer and so on. Therefore by controlling the particle size in the emulsions, the physicochemical properties of these foods can be significantly altered. Emulsions are colloidal dispersions of two immiscible liquids, in which one phase is dispersed as droplets and the other forms a continuous phase around them. In conventional emulsions usually this droplet size ranges from 100 nm to several hundred micrometers. It has been proposed that textural and optical properties of emulsions can be modified significantly by reducing their droplet radii below 100 nm, i.e., converting them into nanoemulsions (McClements et al., 2011).

Nanoemulsions are metastable colloidal dispersions with average droplet radius ranging from 10 – 100 nm. The extremely small droplet size of nanoemulsions make them kinetically more stable to droplet aggregation, gravitational separation and coalescence compared to the conventional microscale emulsions (Huang et al., 2010). Due to the large interfacial area, nanoemulsions have shown to have improved delivery and bioavailability of bioactive materials encapsulated within their droplets (Huang et al., 2010). However, almost all nanoemulsions used to date are liquids, which restrict their use in many soft materials, including, gels, creams, and pastes. An elastic nanoemulsion gel (nanogel) with much improved stability and novel structure can have numerous applications in food, pharmaceuticals and cosmetics (Mason et al., 2007).

Recently, it has been shown that nanoemulsions can be transformed into viscoelastic gels at dispersed phase volume fractions much lower than microscale high internal phase emulsions (HIPE) (Mason et al., 2007; Wilking et al., 2007). In HIPE when droplet volume fraction (ϕ) reaches a disordered close-packing limit, known as maximal random jamming (ϕ_{MRJ}), the droplet surface starts to deform due to the pressure from neighboring droplets and cannot flow past one another without the application of external force (Mason et al., 1997). For disordered packing of

monodisperse hard spheres ϕ_{MRJ} = 0.64 (Berryman, 1983), while for polydisperse emulsions droplet packing and deformation can happen at a larger ϕ ($\phi_{MRJ\text{-}polydisperse} \geq 0.7$) as small droplets can fit into the interstices of larger packed droplets (Groot et al., 2011). The energy needed to compress and deform the disorderly-packed droplets against their interfacial tension leads to the elasticity of the structure (Wilking et al., 2007). The stability of these elastic emulsion gels comes from the presence of emulsifier layer at the oil-water interface and a thin film of water between the compressed droplets (Masalova et al., 2007). Since nanodroplets are more stable to coalescence, gels made from nanoemulsions are expected to be more stable than the conventional HIPE. Moreover, nanoemulsions with extremely small droplet size have stronger elasticity compared to the conventional HIPE as the elastic storage modulus of the gels are proportional to the Laplace pressure ($P_L=2\gamma/r$, where γ is the interfacial tension and r is the droplet radius) of non-deformed droplets, and therefore inversely proportional to their radius (Fryd et al., 2012). For an oil-in-water (O/W) emulsion stabilized with ionic emulsifiers, the charged droplets have a cloud of counterions forming an electrical double layer around their surface (Wilking et al., 2007; McClements et al., 2011). Due to the electrical double layer, droplets' effective radii become larger than their actual size, and effective volume fraction (ϕ_{eff}) become more than the actual volume fraction (ϕ_{core}) and consequently, they pack and deform at a ϕ_{core} below ϕ_{MRJ}. The equation governing this relation can be expressed as (Weiss et al., 2000; Wilking et al., 2007):

$$\phi_{eff} = \phi_{core}\left(1 + \frac{\delta}{r}\right)^3 \qquad 1$$

where, δ is the interfacial shell layer thickness due to electrical double layer. From eq 1 it can be calculated that for a 40% O/W nanoemulsion (ϕ_{core} = 0.4) with a droplet radius and shell layer thickness of 60 nm and 10 nm, respectively, ϕ_{eff} would be 0.64. Thus, by reducing droplet size and increasing shell layer thickness it would be possible to reach ϕ_{MRJ} at much lower ϕ and thereby develop the elastic behavior. This is a significant advantage for nanogels besides that they are more stable than conventional emulsion gels, as much less oil can be used to develop the elastic behavior. Experimental evidence of nanoemulsions' elastic behavior at low ϕ_{core} has also been observed by some research groups (Weiss et al., 2000; Wilking et al., 2007; Kawada et al., 2010). Weiss et al. (2000) found that a liquid 25% n-octadecane emulsion stabilized by 50mM sodium dodecyl sulfate (SDS) transformed into a viscoelastic gel when the droplet radius was

reduced below 80 nm. Similarly, Wilking et al. (2007) showed that liquid 40% silicone oil-in-water nanoemulsion stabilized with 116 mM SDS became elastic gel when the droplet radius fell below 60 nm during multiple passes through the microfluidizer.

Nanogels can also be formed by inducing attractive interactions among the nanodroplets. Bibette et al. (1993) showed that the addition of appropriate quantity of salt can transform a repulsive emulsion with charged droplets into an attractive elastic gel where the droplets are strongly aggregated in secondary minima of interdroplet pair potential. However, the complication with such attractive microscale emulsion gels is that the droplets may lose their integrity under strong adhesion and may coalesce (Ivanov et al., 1999). Nevertheless, small droplets in nanoemulsions have high Laplace pressure that makes them extremely stable against coalescence (Danov et al., 1993; Fryd et al., 2012). Therefore, attractive nanoemulsion gels are generally stable against coalescence. Such attractive gels were developed by Wilking et al. (2006) by adding ~700 mM NaCl to SDS-stabilized nanoemulsions with an average droplet radius ranging from 40 – 50 nm. Attractive interactions among the emulsion droplets can also be generated by depletion interactions where high concentrations of biopolymers or small nanoscale particles or emulsifier micelles in the continuous phase of emulsions lead to an osmotic imbalance between the interdroplet region of two closely approaching droplets and the bulk continuous phase forcing them to aggregate (Mondain-Monval et al., 1996; Berli et al., 2002). The three-dimensional network formed by the droplet aggregates immobilizes the continuous phase leading to the formation of emulsion gels (Berli et al., 2002; Datta et al., 2011). Often in electrostatically stabilized emulsions the repulsive forces caused by the adsorbed emulsifiers on the droplet surface and the attractive interactions caused by the micelles in the continuous phase coexist and the net interdroplet interaction and elastic properties of the emulsions depend on the balance between these interactions (Mondain-Monval et al., 1995). Recently, Datta et al. (2011) showed that while repulsive emulsion gels exhibited elastic properties only when ϕ_{eff} is above ϕ_{MRJ}, attractive emulsion gels are capable of forming elastic gels even when ϕ_{eff} is below ϕ_{MRJ}. However there has been no consensus on what concentration of a particular emulsifier the transition from repulsive to attractive nanogels would be observed and no theory is available for predicting the elasticity of the gels caused by both the electrostatic repulsion and depletion attraction.

As the gelation in nanoemulsions can be obtained at much lower actual dispersed phase volume fraction compared to conventional emulsions, they hold promise in wide applications because of the higher stability of nanoemulsions and lower droplet volume fraction needed for gelation. However, to date no reported application of these nanoemulsion gels in food products can be found. This could be due to the poor understanding of their formation, long-term stability, behaviour in complex food matrices and suitability of food grade ingredients available.

The overall goal of this thesis is to investigate the influence of emulsifier concentration, droplet size and effective dispersed phase volume fraction on the close packing of oil droplets in oil-in-water (O/W) nanoemulsions. The study also includes the investigation of long-term stability of the resulting nanogels.

1.2 Objectives

The following research objectives are developed to reach the overall goal:

- To investigate the influence of emulsifier type and concentration on the gelation of nanoemulsions;
- To study the effect of droplet size on nanoemulsion gelation;
- To investigate the effect of dispersed oil phase volume fraction on nanoemulsions gelation; and
- To investigate the long-term stability of the nanogels

1.3 Hypotheses

The following hypotheses were tested as a part of this research study:

- Ionic emulsifiers, due to the formation of electrical double layer, will be able to contribute to the effective oil phase volume fraction and gel strength (higher G' than G") to a greater extent than that prepared with non-ionic emulsifiers.
- Below a critical nanoemulsion droplet size, influence of interfacial electrical double layer thickness would significantly increase the effective droplet size and oil phase volume fraction (ϕ_{eff}) compared to the actual such that a close-packed network of nanodroplets will form when ϕ_{eff} would be equal to the theoretical volume fraction of maximal random jamming (ϕ_{MRJ}) i.e. $\phi_{eff} \approx \phi_{MRJ}$

- When oil phase effective volume fraction (ϕ_{eff}) become equal or more than the random jamming of nanodroplets (ϕ_{MRJ}) a viscous liquid nanoemulsion will convert into a viscoelastic gel-like material such that the storage modulus (G') of the nanoemulsion will be higher than the loss modulus (G").
- Ionic emulsifier concentration would influence nanoemulsion gelation based on whether the interdroplet interaction falls within repulsive or attractive regimes.
- Gel strength of the nanogels would increase with decrease in droplet size
- With an increase in ϕ, repulsive nanoemulsion should transform from liquid to glassy to jammed state, while attractive nanoemulsion change from liquid to fractal gel where a network of droplets is responsible for gelatin.
- Extremely small droplet sizes of nanogels make them more stable to droplet coalescence and creaming for long periods of storage time.
- The gel strength of nanogels will be stable with time during their storage.

The first five hypotheses are common for the objectives 1 and 2 in which the influences of emulsifier concentration and droplet size on nanoemulsion gelation were investigated. Third and sixth hypotheses were tested as a part of objective 3 in which the influence of ϕ on the gel strength of nanogels was investigated. Seventh and eighth hypotheses were developed for objective 4 which investigated the stability of nanogels during storage time of 90 days.

2 LITERATURE REVIEW

2.1 Emulsions

Emulsions are dispersions of two or more immiscible phases, one being dispersed as droplets in the other (McClements, 2005). The phase which makes up the droplets is called dispersed phase, and the phase surrounding the droplets is called a continuous phase. Emulsions are found in many foods products like whipped cream, dips, infant formulas, coffee whitener, sauces and soups (McClements, 2005). Emulsions are also used in many pharmaceutical industries for drug delivery and in the manufacturing of cosmetics like lotions and creams (Hatanaka et al., 2010; Mihranyan et al., 2012).

2.1.1 Types of emulsions

Based on the composition of dispersed and continuous phase, emulsions are classified as oil-in-water (O/W) and water-in-oil (W/O) emulsions. In O/W emulsions oil droplets are dispersed in continuous water phase (e.g., mayonnaise, salad dressings etc.), whereas in W/O emulsions water droplets are dispersed in the continuous oil phase (e.g., butter, margarine). Based on the number of dispersed phases, emulsions can also be classified as single, double or multiple emulsions. Single emulsions have only one dispersed phase, while double emulsions have two or more dispersed phases, one phase dispersed as droplets in the other, which in turn dispersed in another continuous phase (Muschiolik, 2007). Examples are oil-in-water-in-oil (O/W/O) emulsions and water-in-oil-in-water (W/O/W) emulsions. These emulsions are not very common in food, but they are used as a drug delivery medium in pharmaceutical industries (McClements, 2005). Depending on the stability of dispersed phase, emulsions can also be classified as conventional emulsions, and microemulsions (McClements, 2012). Conventional emulsions are thermodynamically unstable and the stability of the two phases can only be controlled kinetically (Mason et al., 2007), whereas, microemulsions are thermodynamically stable under a given sets of conditions (McClements, 2012). The droplet radii of microemulsions are in the range of 2-50 nm, whereas conventional emulsions have a broad range of droplet radii from few hundred nanometers to several micrometers (100nm – 100µm) (McClements, 2011). A

new class of emulsions, called nanoemulsions has become popular in recent years due to improved stability compared to the conventional emulsion and the need for much less emulsifiers compared to microemulsions (Rao et al., 2012). Nanoemulsions are prepared under very high-pressure homogenization conditions, and the droplets radius is in the range 10-100nm (McClements, 2011), i.e. in the range of microemulsions and less than conventional emulsions. However, these limits are somewhat arbitrary and at present there is no consensus in the literature as to what should be the cut-off droplet radius to be classified as nanoemulsions (McClements, 2011).

2.1.2 Emulsion composition

Many foods are made of emulsions, either partly (e.g., sauces, beverages with the emulsions for flavor delivery) or as a whole (e.g., milk, mayonnaise, spreads etc.) (McClements, 2005). Most of these emulsions are comprised of a wide variety of both oil and water soluble constituents like emulsifiers, thickening agents, preservatives, antioxidants, sweeteners, flavours, etc. The concentration and distribution of ingredients in dispersed and continuous phases significantly influence the physicochemical and organoleptic properties of foods, which in turn impact their consumer acceptability (Malone et al., 2003). The distribution of ingredients in food emulsions can be broadly divided into the following three groups.

2.1.2.1 Lipid phase

The composition of the lipid or oil phase of food emulsions has a high influence on the nutritional, physicochemical and organoleptic properties (McClements, 2005). Besides oil, this phase also contains other lipid soluble constituents like flavors, vitamins, etc. which influence the organoleptic properties of emulsions. The appearance of emulsions, namely turbidity, opacity or color is due to light scattering by the oil droplets. The viscosity and texture of emulsions (e.g. creaminess) also depends on the concentration and droplet characteristics of the oil phase. For example, emulsions with higher oil concentrations are more viscous than emulsions with low oil concentration (McClements, 2005).

2.1.2.2 Aqueous phase

The aqueous phase of an emulsion consists of water-soluble ingredients (e.g. colorants, preservatives, vitamins, proteins, polysaccharides) which influence the organoleptic properties, flowability and stability of food emulsions. When emulsions are used as part of a frozen food, freeze/thaw stability of the emulsion is significantly influenced by aqueous phase composition (Ghosh et al., 2006). Aqueous phase viscosity also influences emulsion stability for example, an O/W emulsion with higher aqueous phase viscosity would be more stable against creaming as the droplet movement can be restricted by the viscous continuous phase (McClements, 2005).

2.1.2.3 Interface

The interface is the area of the surface around the dispersed droplets. The composition of emulsifiers at the interface has a significant influence on emulsion stability (McClements, 2005). Emulsifiers are surface active amphiphilic molecules which adsorb onto the interface and reduce the interfacial tension between oil-water interfaces. Thus, they aid in the formation of emulsions as the amount of energy required for emulsification is less when the interfacial tension is low. They also prevent droplet recoalescence during and after emulsification (Walstra, 1993).

Different types of surface active agents used for emulsion stabilization are low molecular weight emulsifiers, amphiphilic biopolymers and solid particles (Figure 2.1.1). Depending on the characteristics of the head and tail groups emulsifiers can be classified into ionic (fatty acid salts and sodium stearoyl lactate, sodium dodecyl sulphate), zwitterionic (which has both positively and negatively charged groups on the same molecule e.g. lecithin and other phospholipids) and non-ionic (sorbitan esters, monoglycerides etc.). Surface active biopolymers have both polar and nonpolar groups attached to them and the common biopolymers used in food emulsions are proteins (e.g. Caseins, whey proteins, gelatins) and polysaccharides (e.g. gum Arabic). Solid particles (e.g. triglyceride crystals) which are adsorbed on the droplet interface can impart stabilization, and this process is known as Pickering stabilization (Dickinson, 2010). Small molecule emulsifiers' functional properties are determined by their molecular structure (the ratio of cross sectional area of the hydrophilic head group and hydrophobic tail group) (Holmberg et al., 2003). For example emulsifiers with the larger polar head group and smaller tail group are

effective in stabilizing O/W emulsions, and those with the smaller head group and larger tail group will stabilize the W/O emulsions.

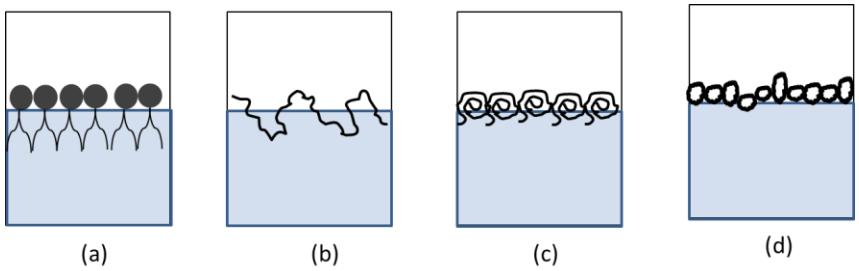

Figure 2.1.1 Stabilization by different types of surface active agents. (a) small molecule emulsifier, (b) flexible proteins (caseins), (c) globular proteins (whey proteins) and (d) particles (triglyceride crystals)

2.1.3 Emulsion preparation

As the two phases in emulsions are immiscible, external energy is required to disperse one phase as droplets into other. The energy supplied should be sufficient for droplet deformation and disruption, which is opposed by the internal pressure of the droplets (also known as Laplace pressure, P_L) and is given by the equation:

$$P_L=\frac{2\gamma}{r} \qquad 2.1.1$$

where, γ is the interfacial tension between oil and water, and r is the radius of the droplet (Walstra, 1993). From eq 2.1.1 it can be observed that the Laplace pressure is directly proportional to the interfacial tension and inversely proportional to the droplet size. Therefore, as the droplet radius becomes smaller during homogenization, it becomes increasingly difficult to break them up further.

The process of emulsion preparation is called homogenization (Walstra, 1993). It is normally a two-stage process where a primary coarse emulsion is prepared in a high-intensity blender (in order to disperse the droplets in the continuous phase) followed by homogenization using high-pressure homogenizers or microfluidizer to further reduce the droplet size and polydispersity. The droplet size of a freshly prepared emulsion depends on the homogenization pressure, time and number of passes. The mechanism of homogenization can be characterized by

two opposite processes i.e. droplet disruption and droplet re-coalescence which occur simultaneously during homogenization (Qian et al., 2011; Lee et al., 2013). Newly formed droplets tend to coalesce with surrounding droplets on their encounter during homogenization as they are thermodynamically unstable (Jafari et al., 2008). This process is opposed by emulsifier adsorption at the interface of newly created droplets. But if the rate of adsorption of emulsifier at the interface is slower than interdroplet collision, the droplets would coalesce. Hence, in order to get smaller droplets the rate of emulsifier adsorption at the interface should be much faster than the rate of recoalescence (Jafari et al., 2008; Qian et al., 2011). The presence of insufficient amount of emulsifier to stabilize newly formed droplets would lead to coalescence, and the droplet size cannot be further decreased with an increase in homogenization pressure (Olson et al., 2004).

2.1.4 Droplet characteristics

Droplet characteristics like concentration, size, charge, etc. strongly influence the physicochemical properties of food emulsions (e.g. rheology, stability and appearance). Droplet concentration and size of an emulsion has significant impact on the stability (e.g. stability to gravitational separation, flocculation and coalescence), optical properties, rheology and sensory attributes (creaminess) of emulsions (McClements, 2005). Droplet concentration is expressed as the dispersed phase volume fraction (ϕ) or mass fraction (ϕ_m). As most food emulsions are polydispersed, they have a range of droplet sizes. Hence, it is better to characterize emulsions by droplet size distribution. However, in many cases it is convenient to use volume weighted (d_{43}) or surface weighted mean droplet size (d_{32}). This also gives an estimation of the concentration of droplets in different size classes (McClements, 2007). Generally, the volume-weighted mean is more sensitive to the presence of large droplets than the number-weighted mean. Appreciable differences between the d_{32} and d_{43} generally indicate that the particle size distribution is broad (McClements, 2007).

Droplets in most food emulsions are charged due to the inherent charge of food emulsifiers adsorbed at the surface of the droplets (McClements, 2005). Droplet charge determines electrostatic interactions among themselves and with other particles in emulsions. For example, an anionic emulsifier (e.g. sodium dodecyl sulfate) could be used to prepare an O/W

emulsion such that electrostatic repulsions between the negatively charged droplets would prevent aggregation (Dickinson, 1992).

2.1.5 Droplet interactions

Droplet interactions have a significant impact in deciding whether they will remain separate or form aggregates (Friberg et al., 2004). The stability of many food emulsions depends on the interdroplet interactions, which in turn influence gravitational separation, flocculation, and coalescence. Droplet interactions are expressed in terms of the interdroplet pair potential, which is the energy required to bring two droplets from an infinite distance to a close separation (Ghosh et al., 2010) (Figure 2.1.2). The interdroplet pair potential is shown in Figure 2.1.2. is the sum of van der Waal and electrostatic interactions. In Figure 2.1.2, the interdroplet interaction energy (JK^{-1}) is shown on the Y-axis, and the distance of separation (meters) between two droplets is represented by the X-axis. The electrostatic potential component is repulsive which increases exponentially with a decrease in distance between the droplets. On the other hand van der Waal forces are attractive and increases as the droplets approach each other. The total interaction potential is the sum of these two forces. It decreases as the particles come near, and the droplets form loose aggregates when the interaction potential drops to a secondary minimum. Upon further droplet approach, the electrostatic repulsion dominate over the van der Waal interaction and if the thermal energy of the droplets is not enough to overcome the repulsive energy barrier they return back to initial non-aggregated state (reversible flocculation). On the other hand, if thermal energy of the droplet pair is more than the repulsive energy barrier, the interaction potential passes through the energy barrier and the droplets form strong irreversible aggregates (also known as coagulation) at the primary energy minima. In the presence of an electrolyte wherein the electrostatic repulsions are reduced by the screening of droplet charge, the potential energy barrier is small compared to the thermal energy of the system and the droplets will aggregate easily. This theory of interdroplet potential was first proposed by Derjaguin, Landau, Verwey and Overweek and is known as DLVO theory (Ghosh et al., 2010). Original DLVO theory did not take into account steric repulsions, depletion forces, hydrophobic and hydration interactions, so it is only an approximate estimate of droplet interactions. However, for specific

cases, these factors can be included in a modified DLVO theory that could be used to predict inter-droplet interactions and hence emulsion stability (McClements, 2005).

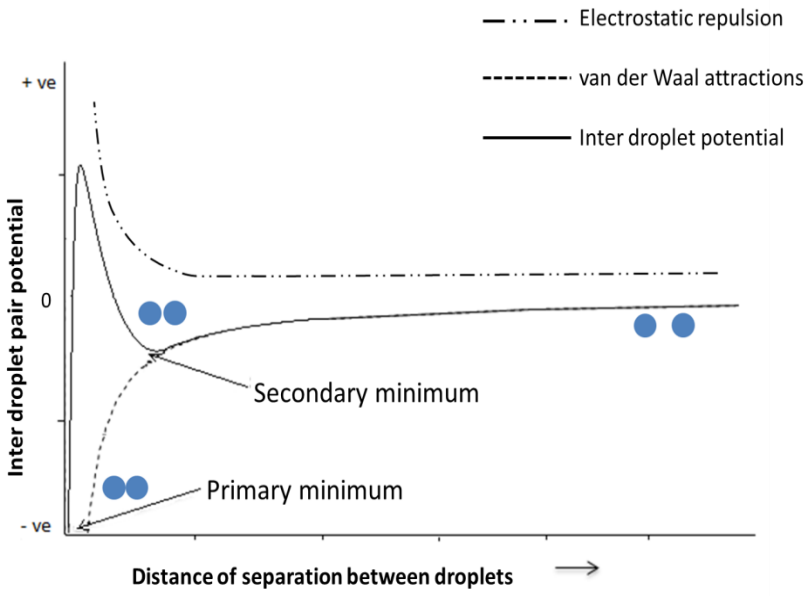

Figure 2.1.2 DLVO interdroplet pair potential between two droplets (adapted from Ghosh and Rousseau, 2010)

2.1.6 Emulsion stability and destabilization mechanisms

Emulsions are thermodynamically unstable systems and they tend to form completely separate oil and aqueous phases over time which is energetically more favoured as it minimizes Gibb's free energy of the system (McClements, 2007). However, they can be made kinetically stable over time with the help of emulsifiers and other ingredients. Therefore, it is important to understand the various physicochemical mechanisms of emulsion destabilization (Figure 2.1.3) (Dickinson, 1992; McClements, 2007). Often these mechanisms are interrelated, and they occur simultaneously (McClements, 2007).

2.1.6.1 Gravitational separation

Gravitational separation is the process in which the two immiscible phases with different densities tend to separate under the influence of gravity (McClements, 2007). Droplets tend to cream if their density is less than that of continuous phase (for O/W emulsion) (Figure 2.1.3c) and they tend to sediment if their density is more than that of continuous phase (for W/O emulsion) (Figure 2.1.3d). The creamed layer can be re-dispersed uniformly when gently mixed, thus creaming can be reversible (Dickinson et al., 1988; McClements, 2007). The rate of creaming can be measured by Stokes' law which states that a particle moving at a constant velocity through a surrounding liquid will have an opposing hydrodynamic frictional force equal to the gravitational force acting on it. The creaming velocity of an isolated spherical particle in an emulsion can be determined by Stokes' formula:

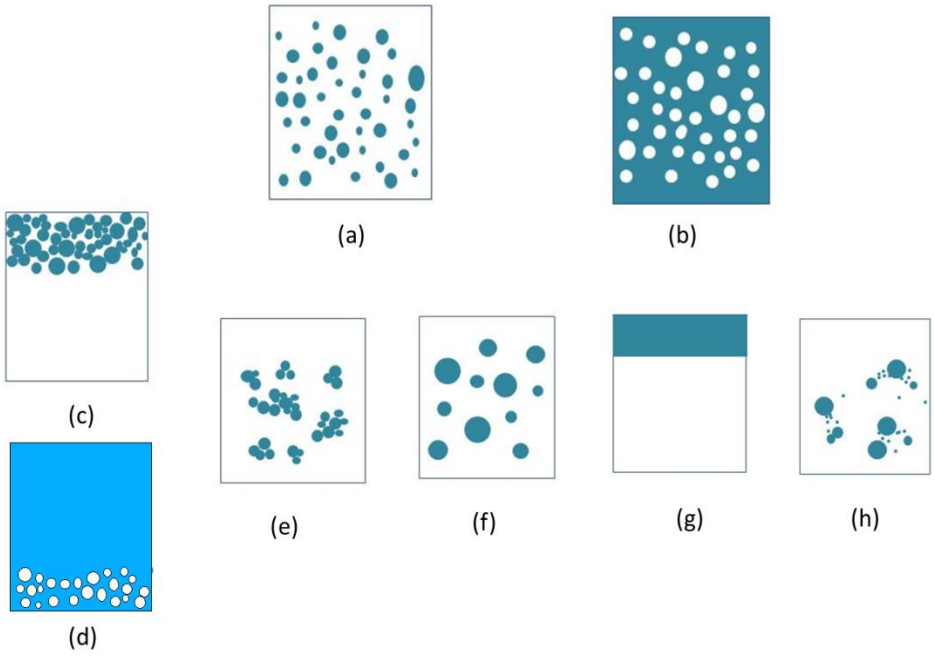

Figure 2.1.3 Mechanisms of emulsion destabilization (a) kinetically stabilized O/W emulsion, (b) phase inversion into W/O emulsion, (c) creaming of oil droplets (d) sedimentation of water droplets, (e) flocculation, (f) coalescence, (g) phase separation, (h) Ostwald ripening (adapted with modification from McClements 2007).

$$\nu = \frac{2g\Delta\rho r^2}{9\eta} \qquad 2.1.2$$

where ν is the velocity of the droplet and $\Delta\rho$ is the density difference of the two phases of the emulsion, r is the radius of the droplet, η is the viscosity of the surrounding continuous phase and g is the acceleration due to the gravity. From this equation it is evident that creaming rate of an O/W emulsion can be reduced by decreasing the droplet size and increasing the continuous aqueous phase viscosity. Actual creaming velocity in a typical food emulsion is less than the value predicted by stokes' law as the emulsions are not dilute enough and movement of each droplet is influenced by surrounding droplets (Dickinson et al., 1988).

2.1.6.2 Flocculation

Flocculation (Figure 2.1.3e) is the process where two or more droplets form an aggregate retaining their individual identity (McClements, 2007). Flocculation increases the overall size of droplet aggregates which in turn increases creaming. The rate of flocculation depends on colloidal interactions and collision frequency of the droplets as a result of Brownian motion and gravitational flow (McClements, 2007). Flocculation can be prevented by inducing electrostatic or steric repulsion among the droplets.

2.1.6.3 Coalescence

Coalescence (Figure 2.1.3f) is the process in which two or more droplets merge to form one large droplet (McClements, 2007). Similar to flocculation coalescence also depends on droplet interaction and collision frequency. Droplet encounter and interdroplet film rupture are the essential steps of coalescence (McClements, 2007). Coalescence increases the rate of creaming due to increase in droplet size. Close encounter of droplets in the cream layer may also lead to rupture of interdroplet film leading to coalescence.

2.1.6.4 Ostwald ripening

In Ostwald ripening (Figure 2.1.3h) mass transport of the molecules of dispersed phase droplets occurs from smaller droplets to larger droplets, increasing the size of larger droplets at the expense of smaller ones (Kabalnov, 2001; McClements, 2007). Ostwald ripening depends on the solubility and diffusion of the dispersed phase molecules in the aqueous phase (Weiss et al.,

2000). It can be inhibited by proper selection of oil that is insoluble in the aqueous phase (e.g., vegetable oil in water) Ripening inhibitors (e.g., polyvinyl alcohol) are also used which reduces the solubility of dispersed phase molecules in the continuous phase (Chang et al., 2012).

2.1.6.5 Phase inversion

Phase inversion (Figure 2.1.3b) is the process whereby an O/W emulsion changes to a water-in-oil (W/O) emulsion, or vice versa (McClements, 2007). This could happen when the dispersed phase concentration of a highly concentrated emulsion exceeds the critical packing limit and becomes continuous phase. Changing emulsifier composition from a low HLB system to a high HLB system could also promote emulsion phase inversion (Solans et al., 2012).

2.1.7 Measuring emulsions stability

Emulsion stability can be measured by monitoring gravitational separation (creaming or sedimentation), droplet aggregation and increase in droplet size. The gravitational separation can be determined by calculating the height of cream or sedimentation layer of an emulsion in a test tube. Quantitative determination of creaming or sedimentation rate is done by light scattering experiments by measuring the back-scattered and/or transmitted light as a function of the height of emulsion in a test tube (McClements, 2007). This way complete droplet distribution at different heights of an emulsion in a test tube can be obtained. It can also be measured by accelerated stability tests which often involve centrifugation (see section 3.6 for more details). Flocculation and coalescence can be experimentally determined by microscopy (floc structure and dimension) and particle size measurement. Particle size measurement is more often used in understanding flocculation and coalescence of emulsion. However, care must be taken to ensure that the increase in droplet size is due to flocculation or coalescence alone and not due to Ostwald ripening, which is often difficult. Phase inversion can be easily detected by the changes in the electrical conductivity of emulsions at the phase inversion point where a sudden change in conductivity indicates conversion of water continuous system is converted into oil continuous system, or vice versa (McClements, 2007).

2.2 Nanoemulsions

2.2.1 Definition

Nanoemulsions are the emulsions whose mean droplet radius varies from 10 to 100 nm (Tadros et al., 2004; Mason et al., 2007). This range of droplet size is arbitrary, and some authors consider the upper range to be 500 nm (Gutierrez et al., 2008). Nanoemulsions are kinetically very stable, sometimes over the years. Dilute nanoemulsions are less turbid or can even be transparent if their droplet size is much smaller than the visible light wavelengths (McClements, 2011).

2.2.2 Nanoemulsions formulation

The physicochemical properties of the oil phase (e.g., viscosity, water solubility) have high impact on the formation, stability, and rheological properties of nanoemulsions (Tadros et al., 2004; McClements, 2011). Proper choice of oil type is to be made while preparing O/W nanoemulsions, as the solubility of oil in water might lead to Ostwald ripening. The oil phase may also contain other ingredients like weighting agents (which match the density of oil and aqueous phase, thereby improving their stability to gravitational separation) and ripening inhibitors (components which are soluble in oil and insoluble in aqueous phase and reduce the solubility of oil phase in water thus inhibiting Ostwald ripening). The aqueous phase is also important in deciding the stability of nanoemulsions. The viscosity ratio of dispersed to continuous phase (η_d/η_c) influences droplet breakup and nanoemulsion stability (Walstra, 1993; McClements, 2011). If the (η_d/η_c) is greater than 4, the flow behaviour inside a homogenizer turns less turbulent, making it difficult to achieve droplet breakdown (Walstra, 1993). It was also shown that and if (η_d/η_c) is greater than 10 droplets cannot be broken down (Walstra, 1993). In other words, with an increase in the oil phase viscosity, it will be difficult to get extremely small droplet size. Emulsifiers are also very important in the formation of nanoemulsions. As mentioned earlier in section 2.1.3, in order to form nanoscale droplets emulsifiers need to be adsorbed immediately onto the interface of oil droplets before they coalesce (Jafari et al., 2008). For this reason, small molecule emulsifiers are better than polymeric emulsifiers to form nanoscale droplets (e.g. proteins, polysaccharides) and in preparing nanoemulsions. Besides the

higher rate of adsorption at the interface, the emulsifier concentration should also be sufficient to stabilize extremely high droplet interfacial area in nanoemulsions.

2.2.3 Preparation of nanoemulsions

The energy required to prepare nanoemulsion is much higher compared to normal emulsions because of creation of extremely small droplets with very high interfacial area and the corresponding higher internal Laplace pressure (eq 2.1.1) of the droplets that must be overcome in order to create nano-droplets (McClements, 2011). Commonly used mechanical devices that generate intense disruptive forces to break the oil phase into nano-droplets are, high-pressure homogenizers, microfluidizers and ultrasonic transducers (Maali et al., 2013). It has been shown that the droplet size of nanoemulsion reduced with homogenization pressure and time (Walstra, 1993; Qian et al., 2011). However, for every homogenization process there is a limit beyond which the droplet size cannot be further reduced with an increase in pressure (Qian et al., 2011).

Nanoemulsions can also be prepared by low energy methods. In low energy methods small oil droplets are spontaneously formed when the solution conditions (e.g., dispersed phase concentration, emulsifier type and concentration) or environmental conditions (e.g. temperature) are altered accordingly (McClements, 2011; Solans et al., 2012). Often these low energy approaches use a high amount of surfactant compared to high energy methods, which is a drawback for its use in food emulsions.

2.2.4 Influence of interfacial layer on nanoemulsion properties

The droplets in O/W nanoemulsions have a lipophilic core surrounded by a shell of surface-active material (McClements, 2005). The thickness of the shell has a significant influence on the stability of nanoemulsions and also on the effective volume fraction of oil droplets (Lee et al., 2010; McClements, 2011; Rao et al., 2012). In conventional emulsion, the shell thickness can always be neglected, as it does not influence overall droplet size. However, if shell thickness (δ) becomes the same order of magnitude as that of droplet radius (r), it contributes a lot to the effective droplet size. The overall effective oil phase volume fraction ($\phi_{effective}$) is the sum of volume fractions of core droplet(ϕ_{core}) and the shell (ϕ_{shell}).

$$\phi_{effective}=\phi_{core+}\phi_{shell} \qquad 2.2.1$$

The shell layer thickness of sterically- stabilized systems depends on the thickness of the adsorbed biopolymer. However, for electrostatically-stabilized systems it is greater than the adsorbed layer because of the Debye screening length (κ^{-1}) (Mason et al., 2007). Debye screening length is the characteristic distance above a droplet in which the opposite charged counterions are electrostatically attached to the droplets (Israelachivili, 2011). The electric charge (zeta-potential, ζ) and the debye screening length has a positive effect on the shell layer thickness (McClements, 2011; Fryd et al., 2012). The interfacial shell thickness can also be altered by emulsifier composition and concentration.

2.2.5 Stability and destabilization mechanisms of nanoemulsions

Nanoemulsions are kinetically more stable than conventional emulsions due to the small droplet size (Tadros et al., 2004). The destabilization mechanisms in nanoemulsions are similar to conventional emulsions and only differ by the magnitude. Extremely small droplet size in the nanoemulsions leads to more kinetic stability against particle aggregation and gravitational separation (Tadros et al., 2004; Rao et al., 2012). This can be explained using Stokes' law (equation 2.1.2), which states that the velocity of droplet movement is proportional to the square of droplet radius. Therefore, below a certain droplet size destabilization mechanism in nanoemulsions is mostly due to the Brownian motion whereas in case of normal emulsions it is gravitational separation (McClements, 2011). Brownian motion is the random movement of particles suspended in a fluid (liquid or gas) (Kikoin et al., 1973). Droplet movement due to Brownian motion may lead to interdroplet collision, and this may induce droplet destabilization. Flocculation and coalescence in nanoemulsions are less compared to conventional emulsions as the range of attractive interactions between the droplets decreases with the droplet size (Tadros et al., 2004; Rao et al., 2012). In nanoemulsions, the surfactant film thickness is significant relative to droplet radius, therefore thinning or disruption of the liquid film between the droplets is reduced making them more stable to flocculation and coalescence (Fryd et al., 2012).

2.2.6 Applications of nanoemulsions

Nanoemulsions have many potential advantages compared to the conventional emulsions. They are extremely stable compared to conventional emulsions which make them attractive to

use in commercial products with better shelf life (Silva et al., 2012). Nanoemulsions hold great promise for use in food application due to their stability and flow behaviour ranging from liquid to viscoelastic gels at a lower oil phase volume fraction compared to conventional emulsions. Their optical properties (significantly less turbid or translucent) also make them useful in many applications, e.g. flavour delivery medium in clear beverages (Gutierrez et al., 2008). nanoemulsions are also shown to increase bioavailability of bioactive lipophilic substances because of their high surface-to-volume ratio (hence higher release of internal bioactive compounds in the guts), making them preferable over normal emulsions in functional foods, nutraceuticals and pharmacological applications (Silva et al., 2012; Maali et al., 2013).

2.3 Rheological behaviour of materials

2.3.1 Theory of rheology

Rheology is the science that represents the study of deformation and flow of matter (ranging from liquids to soft solids) in response to mechanical stress (Barnes et al., 1989). Knowledge of rheological properties of the material is very important in food industries for many reasons. It helps food engineers in designing processing operations such as stirring, mixing, the passage of food through a heat-exchanger, packing of food into containers, etc. that are based on material flow behaviour. Rheological properties such as creaminess, thickness, spreadability and hardness also significantly influence the sensory properties of foods (Rao, 2007; Fischer et al., 2011).

The term Rheology was coined in 1920's by chemists Eugene C. Bingham and Markus Reiner. In 1678, the theory of elasticity was proposed by Robert Hooke, which explains the elasticity of solids (Macosko et al., 1994; Rao, 2005), 1994. He proposed that the relative change of length of spring was proportional to the force applied (Barnes et al., 1989). He also observed that the spring returned back to its original length when the tension is released. For example, when shear stress (τ) (equivalent of force (F) per unit area (A) required to produce deformation) is applied on a Hookean solid block shown in Figure 2.3.1A, an instantaneous deformation is observed. However, removing the stress would lead to complete recovery to the original state of the solid block. The constitutive equation for elasticity of such solid is given by eq 2.3.1, in which angle 'γ' is the strain and G is the elastic modulus (Barnes et al., 1989; Meyers, 2009).

Energy is stored in the intermolecular bonds when an external stress is applied to compress or expand the material. When the stress is removed this energy is released, and the material returns to its original shape. Thus, the elastic modulus of an elastic solid depends on the number and strength of intermolecular bonds per unit area (McClements, 2005).

$$\tau = G\,\gamma \qquad 2.3.1$$

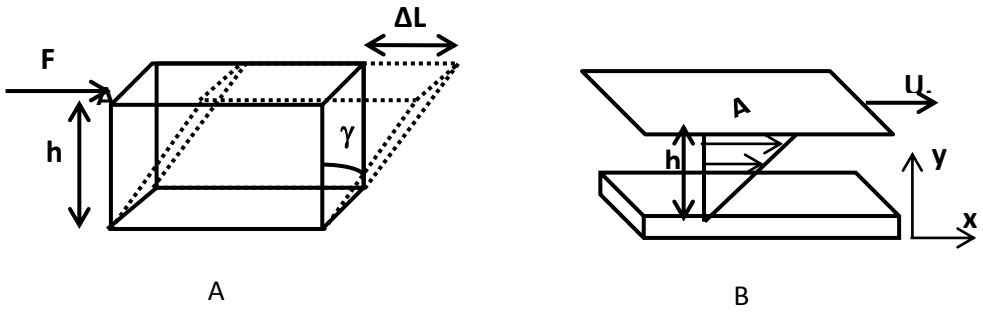

Figure 2.3.1 (A) Hookean solid which is deformed by a length of ΔL by the application of shear stress τ. (B) Shear flow between parallel planes of area A, separated by a distance h. Liquid filling the space between them is sheared by the upper plane moving whole relative velocity is U. The local velocity of fluid is proportional to the lengths of arrows between the two layers.

In the year 1687, Isaac Newton postulated his theory of the flow of liquids and the conjecture of viscosity. According to him, viscosity, a measure of resistance to flow in liquid, is proportional to the velocity of the liquid (Barnes et al., 1989; McClements, 2005; Rao, 2005). It can be understood with an example of the liquid flowing between two parallel plates as shown in Figure 2.3.1B. The upper moving plate shears the fluid with a velocity U, and the bottom plate is at rest. Assuming that the fluid between plates consisted of a series of thin layers, the velocities of layers in direct contact with the bottom and top plates will be 0 and U respectively. The intervening layers would slide over each other with an intermediary velocity between 0 and U. In an ideal liquid, the stress τ is proportional to the change in displacement of layers per unit time ($d\gamma/dt$) which can also be referred as rate of strain ($\dot{\gamma}$) and is given by eq 2.3.2 in which the constant of proportionality η is called the coefficient of viscosity.

$$\tau = \eta\dot{\gamma} \qquad 2.3.2$$

The type of flow shown in Figure 2.3.2B is known as the laminar flow that occurs at low applied shear rates. At higher shear rates, the fluid shows turbulent flow pattern and eddies are formed which makes it complex to mathematically derive a relation between shear stress and shear rate (Walstra, 2003). Hence, instruments that measure the viscosity of liquids are designed to eliminate any non-laminar flow. Water and pure vegetable oil are some of the liquids that obey the viscosity behavior postulated by Newton and are called Newtonian fluids. However, the majority of the liquids does not follow the Newtonian fluid behavior as their viscosity change with the rate of strain (Figure 2.3.2). These fluids are generally referred to as non-Newtonian fluid whose viscosity either decrease (pseudoplastic or shear-thinning) or increase (dilatant or shear thickening) with the rate of shear. For example, the viscosity of chocolate milk diminishes as shear rate increases (Pseudoplastic behavior) and the viscosity of corn starch dispersion heated to a temperature of 70° C increases as shear rate increases (Dilatant liquids) (McClements, 2005; Mewis, 2012). The viscosity of some materials also changes as a function of time at constant shear/strain rate (Meyers, 2009). Such type of behavior is called thixotropy when viscosity decreases with time or rheopectic when viscosity increase with time.

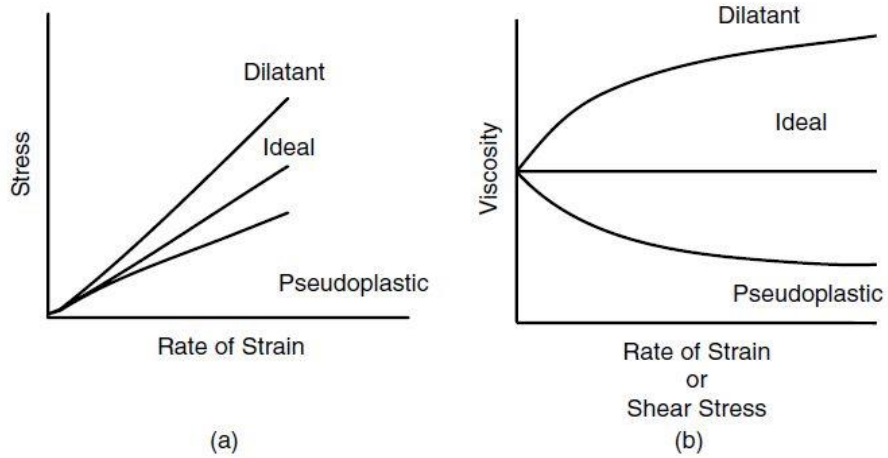

Figure 2.3.2 Comparision between ideal and nonideal liquids (a) Shear stress vs. rate of strain and (b) apparent viscosity vs. rate of strain for ideal, dilatant and pseudoplastic liquids

Some studies in 1800's found that many materials such as paints and oils are not perfectly viscous, but possess some elastic properties and their viscous behavior cannot be solely explained by Newtonian fluid mechanics (Barnes et al., 1989; Macosko et al., 1994). In 1835,

Wilhelm Weber found that silk threads were not perfectly elastic, as a longitudinal load on it produced an instantaneous extension followed by a continued slow stretching with time (Barnes et al., 1989). Removal of the load on it resulted in an immediate contraction but delayed shrinking to the original length. He theorized that it was a solid-like material, with elements of flow properties associated with liquids and found that Hooke's law alone can not describe the response of such material. In the year 1867 James Clerk Maxwell first proposed a mathematical model to explain elastic properties of non-Newtonian fluids (Maxwell, 1866; Barnes et al., 1989). Such material that exhibits both elastic and viscous characteristics under stress are known as a viscoelastic material.

In a viscous material, energy is lost upon application of stress. On the other hand, in purely elastic material, energy is not dissipated when a load is applied and removed. However in a viscoelastic material, the viscous component results in loss of energy upon removal of applied load. This results in a hysteresis loop observed in a stress-strain curve after loading and during unloading passes, and the area of the loop is equal to the energy lost (Meyers, 2009). Unlike elastic solid material where deformation under stress is caused by atomic displacements on specific crystallographic planes, in viscoelastic material, a constant load results in the continuous displacement of atoms or molecules with time.

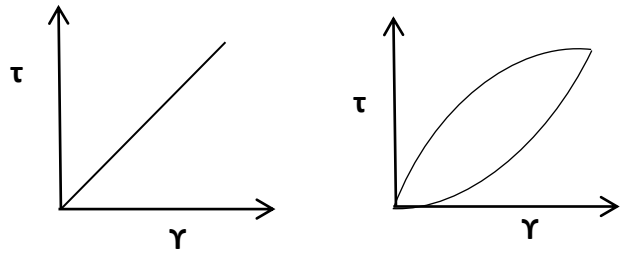

Figure 2.3.3 Shear stress vs. strain graphs of (A) perfect elastic material which has a linear relationship and (B) a viscoelastic material in which hysteresis loop is observed whose area is equal to the energy lost.

Characterization of material viscoelastic behavior is usually done by sinusoidally deforming the material and recording the resultant stress (Courtney, 1990). Let us consider a

material is being subjected to an oscillatory strain with frequency ω. In the viscoelastic material, there is a phase lag δ, between the applied stress (τ) and the resulting strain as shown in Figure 2.3.4. In the case of ideal elastic material, the phase shift $\delta = 0$, while for an ideal viscous material $\delta = 90$ ° (McClements, 2005; Meyers, 2009). The subsequent expression for stress and strain in sinusoidal deformation can be written as:

$$\tau = \tau_0 \sin \omega t \quad 2.3.3$$

$$\dot{\gamma} = \gamma_0 \sin(\omega t + \delta) \quad 2.3.4$$

where τ_0 and γ_0 are stress and strain amplitudes respectively. From these expressions, we can define two moduli that characterize the elastic and viscous behaviours of viscoelastic materials.

$$G' = \left(\frac{\gamma_0}{\tau_0}\right) cos\delta \quad 2.3.5$$

$$G'' = \left(\frac{\gamma_0}{\tau_0}\right) sin\delta \quad 2.3.6$$

where G' is the storage modulus which is the measure of stored energy or the elastic part and G'' is the loss modulus which is the measure of lost energy in the form of heat or viscous component. Alternatively there is a complex modulus G* which represents both the G' and G'' by the following equation in which *i* is the complex number and is equal to $\sqrt{-1}$.

$$G^* = G' + iG'' \quad 2.3.7$$

The initially stated definition of rheology signifies the study of the flow behavior of all material which includes the material that falls into the category of classical extremes of Hookean elastic solids and Newtonian viscous liquids. However, many scientists see these classical extremes of Hookean elastic theory and Newtonian fluid mechanics as outside the scope of rheology whose study is majorly in understanding the material between these extremes (Barnes et al., 1989).

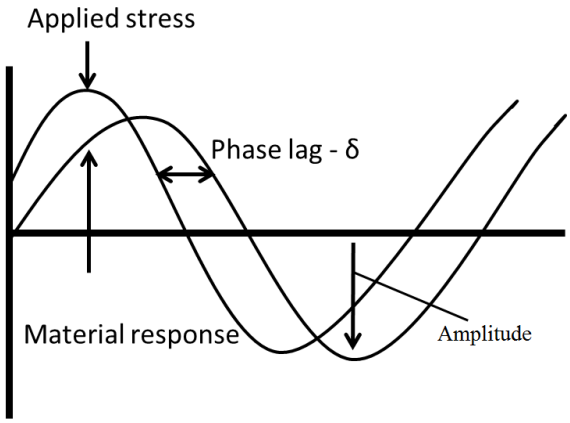

Figure 2.3.4 Viscoelastic response of the material subjected to oscillatory strain with frequency ω

2.3.2 Measurement techniques

Rheological behaviors of a wide range of materials, including dilute and very viscous liquids, solids, plastic and viscoelastic material, can be characterized by a variety of instrumental methods (Schowalter, 1978; Steffe, 1992). The different instruments vary depending on the type of measurement techniques they use, which include shear, compression, elongation or any combination thereof. These methods provide information about the fundamental rheological constants of the material, such as η, G', G'' (Steffe, 1992; Rao, 2005).

2.3.2.1 Simple compression and elongation

This technique is mostly used for solids or semisolids that are consistent enough to support their own weight such as gels, pastes, etc. In this method, the material to be tested are subjected to compression or elongation by specially designed probes (McClements, 2005). These probes move vertically at a particular speed and deform the material, during which the stress and strain experienced by the material are calculated by instruments based on the probe dimensions, force applied and deformation recorded (Rao, 2007).

2.3.2.2 Shear measurements

In this technique, rheological properties of different material are characterized by shear measurements. The type of shear applied and the test method used is based on the rheological

constants to be determined and the physiochemical characteristics of the sample. There are many instruments designed to test the rheology of materials that range from liquid to solids (McClements, 2005). Some instruments such as Capillary viscometers in which the applied shear rate cannot be controlled are only suitable for analyzing ideal liquids. However, many types of advanced mechanical viscometers and dynamic rheometers are designed that can characterize fluids over a wide range of shear rates and are used to analyze both ideal and nonideal liquids (Morrison, 2001). In such type of dynamic rheometers, shear is applied to material held between different measurement cells (e.g., concentric cylinders, cone and plate, parallel plate measurement cells etc.). These measurement cells are used to apply various types of shear on the material. The following are some measurement techniques which employ various types of shear:

2.3.2.3 *Rotational rheometry*

The principle of this technique is that the deformation of the sample held between two plates is obtained by rotating of one plate relative to the other, hence the name rotational rheometry (Steffe, 1992). This technique can be used to determine both transient and steady shear flow properties of materials; typically shear viscosity, creep or stress relaxation.

2.3.2.4 *Oscillatory rheometry*

The viscoelastic properties of the material can be determined using oscillatory rheometry. The principle of the technique is that the material to be tested is held between the two plates of the rheometer and is subjected to a sinusoidal torque by oscillating one plate relative to the other (Findley, 1989), Creep and Relaxation of Nonlinear Viscoelastic Materials, Dover Publications). The response of the sample to sinusoidal displacement is used to record viscoelastic moduli (G', G", G*) and phase angle (δ).

There are other sophisticated measurement techniques such as melt flow rate, capillary and slit dye extrusion rheometry, extrudate swell and draw-down rheometry techniques that are used to measure rheological characteristics in line with the material processing (Morrison, 2001).

2.3.3 Rheology of emulsions

Food emulsions exhibit a broad range of different rheological properties, ranging from low viscosity liquids (e.g., milk, pourable salad dressings) to viscoelastic solids (shortening, margarine, butter and other solid-like soft materials) (McClements, 2005; Rao, 2007). Many foods constitute of emulsions, either partly or wholly. Hence, the knowledge of rheology of food emulsions can be used to design novel foods with different textural properties. Sensory properties of food emulsions are also associated with their rheological properties such as spreadability, consistency, etc. (Mewis, 2012). Rheological properties of emulsions provide information that helps to understand structural organization and interactions within emulsions. For example, viscosity versus shear rate data can provide an insight into the type and strength of interactions between the dispersed droplets in emulsions (Tadros, 1994; Berli et al., 2002). Shelf life of food emulsions also depend on its rheology (McClements, 2005). For example, continuous phase viscosity can influence the creaming or sedimentation of dispersed droplets leading to destabilization. Due to the above reasons studying the rheology of emulsions is crucial (Dickinson, 1982; Doublier, 1992).

Rheological properties of emulsions depend on many factors such as packing or volume fraction of the dispersed phase droplets, properties of the continuous phase, and the type, size and strength of interactions between the dispersed droplets (Mason et al., 1997; McClements, 2005; Datta et al., 2011; Mewis, 2012). Among all, dispersed phase volume fraction (ϕ) is an important factor influencing the rheological properties of emulsions. Emulsions' rheological behaviour can transform from liquids to viscoelastic solids depending on the ϕ (Figure 2.3.5).

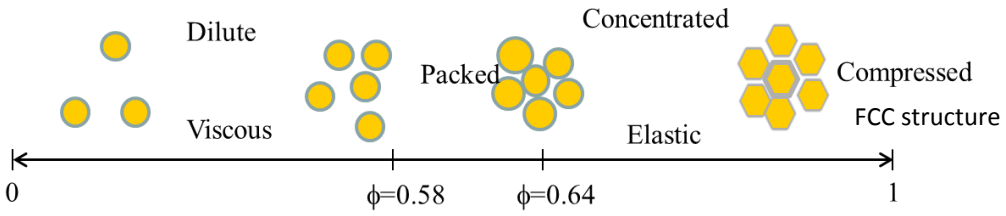

Figure 2.3.5 Rheological behavior of emulsions containing various amount of soft oil droplets (ϕ). (modified image adapted from Mason 1999).

In dilute emulsions (ϕ < 0.05) the droplets do not interact with each other as they are sufficiently far apart. Such emulsions exhibit relatively low viscosity which is dominated by the influence of the continuous phase. As the system becomes more concentrated, (0.05< ϕ < 0.49), interactions between the droplets through droplet collisions, hydrodynamic interactions become appreciably higher hindering their movement within the continuous phase resulting in an increase in emulsion viscosity (Sun et al., 2009a; Ochowiak et al., 2012). Sun et al. (2009b) observed that viscosity of whey protein isolate-stabilized oil-in-water emulsions at 1 s^{-1} shear rate increased from 0.4 to 1.2 Pa.s ϕ increased from 0.05 to 0.4 (Sun et al., 2009b).

In further concentrated systems (0.49 < ϕ < 0.58) viscoelastic behavior begins as a result of closer packing of droplets. For 0.58 < ϕ < 0.64, the movement of droplets become severely restricted as each droplet is caged between the neighbors and separated by a thin layer of continuous phase between them (Mason et al., 1995). These systems are known as colloidal glasses where the droplets can only vibrate but cannot move past each other smoothly. When ϕ is close to 0.64 dramatic increase in viscosity and viscoelastic behavior of emulsions has been observed by many researchers (Weiss et al., 2000; McClements, 2005; Scheffold et al., 2013; Mason et al., 2014). For monodispersed emulsions at ϕ = 0.64 droplets surface touch with each other and when ϕ is higher than 0.64 droplets become compressed and deformed. This deformation lead to an increase in interfacial area, which results in energy stored in the droplets that manifest as elasticity (G' > G'') (Mason et al., 1995; Masalova et al., 2007). Many simulation and experimental works done by different researcher groups have found jamming transition of monodispersed droplets at ϕ = 0.64. This point was referred as random close packing (RCP) which was later termed as maximal random jamming (MRJ) (Truskett et al., 2000; Wilking et al., 2007). At very high ϕ, the emulsions behave as crystalline systems in which the droplets are more densely packed and droplets' surface become so deformed that they exist as hexagonal droplets (Figure 2.3.5) (Meleson et al., 2004). These emulsions are also called as high internal phase emulsions (HIPE). At or above MRJ the G' and G'' become independent of strain at low strain rates resulting in the linear viscoelastic region (LVR) (Datta et al., 2011; Knowlton et al., 2014). Figure 2.3.6 represents a typical viscoelastic behavior as a function of strain rate for oil-in-water emulsions with ϕ = 0.8 as observed by Knowlton et al. (2014). As the applied strain increased, G'' grew due to rearrangements between the droplets while G' is still

higher than G″. Within this region, the emulsions retained an overall solid-like behavior, and both the moduli were independent or weakly dependent on strain (Meleson et al., 2004; McClements, 2005; Knowlton et al., 2014). Beyond this, an increase in strain resulted in a significant drop of G′ while G″ kept increasing. At a higher strain called fluidization strain, both the moduli decreased with strain, with G″ dominating over G′ indicating loss of elasticity and dominating viscous behavior. In concentrated systems discussed above the transition from viscoelastic solid to fluid behavior under strain is smooth and extends at least one decade in strain amplitude (Knowlton et al., 2014). The strain at which the crossover of G′ and G″ occurs is called crossover the strain or yield strain, and it is the point where the system begins to flow. Some researchers consider the yield strain as the strain at which the moduli deviate from the LVR. Knowlton et al. (2014) noticed that strain dependence of shear stress measured deviates from the initial power-law behaviour at this point (Figure 2.3.6).

Another major factor that influences the rheological properties of emulsions is the interactions (repulsive or attractive) between the dispersed droplets (Berli et al., 2003; McClements, 2005; Graves et al., 2008; Datta et al., 2011). Electrostatic interactions are often the result of surface charge caused by adsorption of charged emulsifiers on the droplets surface. These electrostatic interactions play a significant role in preventing droplets from aggregation. Due to this charge, a counterion cloud is formed around the droplets resulting in an increase of ϕ, known as effective volume fraction (ϕ_{eff}) (See section 2.2 on nanoemulsions). As a consequence, rheological properties of such repulsive emulsions with a high value of ϕ_{eff} would be similar to that of HIPE (Graves et al., 2008). In some emulsions, long-range attractive interaction such as depletion force leads to extensive droplet aggregation and formation tenuous network which entraps continuous phase and forms colloidal gel (Datta et al., 2011). These emulsions exhibit yield stress, which is the minimum amount of stress needed to make them flow (Berli et al., 2003). They also exhibit elastic properties similar to that of HIPE even at very low ϕ ($\phi << \phi_{\text{MRJ}}$) (Datta et al., 2011). The flow and viscoelastic properties of these emulsions are characterized by the interdroplet network structure. Any external stress beyond yield stress would break the attractive bonds between droplets which in turn break the network. This results in smaller clusters of droplets which can flow past each other easily (Sherman, 1968). Koumakis et al. (2011) Proposed a two-step yielding of colloidal gels according to which the inter-cluster bonds

break yielding to smaller clusters in the initial step followed by the breakdown of clusters into individual particles. Similar observation based on the rheological experiments on attractive gels have been made by Datta et al. (2011). The magnitude of yield stress or gel strength of these attractive emulsions essentially depend on the strength of attractive forces between the emulsion droplets, the stronger the attractive interaction the greater the gel strength (Pal, 1996b; Dickinson, 2013b). However, other factors like number, volume fraction and structural organization of droplets, number of attractive bonds per droplet also influence emulsion rheological properties (Bremer et al., 1993; Pal, 1996b; Narine et al., 1999).

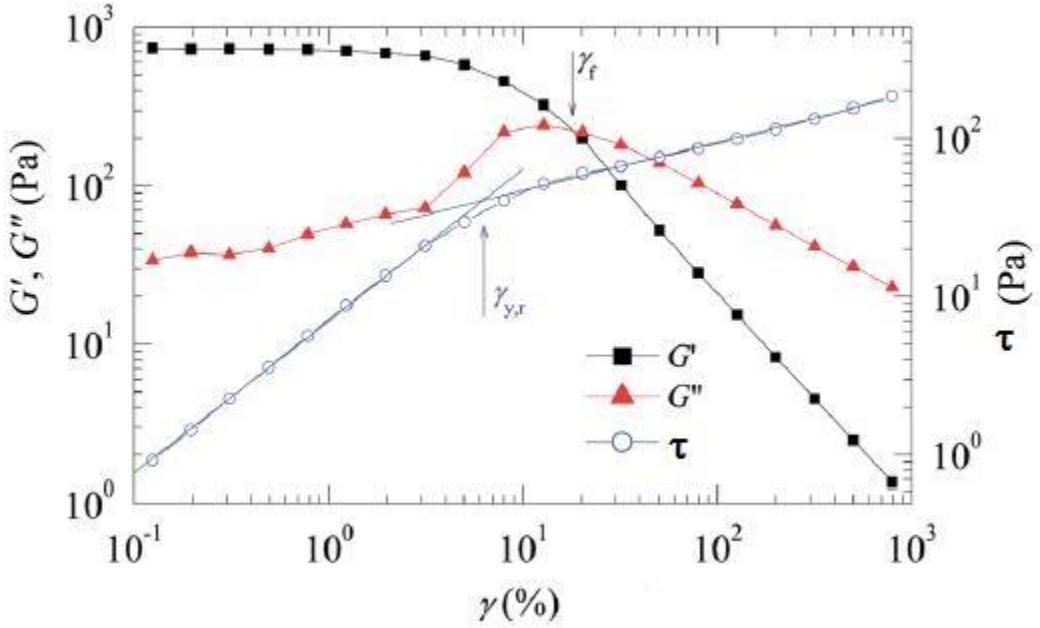

Figure 2.3.6 Typical behavior of viscoelastic moduli of O/W emulsion (ϕ = 0.83) as a function of % strain as observed by Knowlton et al. (2014). Left axis represent the elastic and loss moduli (■, ▲) as a function of % strain amplitude given in the x-axis. γ_f represents the fluidization strain at which the cross-over of G′ and G″ occur. Axis on the right represents the shear stress (τ) vs. % strain amplitude. $\gamma_{y,r}$ represent the rheological yield strain, which is the intersection of two lines describing the behavior of shear stress at small and large strain. Figure obtained from Knowlton et al., 2014.

Droplet size is another major factor that influences emulsion rheological properties (Pal, 1996a; McClements, 2005). As mentioned above in the case of emulsions with ϕ > 0.64, elasticity results from the energy stored by deformation of droplets. The deformation is dependent on the Laplace pressure of droplets which is equal to γ/r, where γ is the interfacial tension and r is the radius of the droplets before deformation. Thus elasticity is inversely related to the droplet size of emulsions. Princen et al. (1986) have derived expressions for yield stress (τ_0) and G′ of HIPE:

$$\tau_0 = 1.05 \frac{\gamma \cos\theta}{r} \phi^{1/2} F \qquad 2.3.8$$

$$G' = 0.525 \frac{\gamma \cos\theta}{r} \phi^{1/2} \qquad 2.3.9$$

where θ is the contact angle between the droplets and the thin film of continuous phase between them and F is a dimensionless parameter (Pal 2005). According to these equations elastic strength and yield stress of HIPE increases with decrease in droplet size. In electrostatically stabilized emulsions, decrease in droplet size also results in an increase of ϕ_{eff} (see section 2.2 on nanoemulsions), further enhancing the rheological properties (yield stress and G') of emulsions (Fryd et al., 2012).

In addition to above factors, properties of continuous phase also have an influence on the emulsion rheology. Particularly in many food emulsions (e.g., salad dressing, coffee creamer), where the droplet concentrations are well below the $\phi_{MRJ,}$ continuous phase characteristics most effectively influence emulsion rheology (McClements, 2005). This is one of the reason for which many additives such as thickening agents, gelling agents, polysaccharides and proteins are often added to the aqueous phase of emulsions to modify their rheological properties (Pal et al., 1992; Pettitt et al., 1995). Apart from the above-mentioned factors, crystalline properties and structure of the dispersed and continuous phase also affect emulsion rheology (e.g., ice cream, whipped cream, butter and margarine) (Doublier, 1992; Fischer et al., 2011).

2.4 Gelation

Gelation is the process of formation of gel from sol. The word “gel” was coined in 19th Century by the Scottish Chemist Thomas Graham, known as the father of colloidal chemistry

(Oakenfull, 1997). According to the International Union of Pure and Applied Chemistry (IUPAC), the gel is defined as a "Non-fluid colloidal or polymer network that is expanded throughout its whole volume by a fluid". However, there is no explicit definition that includes all the different characteristics of gels. For example in some colloidal gels, the colloidal network is comprised of fluid rather than non-fluids as stated in the above definition. Also in some aerogels (e.g., silica aerogels) there is no continuous phase fluid between the silica particle network; instead, air fills the void between (Hrubesh, 1998). According to a widely cited definition given by Dorothy Jordan Lloyd, "gel", is one which is easier to recognize than to define" (Djabourov et al., 2013). Nevertheless, a gel can be recognized as an intermediate state between liquid and solid, i.e., they are liquid rich system, yet possess solid like property with no flow under gravity.

One of the most important characteristic properties of the gel is its mechanical or rheological property. As gels are intermediate state between viscous liquid and elastic solid, their rheological characteristics vary between Newtonian viscosity and Hookean elastic properties (Katsuyoshi, 2009). In other words, they display viscoelastic behaviour manifested by the network structure that prevents the fluid from flowing. Upon breaking the structure by external stress, the fluid flows resulting in the viscous behavior (Tanaka, 1981).

2.4.1 Types of gels

There are different classifications of gels depending on their characteristics. Often the network structure is the prime basis for differentiating the types of gels (Katsuyoshi, 2009). One of the most common classifications of gels is based on the types of bonds between the network structure that holds the gel (Katsuyoshi, 2009); (1) Chemically crosslinked gels in which the network structure is formed by the chemical bonds between the polymers. One such example would be a hydrogel in which a network of β-lactoglobulin monomers is formed by the di-sulphide covalent bonds between the cysteine amino acids on them (Jost, 1993). (2) Physical gels in which the network is formed by the secondary molecular forces such as hydrogen bonds, electrostatic and hydrophobic interactions between the polymers or colloids. These type of gels are more common in foods, for example, gelatin desserts and jellies that are viscoelastic due to the network formed by hydrogen bonds between partially regained triple helical structure of gelatin molecules (Banerjee et al., 2012). Another such example in case of colloids would be

chocolate milk in which k-carrageenan forms an intermolecular network with dispersed casein micelles due to their electrostatic interactions, thus forming thin pourable weak gel whose structure prevents settling of cocoa particles (Arltoft et al., 2007). Usually, the secondary molecular interactions are weak. Hence, the bonds in physical gels are reversible and can be altered when thermodynamic properties like pH, ionic strength or temperature are varied (Masuelli, 2012). In contrast, bonds in chemical gels are covalent and hence they are strong and not reversible.

Gels can also be classified based on their reversible nature with varying temperature, (Banerjee et al., 2012). (1) Thermo-reversible gels, in which gels turn to solution upon heating and again gel when cooled. For example, in κ-carrageenan and I-carrageenan gels, the network of carrageenan helices aided by cation electrostatic bridging between them can undergo transformational changes to coils upon heating. This results in the loss of gelation and form a solution, which is capable of reforming a gel when cooled (Mangione et al., 2003). A similar type of the heat reversible gelation can also be observed in the case of gelatin and agar gels. (2) Thermo-irreversible gels in which the gelation process is not reversible. For example, in alginate gels, heating has no effect on alginate network in which calcium ions form junction zones between them by associating with its guluronic acid making them thermo-irreversible (Florian et al., 2005).

Two different types of gels can also be observed based on the temperatures at which the transition from sol to gel occurs (Banerjee et al., 2012). (1) Cold-setting gels in which the gelation or the formation of a rigid network occurs when the temperature of the solutions are decreased. For example, at high temperature agarose molecules exist as a random coil. When cooled to 39˚ C, L-galactose components on agarose form a double helix structured junctions between the chains leading to gelation (Florian et al., 2005). However, the helix junction zones denature when heated, making it a cold-set gel as well as a thermo-reversible gel. (2) Heat-setting gels in which gelation occurs on heating. During heating of egg white, the structure of the Ovalbumin protein in it undergo conformational changes and denaturation, which facilitate the intermolecular disulphide bonds and hydrophobic interactions between them leading to a network structure and subsequent gelation. Due to the disulphide bonds, the resultant gel is a thermo-irreversible heat-setting gel (Alleoni, 2006).

Based on the constituents of the network structure that forms the gels, they can also be classified as polymer or particulate gels (Nishinari, 2009). (1) In polymer gels, the network constitutes of polymer molecules dispersed in the continuous phase. Polymers can be both natural and synthetic. Examples include the biopolymer gels such as ovalbumin, agarose, alginate gels, etc. (2) Particulate or colloidal gels in which the network is comprised of colloidal particles dispersed in a continuous phase. One such example would be curd formed during cheese manufacture by the addition of rennet, in which colloidal casein network forms gel (Djabourov et al., 2013).

On the basis of the type of solvent present that serves as swelling agent, gels can be classified as follows (Katsuyoshi, 2009); (1) Hydrogels in which water is entrapped between networks of polymer or colloidal particles that are water-insoluble. Common household examples of hydrogels are food jellies and jams which have pectin network and gravies that have a starch network (Banerjee et al., 2012). (2) Organogels that constitute liquid organic phase as a solvent which is usually entrapped in a thermo-reversible network structure. The network structure in organogels is usually facilitated by non-covalent interactions, and the compounds are called organogelators (Co et al., 2012). The organic liquids in organogels can be organic solvent, mineral oil, vegetable oil, etc. There are not many commercial food grade organogels available except for the vegetable oil (corn, soy etc) organogel in which β-sistosterol and γ-oryzanol molecules self-assemble to form a tubular microstructured network leading to a strong gelation (Co et al., 2012). (3) Xerogels in which the solvent is removed or dried resulting in unhindered shrinkage of the network. Horst et al. (2012) have developed solutions with SiO_2 particle network dispersed in alcohol solution containing food additives. They were able to prepare a food grade xerogel from these solutions by removing the alcohol solution by spray drying, which leaves only the food additives embedded in the silica network (Horst et al., 2012). These xerogels are believed to have better stability and can be employed for control release of food bioactive compounds. When drying of the solvent between the network occurs under supercritical conditions, the network will not shrink leaving it with high porosity, and they are referred to as aerogels. Aerogels with a network structure formed by polysaccharides such as hemicellulose, starch, alginates etc. in which the solvent is removed by supercritical drying using CO_2 were developed by a few researchers (Garcia-Gonzalez et al., 2011; Mikkonen et al., 2013).

These aerogels are believed to have potential applications in packaging and controlled release applications. However, they are not yet used in commercial food applications.

2.4.2 Gelation mechanisms

The mechanism of gelation essentially refers to the process of the network formation as it is the cardinal component of the gel. Initially, the polymers and colloids are dispersed in a solvent and upon initiation of the linkage between them clusters are formed. These clusters grow by condensation of polymers or aggregation of particles. Physical or chemical links between these clusters lead to the formation of a single giant cluster that reach across the vessel that contains it and holds the sol between it (Katsuyoshi, 2009). In theory, this condition of the solution is called a gel. This process is referred as sol-gel transition and the critical point at which the gel first appears is called gel point. With time, other smaller clusters will aggregate to the infinite cluster, leading to an increase in gel strength. Dramatic changes in the flow, mechanical and viscoelastic properties are brought about by the sol-gel transition and hence it has been a topic of interest of many research works. There have been many theories proposed to understand the sol-gel transition. Paul Flory proposed the first classical theory of sol-gel transition (i.e. Flory-Stockmayer ('classical') theory) in 1930, which was extended by Stockmayer in 1943. This theory explains the idea that the polymerization leads to branching that takes place repeatedly which eventually forms the infinite network structure (Flory, 1941). There have been many complex models since then that explain the viscoelastic behavior associated with the sol-gel transition. Winter and Chambon (1986) proposed one such model, based on the percolation theory. This model describes the behavior of storage modulus G′ and loss modulus G″ of a system around the transition point, in small amplitude oscillatory rheological measurements (Winter et al., 1986). According to the theory, at a constant frequency ω, G″ of a sol is large while its G′ is small and negligible. With the increase in network structure, G″ increases while G′ rises sharply until it intersects and then exceeds the G″. G′ continues to increase with the increase in network structure, whereas G″ shows a slight maximum. Ultimately both the moduli reach a plateau as the development of the network is completed. This gives the most accepted criterion for gelation i.e. $G' > G''$, which holds good for most gels (Djabourov et al., 2013).

The gelation mechanism depends on several factors that influence the interactions between the network forming polymer molecules or colloidal particles. Examples of such factors include the concentration of polymers or colloidal particles, temperature, pH and ionic strength of the solvent, etc. There should be a critical concentration of polymers or colloids to form a network (Katsuyoshi, 2009). At high concentration, they result in the stronger network forming an elastic gel in which the G′ is far larger than G″, and both moduli are independent of frequency and strain until a critical point. Such type of gels in case of emulsion can be observed at a high dispersed phase concentration (Zha et al., 1991). Datta et al. have observed a significant increase in G′ with an increase in the oil volume fraction from 0.62 to 0.73 for oil-in-formamide emulsion gels (Datta et al., 2011). A similar increase in viscoelastic properties as a function of dispersed phase volume fraction has also been observed by other researchers (Koumakis et al., 2011). Lower concentrations result in weak gelation in which G′ is slightly larger than G″, and both of them show dependency on frequency and applied strain (Mason et al., 1997)

Gelation also depends on the temperature that helps to form crosslinks between the polymers. Examples of gels in which temperature influences the gelation are cold set gels and heat set gels, in which the network structure forms when subject to cooling or heating. It was widely known that some of the globular proteins like β-lactoglobulin and WPI need to be heated in order to unfold their structure. This facilitates the physical or chemical links between the functional components of protein structure that lead to network formation. Along with temperature, other factors such as pH and ionic strength (addition of salt) also influence the gelation mechanism. However, depending on the types of polymer or colloids, the mechanism of influence would be different. In the case of gelation in β-lactoglobulin thiol groups inside their globular structure are exposed due to conformational changes on heating. When pH is acidic protonated thiol groups are not capable of forming sulphide bonds with other β-lactoglobulin monomers, hence gelation would be possible. But when pH is basic (ideally above 8), thiol groups are capable of forming disulphide bonds with other monomers, leading to a network formation (Hoffmann et al., 1997).

Besides temperature and pH, enzymes can also induce gelation. Enzymes like Transglutaminase are capable of inducing covalent bonds between protein molecules leading to gelation (Otte et al., 1996). Besides the above factors, gelation can also be influenced by the type

and nature of the solvent and the presence of ingredients that competes with proteins for hydrogen bonding with water. Oakenfull et al. (1984) have observed that sugars and polyols in solutions gelled by high methoxyl pectin will stabilize the hydrophobic bonds between pectin and giving the gels better strength and stability at higher temperatures. Finally it can be said that the mechanism of gelation essentially depends on the process of cross-linking or network formation by dispersed proteins or colloidal particles, and any factor that can influence it will have significant effect on the process of gelation.

2.4.3 Applications of gels

Gels are widely used in our day-to-day lives, from toothpaste used in the morning to foam mattress used for a comfortable sleep in the night. They are widely used in pharmaceutical, biomedical, cosmetic and food applications. In pharmaceuticals, many formulation includes gels for sustained drug release (Garcia-Gonzalez et al., 2011; Djabourov et al., 2013). Gels containing human cells are being used as scaffolds for tissue engineering (Katsuyoshi, 2009). The contact lenses which we use are silicone gels. They are also essential components of many cosmetics. Gels and gelling agents are used for obtaining desired textural and sensory properties of food products like jams, custards, yogurts, ice-creams, creams, confectionery etc. (Banerjee et al., 2012). Besides that they are also used for a number of other functions like stabilizing foams and emulsions, controlling syneresis and water retention (Florian et al., 2005). In order to form gels in foods, gelling agents are added. Most of the gelling agents used in foods are food hydrocolloids that constitute polysaccharides and biopolymers like pectins, gums, starches, proteins, etc. (Richardson et al., 1998). For example, pectins are widely used gelling agents in jams and jellies, locust bean gum and guar gum are added in dairy products like ice-cream, yogurt to form gels with milk solids (Hui, 2006) and carrageenan is added to chocolate milk to form a weak gel network that prevent cocoa solids from settling down (Banerjee et al., 2012).

2.5 Gelation in emulsions and nanoemulsions

Depending on the dispersed phase volume fraction, droplet size, interdroplet interactions and continuous phase composition emulsions and nanoemulsions could have wide range of

rheological properties that can vary from liquids to highly viscoelastic gels (McClements, 2005; Wilking et al., 2007; Scheffold et al., 2014). Engineering their rheological properties can make them attractive for many applications. For example, liquid nanoemulsions are used to deliver aroma, bioactives and other functional components in beverages (McClements et al., 2011; Silva et al., 2012; Maali et al., 2013). On the other hand, many pharmaceutical and cosmetic creams, gels and thick paste-like food products such as mayonnaise are also made of emulsions (Graves et al., 2008; Kawada et al., 2010). This chapter focuses on formation and mechanisms of gelation in emulsions and nanoemulsions and their applications in food and related soft materials.

2.5.1 Gelation influenced by microstructure

Structurally emulsion gels can be of two types: (1) dispersed particles filled biopolymer gels, and (2) particulate gels (Sala, 2007; Dickinson, 2013a) In the former droplets are randomly dispersed in a biopolymer matrix that imparts gelation (Batchelor et al., 1972; Dickinson, 2013a). Here gelation is caused by the network of biopolymer or hydrocolloid molecules in the continuous phase and the presence of droplets in the gelled matrix either strengthen (active filler) or weaken (inactive filler) the gel depending on their interfacial properties (Dickinson et al., 1999). It was observed that WPI stabilized oil droplets served as active fillers in gelatin gels as the WPI and gelatin interaction increased the gel strength of gels (Sala et al., 2007). Inactive filler gels can be observed in case of small-molecule emulsifier stabilized emulsions filled with a network of biopolymers in which the droplets may or may not react with the network. Sala et al. have found that Tween 20 stabilized dispersed oil droplets served as inactive fillers in gelatin gels and weakened the gel strength (Sala et al., 2007). Figure 2.5.1A and 2.5.1B shows the representative schematic diagrams of active and inactive emulsion filled gels.

In particulate gels, dispersed particles/droplets form three-dimensional network leading to emulsion gelation. Figure 2.5.1C shows the schematic diagram of a particulate emulsion gel. The network is usually formed by secondary intermolecular forces (e.g., hydrogen bonds, electrostatic and hydrophobic interactions) driven aggregation of dispersed droplets. However in case of some emulsions stabilized by proteins, covalent bonds also drive the droplets aggregation (Dickinson, 2013a). For example, in case of biopolymer stabilized oil droplets dispersed in aqueous phase, interaction among the interfacial biopolymers induced by enzymes, changes in

environmental conditions (temperature, pH, ionic strength etc.) results in the formation of aggregated oil droplets leading to gelation (Chen et al., 2001). It has been showed by many researchers that gelation of β-lactoglobulin or casein stabilized n-tetradecane-in-water emulsion can occur by the addition of an enzyme transglutaminase, which induces covalent crosslinking of proteins at the interface (Færgemand et al., 1997; Yamamoto et al., 1997; Dickinson, 2012). This result in the network formation by droplet aggregation leading to the enhancement of emulsion viscoelastic properties compared to the crosslinked protein solutions. In many practical applications, depending on the concentration and types of biopolymers, the structure of many emulsion gels lies between the particle filled gel and particulate gel (Dickinson, 2012). For example in case of WPI stabilized oil droplets dispersed in aqueous phase containing gelatin, WPI and gelatin can interact and the oil droplets also become a part of network (active filler) enhancing the viscoelastic properties of emulsion gels (Sala et al., 2007) (Figure 2.5.1A).

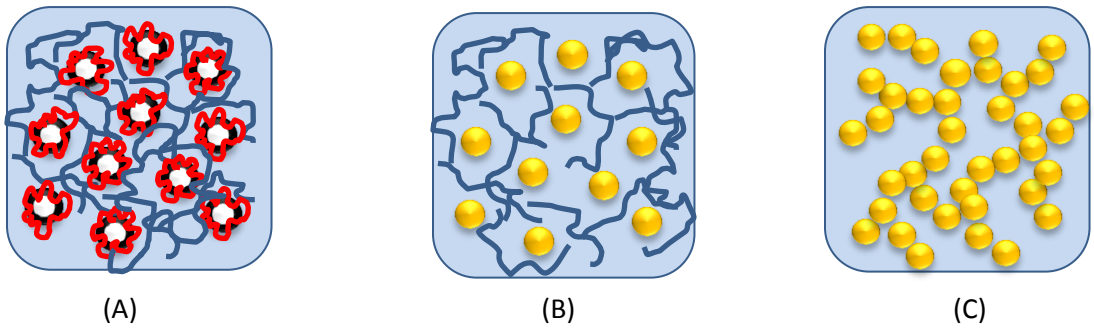

Figure 2.5.1 Schematic diagrams of (A) active particle filled gel in which the network structure is caused by crosslinking the biopolymers/hydrocolloids in the continuous phase, and biopolymer/hydrocolloid stabilized droplets served as active fillers. (B) inactive particle filled gel in which the network structure is caused by crosslinking the biopolymers/hydrocolloids in the continuous phase, and droplets served as inactive fillers. (C) Particulate gels in which network structure is caused by aggregation of dispersed droplets in continuous phase

Particulate gels can be classified into two types based on inter-droplet interactions that lead to their gelation (Fryd et al., 2012). As discussed before, if the droplet network is caused by attractive forces between them they are called attractive gels. On the other hand, if the interaction

between the droplets is repulsive, they are called repulsive gels. The Strength of both these gels depends on the nature and extent of inter-droplet interactions and the dispersed phase volume fraction (Datta et al., 2011; Scheffold et al., 2014).

2.5.2 Attractive gelation

In the case of attractive emulsion gelation, aggregation is caused by the attraction between the emulsion droplets. If attractive interactions (van der Waal interactions, depletion forces etc.) can be induced among the repulsive droplets (stabilized by ionic emulsifiers or thick layers of proteins), secondary attractive minima in their interdroplet pair potential can be developed which would lead to droplet aggregation resulting in gelation (Bibette et al., 1993; Fryd et al., 2012). A common approach towards understanding the structure-function relationship of these gels is by measuring their viscoelastic behaviour using a rheometer and explaining their rheological behaviour with possible inter-droplet interactions. Many researchers have also taken simulation approach to understand the structural characteristics of particle gels to estimate their viscoelastic properties and compare them to the experimental values (Bijsterbosch et al., 1995; Liu et al., 2004; Whitmer et al., 2011). Dickinson (2000) used Brownian Dynamics Simulation technique to understand particle gels and proposed two models for emulsion gelation: (i) Bonding model and (ii) Non-bonding model (Dickinson, 2000; Dickinson, 2013b). In bonding model of aggregation, particles are held together by permanent and flexible crosslinks such as in the previously discussed case of WPI stabilized oil droplets in gelatin filled aqueous phase (Dickinson, 2012). The non-bonding model is characterized by reversible attractive interparticle forces (e.g., depletion interaction) between the particles (Dickinson, 2012). However, it is also possible that the particles in non-bonding model can also interact with other particles by crosslinking. Thus both the models of aggregation can overlap (Dickinson, 2012).

The kinetics of aggregation that leads to attractive gelation can be understood from the viewpoint of the underlying rate limiting processes. The aggregating particles form a complex pattern called fractals which are self-similar at different length scales i.e. they appear the same when viewed over a range of scales (Sorensen, 2001). The mechanisms of aggregation and fractal growth can be explained based on two time scales: (1) diffusion time (τ_D) which is the time needed for the particles or fractal clusters to come close together and aggregate through the process of diffusion through the continuous phase; (2) reaction time (τ_R) which is the time

needed for approaching particles to form bonds (Jullien et al., 1984; Weitz et al., 1985). In this case, the bond formation can be instantaneous upon first contact or can be after many successive attempts (Weitz et al., 1985; Matsushita, 1994). If $\tau_D << \tau_R$, the aggregation process is called diffusion-limited aggregation (DLA) and if $\tau_R << \tau_D$, it is called reaction limited aggregation (RLA). In the process of gelation, rate limited aggregation and growth can be between particles or between clusters (e.g. diffusion-limited cluster aggregation, DLCA). In DLA or DLCA, aggregation results in infinitely strong shear-rigid bonds between the particles and these bonds are not reversible. However, the particles can diffuse around each other to form a more stable fractal cluster. On the contrary, in RLA the aggregated particles can unbind and later rejoin the fractal cluster and hence these bonds are considered reversible (Seager et al., 2007). The attractive interactions required for the above aggregation phenomena and cluster growth can be induced by two methods: depletion interaction or by charge screening due to the addition of ionic salt (Broide et al., 1992; Tuinier et al., 2000; Dickinson, 2013a). Nevertheless, it has been recently proposed that emulsion droplets aggregating under diffusion limited process show a different behavior. Unlike aggregation of solid colloidal particles by DLA where particles form shear-rigid bonds between them, liquid emulsion droplets cannot form shear-rigid bonds. Instead, the droplets form irreversible slippery bonds that lead to formation of dense clusters, in which the droplets can slip around each other to form more favorable structures (Seager et al., 2007; Babu et al., 2008). This type of mechanism is called Slippery-Diffusion Limited Aggregation (SDLA).

2.5.2.1 Depletion attraction

Depletion attraction between colloidal particles or emulsion droplets is observed when they are surrounded by much smaller particles or emulsifier micelles or non-adsorbing polymer molecules (depletants) (Tuinier et al., 2000). A schematic of depletion attraction is given in Figure 2.5.2 where two droplets with radius R and a surrounding depletion zone of thickness σ approach each other. The depletion zones are considered as excluded volumes as the smaller particles or depletants are expelled from these zones due to steric repulsion or similar charge on the droplets (Bibette et al., 1992). When the droplets come closer such that their depletion zone overlap i.e. distance between their centers ‘r’ is less than interspace between droplets ($r < 2R+$

σ), depletants are expelled into the outer continuous phase from the inter-droplet region as shown in Figure 2.5.2. This results in the osmotic pressure difference between the surrounding continuous phase and excluded inter-droplet region. As a result, a force is exerted on the particles to aggregate which is manifested as the attractive interaction between droplets, leading to droplet aggregation (Lekkerkerker et al., 2011).

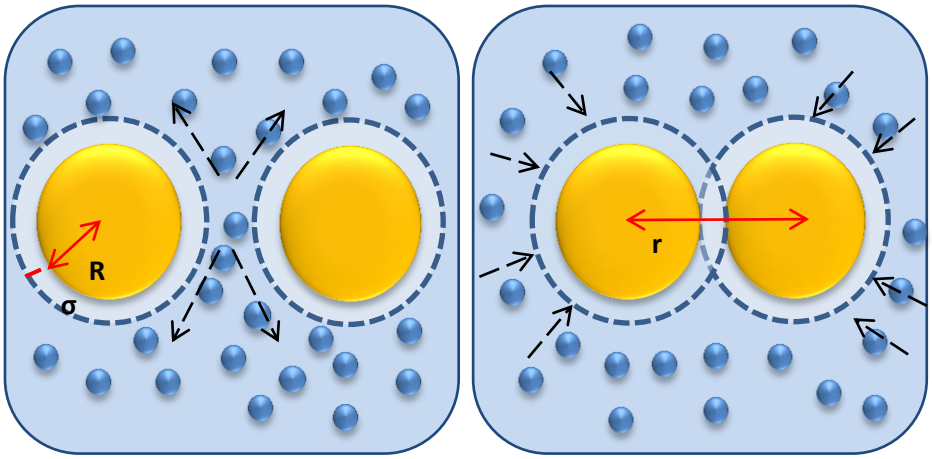

Figure 2.5.2 Schematic representation of aggregation of colloidal particles induced by depletion forces.

The origin of depletion interaction is entropic in nature. Depletants expelled from the inter-droplet region have greater translational freedom due to increased available volume. This leads to a gain in translational entropy of depletants decreasing the free energy of the system, which causes a spontaneous colloidal flocculation (Butt et al., 2005; Sapir et al., 2015).

The first study on the origin of depletion forces and modelling was done by Asakura-Oosawa (Asakura et al., 1954). Since then a lot of researchers have experimentally studied depletion forces (Bibette et al., 1990; Mondain-Monval et al., 1995; Furusawa et al., 2002; Berli et al., 2003). Walz & Sharma (1996) are the first ones to measure the depletion attraction force experimentally. Simulation experiments on depletion forces done by many researchers helped in establishing empirical equations for calculating depletion forces (Sharma et al., 1996). Among them pioneers like Kralchevsky et al. proposed the equation:

$$W_D = -P_0 V_E \qquad 2.5.1$$

where V_E is the volume of the continuous phase confined between the two approaching droplets from which the depleting particles are squeezed out (Petsev et al., 1995) and P_o is the osmotic pressure created by the presence of excess depleting particles in the continuous phase which can be determined by eq 2.5.2 (McClements, 2005):

$$P_0 = \frac{cRT}{M}\left(1 + \frac{2cR_v}{\rho_c}\right) \qquad 2.5.2$$

where c, M, ρ_c are the concentration ($kg.m^{-3}$), molecular weight ($kg.mol^{-1}$), and mass density ($kg.m^{-3}$) of the depletants, respectively. R_v, is the ratio of effective volume to the actual volume of nonadsorbing depletants (McClements, 2000). Rv = 1 for depletants like non-ionic micelles, globular polymers/proteins, but for ionic-micelles with Debye length (due to charge cloud surround the micelles) or polymers that entrain large amounts of solvent Rv > 1 (Dickinson, 2012).

From eq 2.5.2 it can be understood that depletion interaction (i) increases with the concentration 'c' of depletants, (ii) may vary with molecular weight of depletants depending on their volume ratio, R_v (McClements, 2005). In some cases of ionic-micelles or biopolymer induced depletion interactions, the strength is also influenced by the ionic strength of the solvent. For example altering the ionic strength of solvent screens the electrostatic repulsion between the particles or droplets and changes their effective size (Petsev et al., 1995; Mondain-Monval et al., 1996) (more details on the influence of ionic strength on depletion interaction is discussed in section 4.1).

2.5.2.2 Salt induced attraction

Gelation by attractive interactions can also be induced by the addition of ionic salt in the emulsions. In electrostatically stabilized emulsions, droplets repulse each other as they carry he same charge. However, the addition of an appropriate amount of ionic salt screens the charge on the emulsion droplets. According to DLVO theory (section 2.1.5) this charge screening results in the reduction of repulsive barrier between the droplets below the thermal energy of the system. This leads to droplet aggregation in secondary minima of interdroplet pair potential (McClements, 2005; Datta et al., 2011; Fryd et al., 2012). However, salt added in excessive concentration can result in the complete destabilization of emulsions as a result of coalescence (McClements, 2005)(McClements 2005). Salt induced attraction is temperature-dependent, i.e.

raising the temperature above a critical value would increase the thermal energy of the system such that it become greater than the secondary well depth leading to particles re-dispersion and gel breakdown (Derjaguin et al., 1993; Fryd et al., 2012). The addition of salt has also shown to induce gelation in protein-stabilized emulsions (Line et al., 2005; Rosa et al., 2006). Marangoni et al. (2000) and Maltais et al. (2005) have shown that the addition of $CaCl_2$ neutralizes the electrostatic repulsion between whey or soy protein particles and form salt bridges between them leading to gelation.

2.5.2.3 Attractive gelation of nanoemulsions

Attractive interactions induced gelation in nanoemulsions occurs by similar mechanisms as in the case of conventional emulsions discussed above. Attractive gelation in nanoemulsions has been observed by many researchers (Datta et al., 2011; Jorjadze et al., 2011). At the same dispersed volume fraction nanoemulsion gels have shown significantly higher gel strength compared to conventional emulsion gels. This has been attributed to the increase in the number of nanodroplets in nanoemulsions at the same dispersed phase volume fraction leading to large-scale fractal aggregates and stronger cluster network (Lu et al., 2013). Although, the macroscopic properties such as gel strength can be similar for nanogels and conventional emulsion gels, but the mechanism of aggregation of nanodroplets that form the basis of aggregation might differ. Similar to the emulsions, nanoemulsions also show Slippery-Diffusion Limited Cluster Aggregation (SDLCA) (Wilking et al., 2006).

2.5.3 Repulsive gelation

Repulsive gelation in emulsions is characterized by repulsive interactions between the dispersed particles. At low dispersed phase volume fractions (ϕ), these particles are free to diffuse, and the colloidal suspensions are in a fluid state. With increase in volume fraction the droplets become crowded and packed, and for monodispersed systems when ϕ = 0.64 the droplets randomly jam and the emulsion attains yield stress even though they have strong short-range repulsion between them (Liu et al., 2010). This transition from freely flowing to jammed state is termed as jamming transition (Hecke, 2010). The jamming transition has been a topic of interest since dense disordered sphere packaging was first proposed by Bernal and Mason in

1960 (Bernal et al., 1960). Liu et al. (1998) proposed a jamming phase diagram which states that 'For systems with repulsive, finite-range interactions - there is a jamming point that occurs at random close-packing density. It also states that jamming transition can be induced by varying different thermodynamic variables such as temperature or volume and also mechanical variables such as applied stress (Hecke, 2010). The simulation studies on colloidal suspensions have shown that although jamming transition for monodisperse colloidal suspensions occur at ϕ = 0.64, for polydisperse suspensions the transition need ϕ > 0.7, depending on their polydispersity (Schaertl et al., 1994; Clusel et al., 2009; Groot et al., 2011). This shows that the gelation and jamming transitions are often hard to define. The repulsive emulsion gels display elastic properties in rheological experiments (G′ > G″) due to this jamming transition. Thus they satisfy the rheological definition of gels without forming fractal clusters similar to their attractive counterparts.

2.5.3.1 Repulsive nanoemulsion gelation

The repulsive nanoemulsions display unique characteristics of jamming transition and gelation as compared to conventional emulsions. In emulsions stabilized by charged emulsifiers, a layer of charge cloud known as the electrical double layer is formed by the counterions around the droplets. This double layer coupled with droplets behaves as a single entity. The thickness of this layer has negligible influence on the total effective volume fraction of droplets for conventional emulsions. However, when the droplet size is decreased to nanoscale (less than100 nm radius), the thickness of the double layer becomes the similar order magnitude of the nanodroplets, and the overall droplet size and the resulting effective dispersed phase volume fraction (ϕ_{eff}) becomes significantly larger than the actual (ϕ_{core}) (Qian et al., 2011). The resultant ϕ_{eff} and its dependence on droplet size can be given by the following equation (Weiss et al., 2000; Wilking et al., 2007):

$$\phi_{eff} = \phi_{core}\left(1 + \frac{\delta}{r}\right)^3 \qquad 2.5.3$$

where δ is the thickness of electrical double layer and r is the radius of droplets As the droplets size (r) decreases, the thickness of the interfacial layer (δ) surrounding these droplets significantly contribute to the total volume fraction of the droplets (ϕ_{eff}). At sufficient

concentrations of dispersed phase volume fraction, nanodroplets closely pack due to the increased effective volume fraction leading to the jamming transition and development of elastic properties of the resulting nanogels (Wilking et al., 2007; Clusel et al., 2009). The following schematic diagram shows jamming of nanodroplets in O/W nanoemulsions (Figure 2.5.3).

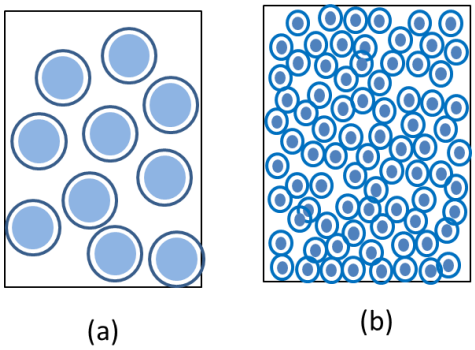

Figure 2.5.3: Schematic representation of the mechanism of repulsive nanogel formation. (a) conventional emulsion with large droplets and insignificant effect of shell layer lead to liquid-like behaviour; (b) random jamming of nanodroplets in repulsive nanogels with similar droplet volume fraction as in the conventional emulsion but with increased effective volume fraction due to the influence of interfacial shell layer thickness.

Using eq 2.5.3 increase in ϕ_{eff} with a reduction in droplet size at three different thickness of shell layer has been illustrated in Figure 2.5.4. When plotted for $\phi = 0.4$, the interfacial shell layer thickness (δ) for microscale emulsions ($r \geq 250$ nm) has a negligible influence on ϕ_{eff} (Figure 2.5.4). However, when r is less than 100 nm, ϕ_{eff} rapidly increases and may even reach close packing ($\phi_{\text{eff}} > 0.7$), where random-jamming of nanodroplets transformed liquid nanoemulsions into particulate gels (the so-called nanogel) at a much lower oil-phase volume fraction. Experimentally, Wilking and Mason showed that an anionic emulsifier-stabilized 20% O/W nanoemulsion can be transformed into an elastic gel when the droplet size falls below 62 nm ($\delta \sim 3$ nm) (Wilking et al., 2007). In these nanoemulsions gels, the shell layer thickness is significantly influenced by the charge cloud (electric double layer) around the droplets. These nanoemulsion gels are referred as repulsive nanogels in the current context of this thesis as they have very strong short-range repulsive electrostatic interactions due to the charge on the droplets.

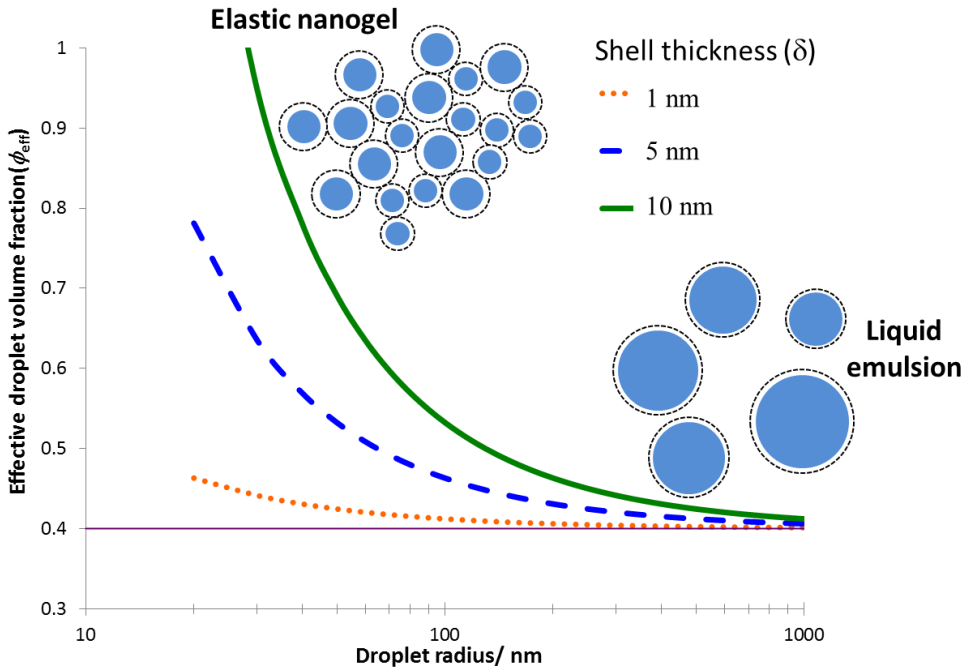

Figure 2.5.4 Schematic representation of increase in ϕ_{eff} with the decrease in droplet size at different thicknesses of shell layer.

The repulsive nanogels can also be prepared by the proteins which may form a thick shell at the interface (Dickinson, 1992, 2012), and increase the ϕ_{eff}. But the constraint of using proteins is that they do not get adsorbed quickly onto the surface of freshly formed droplets during homogenization and hence it is difficult to get extremely small droplets. They also form viscoelastic coating on the interface making it difficult further to reduce the droplet size (McClements et al., 2011). The slow adsorption of proteins onto the interface is due to their large structure, and they have to get rearranged in order to open up their hydrophobic and hydrophilic groups. However, the rate of adsorption varies with the type of proteins, for example, flexible proteins (e.g., caseins) adsorb faster than globular proteins (e.g., β-lactoglobulins). Proteins might also undergo conformational changes during high-pressure homogenization, and this might influence the stability of the nanogels formed (Desrumaux et al., 2002; Floury et al., 2003). Floury et al. (2002) have observed that soy protein stabilized O/W emulsions have shown an increase in viscosity when the homogenization pressure was increased from 250 to 350 Mpa.

They found that high pressure induced structural changes to a protein which facilitated the network formation of interfacial protein and droplet aggregation (Floury et al., 2002).

2.5.4 Applications

Studying the gelation of emulsions and nanoemulsions is very important as a lot of colloidal suspensions in different applications exist in a gelled or jammed disordered state (Hecke, 2010). For example, structure and flow behaviour of toothpaste, shaving foam, cosmetic creams, topical medicine gels depends on the inter-particle interactions and gelation. Emulsion gels used in food applications include yogurt, ice-cream, butter, margarine, salad dressings, cheeses, etc. (Dickinson, 2012). In many of these products structure and functionality can be controlled by modifying the gelation behaviour and interdroplet interactions (McClements, 2005). Gelation in nanoemulsions can be observed at lower dispersed phase volume fractions compared to conventional emulsions due to their increased interdroplet interactions and effective oil phase volume fraction (Mason et al., 2007; Datta et al., 2011). Thus, nanogels can help to reduce the fat content in the emulsion gels while maintaining the structure. Besides, close-packed association of nanodroplets, nanogels are more stable against coalescence compared to conventional emulsion droplets due to their higher Laplace pressure and formation of thick interfacial shell around the droplets (Fryd et al., 2012). Nanodroplets are also known to improve the bioavailability of internal bioactive components which can further enhance nanogel's application (McClements et al., 2007; Huang et al., 2010). However, not much research has been done on the long-term gelation behaviour of the nanogels, and the mechanisms of their interdroplet interactions are not well understood.

3 MATERIALS AND METHODS

3.1 Materials

Canola oil was purchased from a local grocery store and stored at room temperature in the dark. Distilled water (conductivity of 8.2 μS/cm) was used for the aqueous phase. Sodium dodecyl sulfate (SDS) and Tween 20® (polyoxyethylene sorbitan monolaurate) (both with >99% purity) were purchased from Fisher Scientific (Nepean, ON, Canada).

3.2 Preparation of nanoemulsion

O/W nanoemulsions were prepared by pre-mixing the oil phase (40 wt %) with aqueous phase (60 wt %) containing different amounts of emulsifier (either SDS or Tween 20) in a rotor/stator mixer (Polytron, Brinkmann instruments, Mississauga, ON, Canada) for 30 seconds at 20,000 rpm. The coarse emulsions were emulsified in a high-pressure homogenizer (EmulsiFlex-C3, Avestin Inc., Ottawa, ON, Canada) at a pressure of 20,000 psi (137.9 Mpa) for 7 passes. Emulsification was continued either for about 8 passes through the homogenizer or until the nanoemulsion coming out of homogenizer is very viscous that it cannot be further homogenized. Emulsification was performed at room temperature (25.5 °C ± 0.5 °C), although the temperature of the product increased to 60 ºC during the process because high pressure/shear conditions in homogenizer expels a lot of heat. Between the homogenization of different nanoemulsions the homogenizer was cleaned during which it is cooled back to room temperature. After emulsification one part of each nanoemulsion was stored in 40 mL glass vials for visual observation and the rest was stored in 120 mL glass bottles (VWR International, Edmonton, AB, Canada) for further analysis.

In the first study (section 4.1) 40 wt% O/W nanoemulsions were prepared using emulsifier concentrations based on the critical micelle concentration (CMC) of SDS (CMC = 8.3 mM). For nanoemulsions stabilized with SDS, concentrations varied from 0.5 times CMC to 30 times its CMC (4.15 to 249 mM) and the same molar concentrations of Tween 20 (CMC = 0.08 mM) was used in the control nanoemulsions.

In the second study (section 4.2) 40 wt% O/W nanoemulsions were prepared at two concentrations of SDS emulsifier i.e. 2 and 15 times (16.6 mM and 124.5 mM) the CMC of SDS. From the first study (section 4.1) it was seen that gel strength of repulsive and attractive nanogels was highest at SDS concentrations of 2 and 15 times CMC. Hence in the second study, effect of droplet size was studied at these two SDS concentrations. During homogenization nanoemulsions generated after every pass through the homogenizer, each representing a different droplet sizes, were taken for droplet size distribution and rheology measurements (see sections 3.3, 3.4 and 3.5).

Within the third study (section 4.3) nanoemulsions were prepared by passing the premix emulsions with different ϕ through the high-pressure homogenizer. Samples were collected after each pass which resulted in emulsions with different droplet sizes, each having a unique ϕ_{eff} at different ϕ. The influence of oil concentration on nanoemulsion gelation is investigated at six different dispersed oil phase concentrations i.e. ϕ = 0.3, 0.35, 0.4, 0.45, 0.5 and 0.6. Two different concentrations of SDS emulsifier were selected on the basis of 1 CMC and 2 CMC emulsifier concentrations for 40 wt% O/W nanoemulsions described in section 4.1. By keeping emulsifier concentration (mM) to oil volume fraction (ϕ) ratio constant (20.75 for 1 CMC and 41.5 for 2 CMC at 0.4 ϕ, respectively) the emulsifier concentration for each ϕ was calculated according to the following Table 3.2.1. Emulsions with emulsifier concentration to ϕ ratios of 20.75 and 41.5 are named as Low Emulsifier Ratio (LER) and High Emulsifier Ratio (HER) respectively, for convenience. Overall, emulsifier concentration varied from 6.2 mM (0.75 times CMC) to 24.9 mM (3 times CMC) for all emulsions.

In the fourth study (section 4.4), repulsive and attractive nanogels, prepared as a part of study 1 (section 4.1), were analyzed for their long term storage stability. The experimental protocol in this study was divided into three parts. In the first part droplet size distribution of the nanogels after 1, 15, 30, 60 and 90 days of storage time was measured using static laser diffraction technique as employed in previous studies. Change in the droplet size with time gave an estimate of nanoemulsion stability. In the second part of this study, the creaming velocities of the nanogels were measured at different centrifugal forces during accelerated shelf life study using a photocentrifuge (LUMiSizer) (section 3.7). By using this data, the creaming velocity of the nanodroplets as a function of time was estimated at normal storage condition in earth's

gravity. In the final part of this study, the gel strength of the nanogels was investigated by measuring the viscoelastic properties (section 3.3 and 3.4) after 1, 15, 30, 60 and 90 days of storage time using rheology experiments.

Table 3.2.1. Emulsifier concentrations for LER and HER nanoemulsions calculated on the basis of 40 wt% nanoemulsions with 1 CMC (8.3 mM) and 2 CMC (16.6 mM). The emulsifier concentration (mM) to oil volume fraction (ϕ) ratio was kept constant among LER and HER emulsions.

Emulsifier conc./oil volume fraction ratio	Actual oil volume fraction (ϕ)	Emulsifier concentration (mM)
20.75 (Low emulsifier ration (LER) emulsions)	0.30	6.2
	0.35	7.3
	0.40	8.3 (1 CMC)
	0.45	9.3
	0.50	10.4
	0.60	12.5
41.5 (High emulsifier ratio (HER) emulsions)	0.30	12.5
	0.35	14.5
	0.40	16.6 (2 CMC)
	0.45	18.7
	0.50	20.8
	0.60	24.9

3.3 Droplet size distribution

Average droplet sizes of the nanoemulsions were measured by the laser diffraction particle size analyzer (Mastersizer 2000, Malvern Instruments, Montreal, QC, Canada). The relative

refractive index of the dispersed vs. continuous phases used was 1.465. Nanoemulsion droplet size was characterized by surface area mean diameter (d_{32}).

3.4 Apparent viscosity

All rheology experiments were performed using an AR G2 rheometer (TA Instrument, Montréal, QC, Canada) at room temperature. The apparent viscosities of the nanoemulsions and nanogels are measured by the rotational experiments with an applied shear rate continuously ramped from 0.01 to 1000 s^{-1}. Nanogels were gently transferred onto the lower stationary plate of the rheometer by pipettes or a spatula so that the gel structure was not disturbed. A 40 mm diameter cross-hatched geometry plate was used to apply shear on the samples to avoid any wall slip effect. The geometry was slowly brought down on the sample and the gap between the geometry and lower plate (geometry gap) within which the sample is sheared was adjusted to 1000 μm. The sample was equilibrated for 30 s before applying the shear, and any measurements were taken.

3.5 Viscoelasticity

Viscoelastic behavior of the nanoemulsions and nanogels were determined by oscillatory measurements using the same rheometer and geometry settings as in viscosity measurements. Two different types of oscillatory measurements were performed. The strain sweep measurements were performed at 0.01 to 100 % strain and at a constant frequency of 1 Hz (6.28 rad/s). Based on these experiments a linear viscoelastic region (LVR) was identified where the storage and loss moduli were not influenced by the applied strain. From this region, constant strain amplitude of 0.1 % strain was selected for subsequent series of measurements at which the viscoelastic properties of the samples were determined as a function of frequency (ranging from 0.01 to 100 rad/s). For all experiments, storage (G′) and loss (G″) moduli of the nanoemulsions and nanogels were recorded for further data analysis.

3.6 Visual observation of flow behavior

A simple visual observation experiment was carried out to understand the flow behavior of the nanoemulsions. 2-3 hours after preparation, the vials containing nanoemulsions were tilted at

an angle to observe if they flow. They were kept tilted, and the observation was carried out for 30 s after which pictures were taken.

3.7 Accelerated shelf-life study

The accelerated shelf-life study of all nanogels were done using the LUMiSizer (LUM Americas, Boulder, CO, USA). The instrument calculates the creaming rate of O/W emulsion droplets under centrifugal force by measuring Near Infra Red-light transmission as a function of the length of emulsion in the transparent cuvette (Figure 3.7.1). The bigger droplets would cream faster followed by the smaller droplets and as the droplets cream, the bottom of the cuvette would transmit more lasers as it gets devoid of oil droplets with time. After some time all oil droplets would move towards the top of the test tube and form the cream layer such that laser transmission would be almost zero at the cream layer and very high after the end of the cream layer. The sample transmission profiles as a function of the length of test tube after subjecting the sample to centrifugation as a function of time is also shown in Figure 3.7.1 The position of cream layer as a function of time can be calculated and plotted as a function of time using the SEPview® software, and the slope of which gives the creaming velocity of the droplets at a particular relative centrifugal force. Figure 3.7.2 represents a model graph of position vs. time of droplet creaming, whose slope gives the creaming velocity of droplets.

3.8 Statistics

All samples were prepared, and experiments were performed with at least three replicates (n=3) and the statistical significance of the data was analyzed using a pre-programmed function "T test" available in Microsoft Excel 2007 (Microsoft Canada Co, Mississauga, ON, Canada).

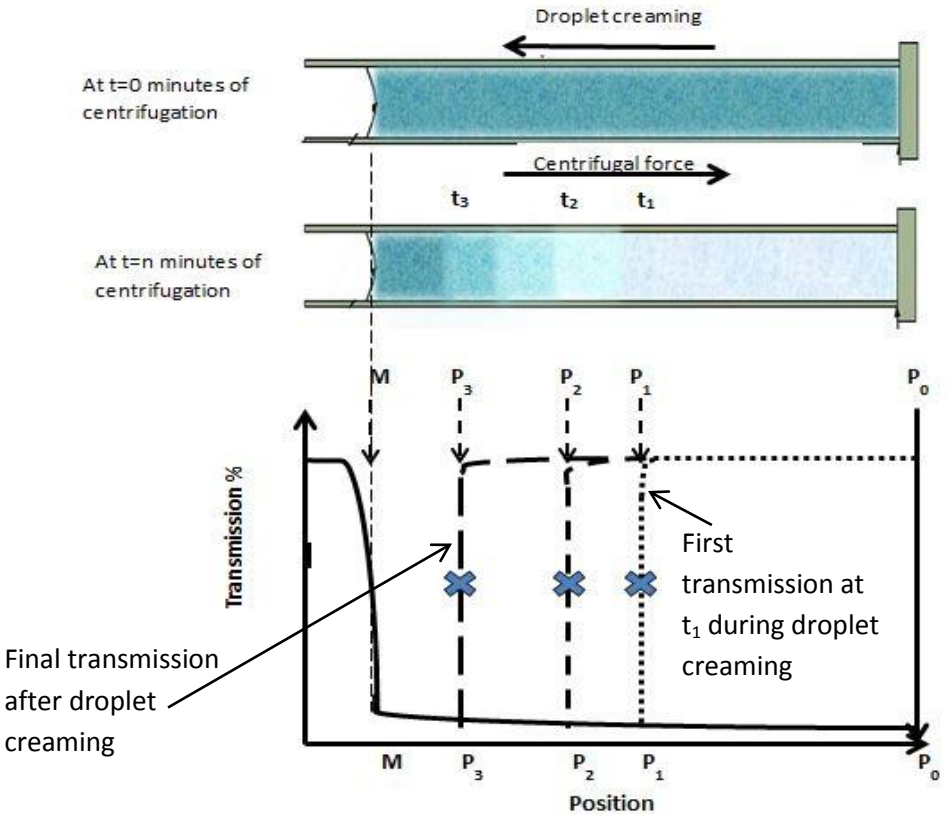

Figure 3.7.1 Schematic representation of the droplet creaming under centrifugal force and transmission profiles of light with time 'n' obtained using a LUMiSizer.

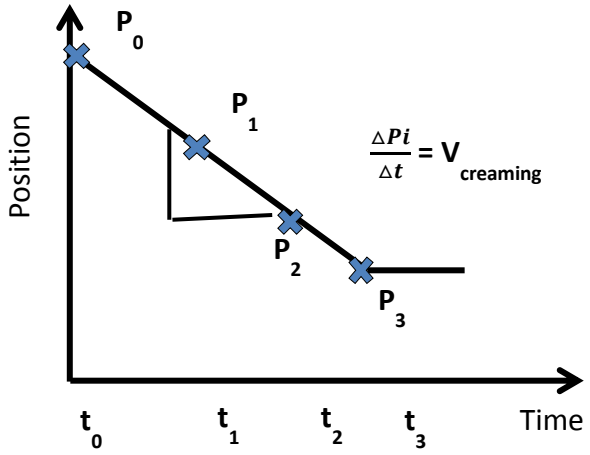

Figure 3.7.2 Model graph of position of cream layer with time obtained using LUMiSizer.

4 RESULTS AND DISCUSSION

4.1 Influence of emulsifier concentration on the gelation of nanoemulsions

4.1.1 Droplet size distribution

The surface area mean droplet diameters (d_{32}) of all nanoemulsions are shown in Figure 4.1.1 as a function of emulsifier concentration. It can be seen that the d_{32} values decrease with emulsifier concentration in power-law fashion ($y = ax^b$, r^2 for SDS and Tween 20 are 0.80 and 0.97, respectively). At higher emulsifier concentration, a plateau is reached in d_{32}. Similar power law decrease in average droplet size with emulsifier concentration was also observed by many research groups (Wilking et al., 2007; McClements, 2011). Meleson et al. (2004) developed an empirical power law model for SDS-stabilized silicon oil nanoemulsions and found the exponent as 0.33, although no significance of the value was provided. The power law exponent can be taken as an estimate of the rate of a decrease in droplet size as a function of emulsifier concentration. It is expected that the rate of decrease would be different for different homogenization devices used, emulsifiers' type, dispersed and continuous phase compositions. In Figure 4.1.1, the power law exponent for SDS and Tween 20 nanoemulsions are 0.20 and 0.61, respectively. The coefficient, on the other hand, expresses the estimated average droplet size when the value of the emulsifier concentration becomes unity. In the present case, the model estimates that with 1 mM emulsifiers the average droplet size for SDS and Tween 20 nanoemulsions would be 338 and 2690 nm, respectively. Such a large difference for SDS and Tween 20 nanoemulsions indicates that at lower molar concentration SDS is more powerful in decreasing emulsion droplet size compared to Tween 20. This could be due to the difference in molecular size and electrostatic charge of the two emulsifiers (molecular mass of SDS 288.4 g/mol vs. Tween 20 1227.5 g/mol). Anionic SDS, with its smaller size, was able to absorb quickly during droplet breakup inside the homogenizer and the negatively charged droplets were able to prevent re-coalescence (Jafari et al., 2008). Nonionic Tween 20, with its larger size, was

not as effectively as SDS in preventing re-coalescence of neutral droplets. With the increase in concentration, however, the difference between the two emulsifiers narrowed and at a molar concentration > 80 mM both emulsifiers provided similar d_{32} values. It is possible that at this higher concentration, there was enough Tween 20 present to cover the droplets sufficiently and prevent re-coalescence. However, merging of d_{32} values at higher concentration could also be due to the homogenizer efficiency, which may have reached its limit in terms of droplet breakup (Qian et al., 2011).

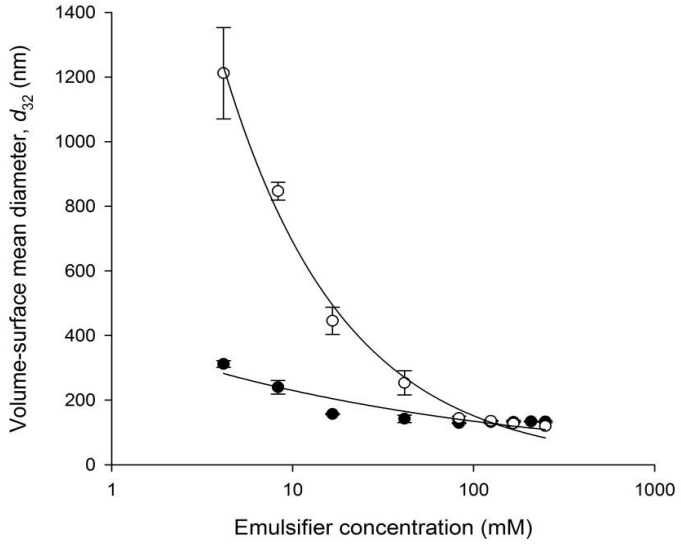

Figure 4.1.1 Effect of emulsifier concentration on the average droplet size (d_{32}) of SDS (●) and Tween 20 (○) nanoemulsions. The line represents a power law model fit to the experimental data (r^2 0.8 and 0.97 for SDS and Tween 20, respectively).

4.1.2 Visual observation of flow behavior

A simple visual observation experiment was carried out to understand the flow behavior of the nanoemulsions. 2-3 hours after preparation, the vials containing nanoemulsions were tilted at an angle to observe if they flow. They were kept tilted, and the observation was carried out for 30 seconds after which pictures were taken. Figure 4.1.2 shows the pictures of tilted vials containing SDS and Tween 20 nanoemulsions. Nanoemulsion prepared with 0.5 CMC SDS immediately flowed under gravity after the vial was tilted. The flow of nanoemulsions slowed

down beginning 1 CMC SDS while 5, 10 and 15 CMC SDS nanoemulsions did not flow at all during the span of observation. Starting from 20 CMC SDS, however, nanoemulsions began to flow again. It is evident that the gravity induced yielding of SDS nanoemulsions subsided at intermediate concentrations of SDS. On the other hand, all the Tween 20 nanoemulsions flowed when the vials were tilted.

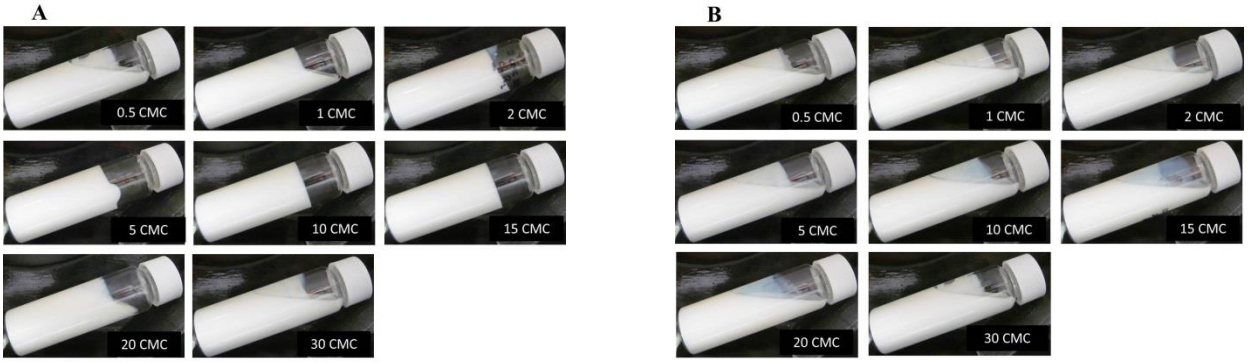

Figure 4.1.2 Pictures from the visual observation experiment of SDS and Tween 20 nanoemulsions. Vials containing nanoemulsions were tilted at a certain angle to record their flow behavior and waited for 30 s after which the pictures were taken.

4.1.3 Nanoemulsion viscosity

Nanoemulsion viscosity is plotted as a function of the shear rate in Figure 4.1.3. For all nanoemulsions, viscosity decreased with shear rate. Such shear thinning or pseudoplastic behavior is common for emulsions and could be due to the breakdown of interdroplet interactions and/or alignment of droplets along the shear field at a high shear rate (Rahalkar, 1992). However, in the present case, the degree of shear thinning behavior was different based on emulsifier type and concentrations. Overall, the degree of shear thinning is higher for SDS emulsions compared to Tween 20 emulsions indicating potential higher order structure formation in the former. For SDS emulsions, however, less shear thinning was observed for 25 and 30 CMC emulsifier concentrations compared to the lower concentrations (Figure 4.1.3B). For Tween 20 emulsions, a low and high-shear plateau was also observed indicating Newtonian behaviour both below and above these shear ranges (Figure 4.1.3C) (Rahalkar, 1992). The viscosity curves progressively increased with emulsifier concentration; except for 20, 25 and 30 CMC SDS concentrations a reverse trend in viscosity was observed.

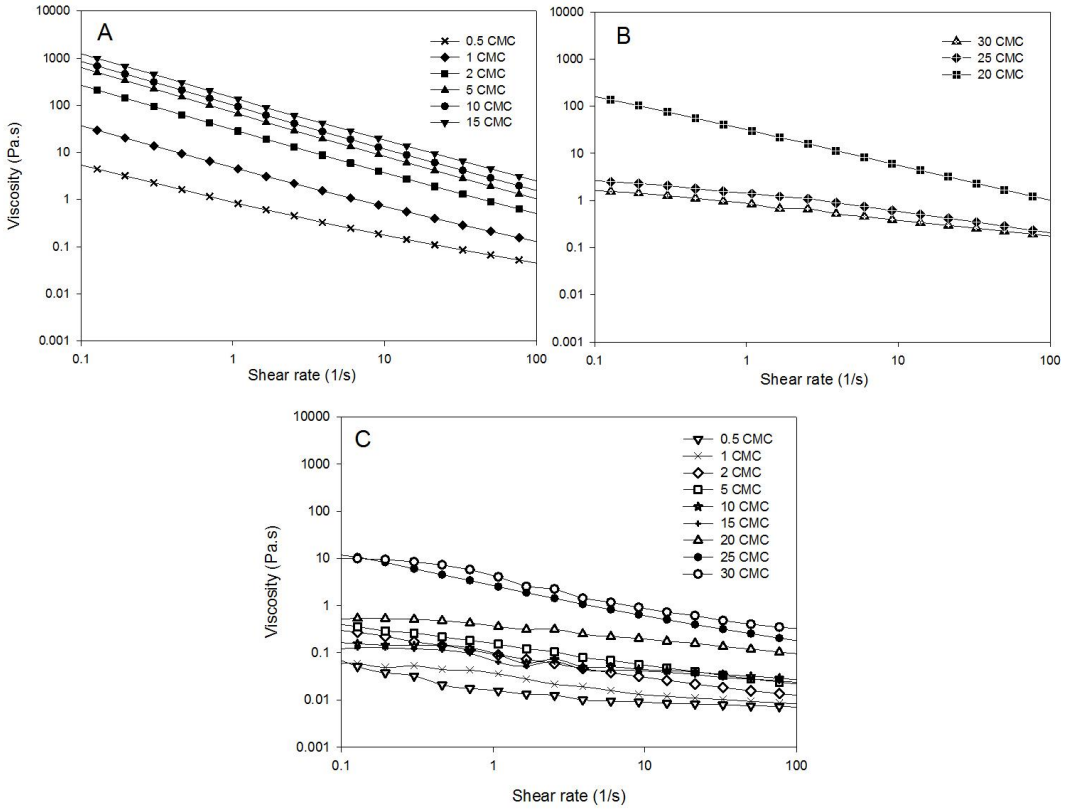

Figure 4.1.3 Change in viscosities of nanoemulsions as a function of shear rate at different emulsifier concentrations. (A) 0.5, 1, 2, 5, 10 and 15 times CMC SDS nanoemulsions, (B) 20, 25, 30 times CMC SDS nanoemulsions, (C) All Tween 20 emulsions. Error bars were not shown for clarity.

The shear stress and shear rate data was fitted to the Herschel-Bulkley (HB) model to quantify emulsion flow behavior:

$$\boldsymbol{\tau = \tau_{HB} + K\dot{\gamma}^{n}} \qquad 4.1.1$$

where *n* is the flow behavior index, *K* is the consistency coefficient, $\boldsymbol{\tau_{HB}}$ is the Herschel-Bulkley yield stress, $\boldsymbol{\tau}$ is the shear stress and $\dot{\gamma}$ is the shear rate. All Tween 20 emulsions and 25 and 30 CMC SDS emulsions showed negligible yield stress and better fit to their viscosity data were obtained with a simple power law model ($\tau = K\dot{\gamma}^{n}$). Good fit to the models was obtained for all emulsions (r^2 ranged from 0.85-0.96 for HB model and 0.8-0.94 for power law model).

All nanoemulsions have flow behavior indices $n < 1$, which corresponds to pseudoplastic behavior (n values were ranged from 0.21 to 0.63 for the SDS nanogels). For comparison, the viscosity of all emulsions at a shear rate of 10 s^{-1} is calculated from the models and plotted in Figure 4.1.4A. SDS-stabilized emulsions showed a maximum in the viscosity profile as a function of emulsifier concentration. Viscosity increased from 0.1 $Pa \cdot s^{-1}$ at 0.5 CMC SDS to 18.3 $Pa \cdot s^{-1}$ at 15 CMC SDS, thereafter steadily decreased until it reached 0.005 $Pa \cdot s^{-1}$ at 30 CMC SDS. Similar behavior of emulsion viscosity with an increase in emulsifier concentration was previously observed by Furusawa et al., in case of anionic latex particle dispersions in different concentration of SDS (Furusawa et al., 2002). The authors proposed that the increase in viscosity was due to depletion flocculation by emulsifier micelles at intermediate SDS concentrations followed by a drop in viscosity due to depletion stabilization by micelles at high SDS concentration. In the present case, the effect of these intermolecular interactions on emulsion rheology is discussed in section 4.1.4.

In contrast to SDS nanoemulsions, Tween 20 nanoemulsions did not show any peak in the viscosity profile, and their viscosity is much lower than SDS emulsions for most of the concentrations (Figure 4.1.4A). Overall, an increase in viscosity from 0.007 to 0.17 $Pa \cdot s^{-1}$ was observed from lowest to highest Tween 20 concentrations. In order to verify whether the aqueous phase viscosity has any impact on nanoemulsion flow behavior, the viscosity of the emulsifier solutions was also measured at 10 s^{-1} shear rate (data not shown). The increase in SDS concentration has no impact on the aqueous phase viscosity; hence the peak in viscosity profile of SDS nanoemulsions must be due to interdroplet and intermolecular interactions. For Tween 20, however, a considerable increase in viscosity (0.003 and 0.01 $Pa \cdot s^{-1}$) was observed with the increase in concentration from 4.15 mM to 249.5 mM. Although both emulsifiers were used at same molar concentrations, their weight fractions were very different due to a large difference in molecular weight. Hence, at 249 mM (equivalent to 30 CMC SDS), while only 0.72 wt% SDS was used, for Tween 20 it was equal to 30.5 wt% of emulsifier in the aqueous phase which led to an increase in viscosity of both the aqueous phase and the corresponding nanoemulsions.

Next, the yield stress of the SDS emulsions obtained from HB model (Figure 4.1.4B) was compared. Tween 20 emulsions did not show any yield stress. Yield stress for SDS emulsions increased with emulsifier concentration until 15 CMC (0.5 Pa at 0.5 CMC to 82 Pa at 15 CMC),

and suddenly decreased to 0.3 Pa at 20 CMC and completely disappeared after that. These values are in accordance with the visual observation of emulsions as shown in Figure 4.1.2. Nanoemulsions with high yield stress (namely, 5, 10 and 15 CMC) did not flow upon tilting (gel-like property) while starting from 20 CMC insignificant or no yield stress allowed them to flow upon tilting.

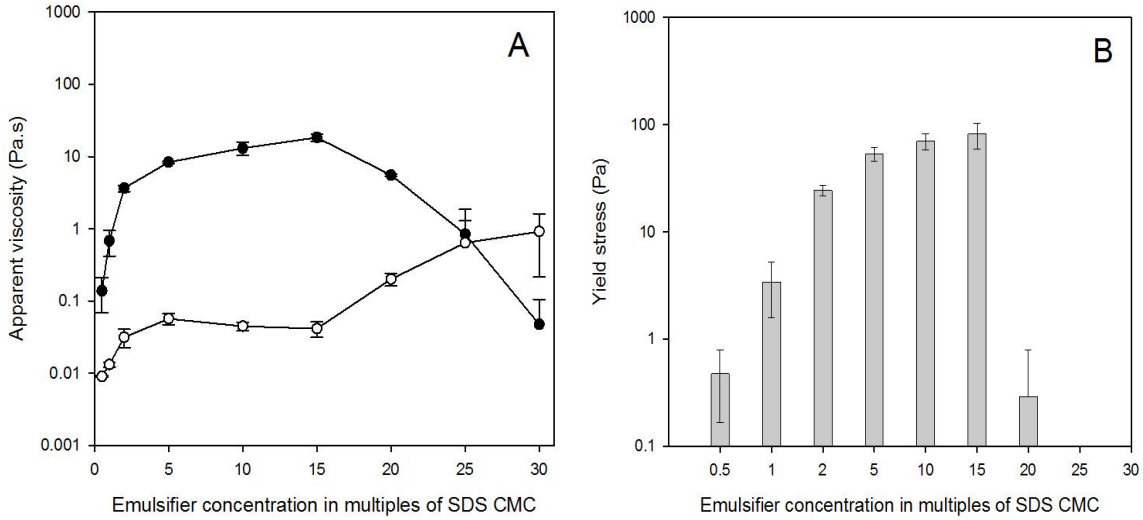

Figure 4.1.4 Average values calculated from Herschel-Bulkley and power law model for SDS and Tween 20 emulsions. (A) viscosity of SDS (●) and Tween 20 (○) nanoemulsions at 10 s^{-1} shear rate, (B) yield stress of SDS nanoemulsions. Error bars represents ± one standard deviation (n=3).

4.1.4 Viscoelastic behavior of nanoemulsions

Figure 4.1.5 shows the strain dependencies of storage and loss moduli for SDS-stabilized nanoemulsions. For all nanoemulsions until 15 CMC SDS concentrations, moduli are independent of strain below 2%, showing the existence of linear viscoelastic region (LVR). For these nanoemulsions, G′ is significantly greater than G″ within the LVR reflecting their dominant elastic nature. However for 0.5 CMC and 1 CMC SDS nanoemulsions despite the higher G′ than G″ and an LVR, they yielded under gravity in the visual observation experiment manifesting weak gelation. At larger strain (beginning 5%), known as yield strain, the G′ values of these nanoemulsions showed a deviation from linearity and dropped gradually. At this time, the G″ values began to rise and formed a peak where it also crossed G′. The distinct peak in G″

was also observed by many researches during viscoelastic study of the soft colloidal materials and is considered to be due to structural relaxation process leading to gel network breakdown and flow of materials (Datta et al., 2011; Koumakis et al., 2011). At higher strain compared to the peak value, G″ dominates over G′, indicating the liquid-like behavior of the nanoemulsions. For Tween 20 nanoemulsions, strain-dependent viscoelastic behavior showed the similar nature of the curves as 20 – 30 CMC SDS nanoemulsions reflecting weak gelation (data not shown).

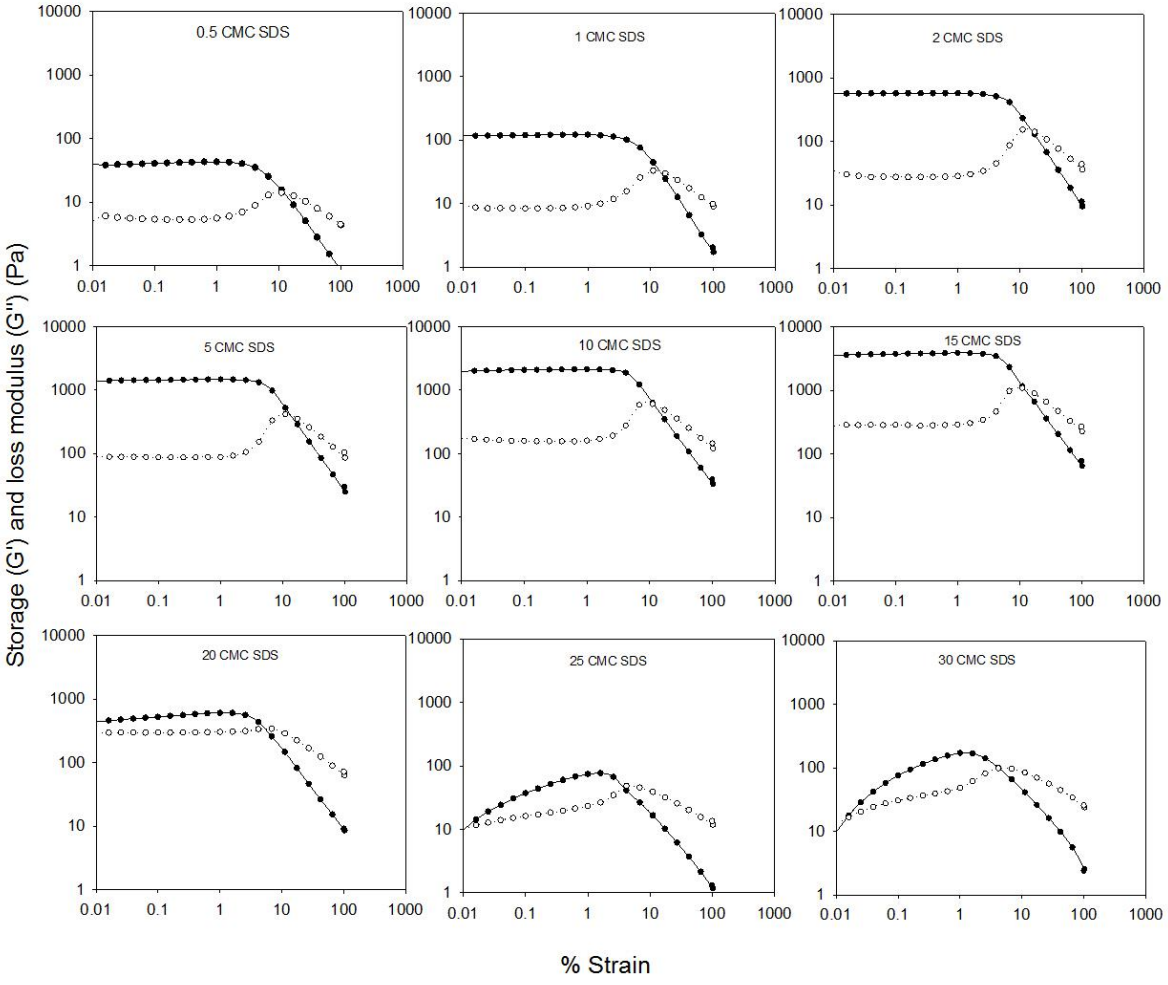

Figure 4.1.5 Average Strain dependent storage (G′) (●) and loss moduli (G″) (○) of different SDS nanoemulsions. SDS concentration is expressed as multiples of its critical micelle concentration (CMC).

In order to compare the elasticity of different nanoemulsions, the plateau storage and loss moduli at 0.1% strain is plotted as a function of emulsifier concentration (Figure 4.1.6). It can be

seen that G′ and G″ increased until 15 CMC SDS and decreased after that, which is in accordance with the viscosity and yield stress behavior discussed before. The apparent increase in G′ and G″ after 25 CMC SDS nanoemulsion is not statistically significant ($p > 0.05$). The viscoelastic moduli for Tween 20 nanoemulsions at 0.1% strain is also plotted in Figure 4.1.6. The G′ and G″ for Tween 20 nanoemulsions are significantly lower than that of SDS nanoemulsions until 20 CMC. Also, within Tween 20 nanoemulsions the G′ is only marginally higher than G″, mimicking the characteristics of weak gel that yielded under gravity as can be seen from Figure 4.1.2.

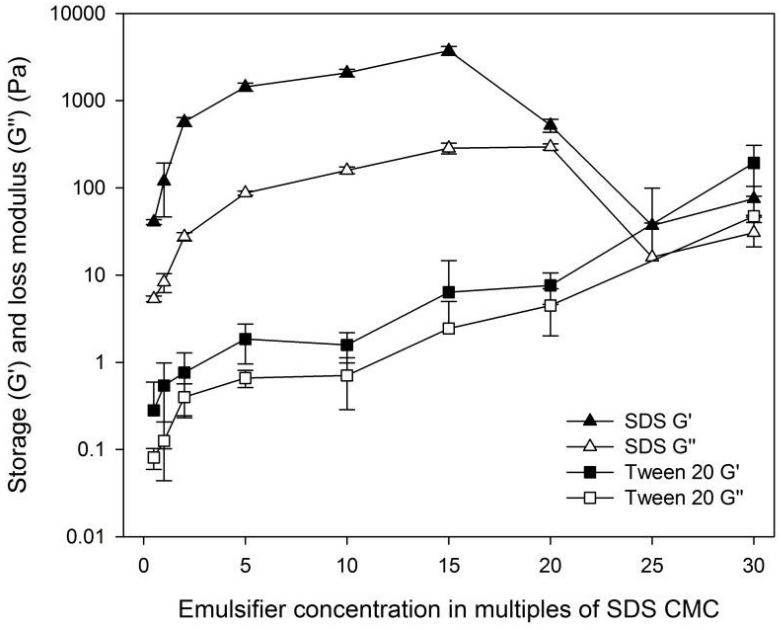

Figure 4.1.6 Characterization of the viscoelastic behavior of SDS (triangle) and Tween 20 (square) nanoemulsions. Values of storage (G′) (closed symbols) and loss (G″) (open symbols) moduli of nanoemulsions (at a frequency of 6.28 rad/sec and 0.1% strain) were plotted from strain sweep measurements data against emulsifier concentration. Lines are used to guide the eye. Error bars represents ± one standard deviation (n=3).

The frequency-dependent mechanical response of the nanogels is shown in Figure 4.1.7. Similar to the strain sweep result, frequency sweep also showed an increase in plateau G′ with increasing SDS concentration until 15 CMC and then it dropped significantly beginning 20 CMC SDS (Figure 4.1.7A and C). For 0.5 to 15 CMC SDS nanoemulsions plateau G′ remained

considerably higher than G″ in the 1 – 100 rad/s range. G″ of these nanoemulsions demonstrated a shallow minima in the frequency range studied (Figure 4.1.7B). Similar minima in frequency dependent G″ for compressed emulsions were also observed by Mason et al. (1997), Datta et al. (2011) and other research groups (Koumakis et al., 2011). Such a minima results as G″ first decreased and later increased with an increase in frequency. The low frequency drop was a consequence of loss of relaxation or very slow structural rearrangements of droplet network, while the high-frequency rise resulted from ultimate domination of viscous flow of the fluid-like phase that could be observed at higher frequency beyond the measured range (Mason et al., 1997). For more detailed analysis and modeling of this frequency dependent rheological behavior, readers are invited to refer to the work by Mason et al.Mason et al. (1997). The frequency-dependent viscoelastic behavior of the nanoemulsions with 20, 25 and 30 CMC SDS concentration showed different behavior from the rest (Figure 4.1.7C and D). G′ no longer has a plateau-like region, instead increased with frequency. Similarly, G″ showed a rapid increase in the viscous flow behavior with increasing frequency and remained very close to G′, reflecting their weak gel-like behavior. Frequency dependence of viscoelastic behavior of Tween 20 nanoemulsions was also measured at a strain rate of 0.1%, although due to the lack of LVR in their strain sweep results it was difficult to measure G′ in the frequency range studied (data not shown).

4.1.5 Mechanism of nanocolloidal gelation

In the present study, three regimes of SDS-stabilized nanoemulsion gelation were observed as a function of emulsifier concentration (Figure 4.1.6). An initial rapid increase in gel strength until 2 CMC SDS concentration followed by slow, but steady increase in gel strength until 15 CMC SDS and then a sudden drop in gel strength leading to weaker gels starting from 20 CMC SDS. We hypothesized that the smaller droplet size of nanoemulsions along with increased influence of electrical double layer formed by the layer of charged SDS at the droplet surface increased the ϕ_{eff} beyond random jamming leading to repulsive gelation. With the increase in SDS concentration, the presence of micelles in the continuous phase induced long-range depletion attraction among the nanodroplets that overcame short-range repulsive interactions and

led to strong interdroplet aggregation and increase in gel strength (Kekicheff et al., 1992; Mondain-Monval et al., 1996)

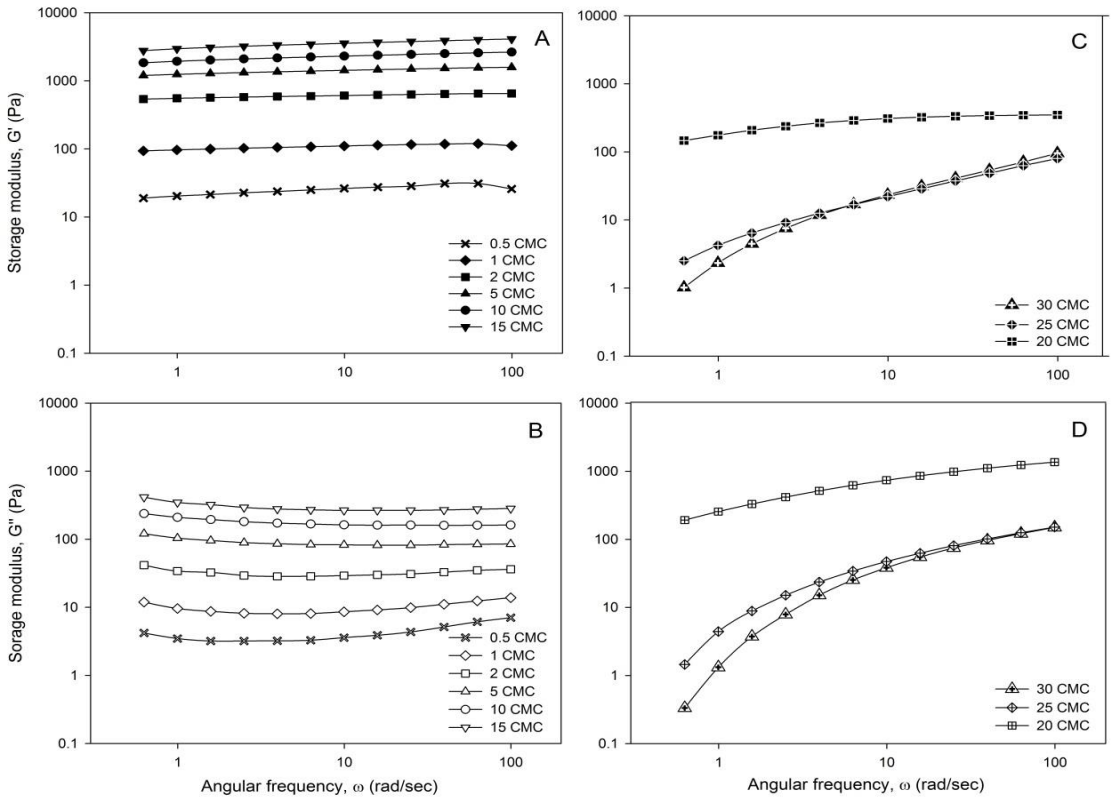

Figure 4.1.7 Frequency dependent storage (G′) and loss moduli (G″) of different SDS nanoemulsions. (A) G′, (B) G″ until 15 CMC SDS nanoemulsions; (C) G′ and (D) G″ for 20 – 30 CMC SDS nanoemulsions.

On the other hand, at a very high emulsifier concentrations, excess micelles in the continuous phase led to depletion stabilization where micelles filled-up the inter-droplet regions. Displacement of layers of micelles from this region resulted in osmotic pressure fluctuations known as oscillatory structural forces (OSF), causing a drop in attractive interactions (Stubenrauch et al., 2003). Many authors have reported the transformation of depletion flocculation to re-stabilization due to OSF at this high emulsifier concentrations (Bergeron et al., 1992; McClements, 2005; James et al., 2014b, 2014a). However, in the present case decrease in attractive interactions among the nanodroplets at high SDS concentrations led to the sudden drop

in gel strength. This type of OSF induced transformation from strong gels with high yield stress to weaker gels that yield under gravity has never been reported before.

Below, is the calculation of κ^{-1} and ϕ_{eff} for all SDS nanoemulsions. Depletion interaction energy was also calculated to show that for the nanoemulsions starting from 5 CMC SDS, attractive interactions dominates. Finally, the decline in gel strength at very high SDS concentration (20, 25 and 30 CMC) is explained by calculating OSF as a function of interdroplet distance. Similar calculations are also done for Tween 20 nanoemulsions to explain their weak-gel behavior at all concentrations.

4.1.6 Calculation of κ^{-1} and ϕ_{eff}

ϕ_{eff} of all the SDS nanoemulsions was calculated using the eq 2.5.3 in which the interfacial shell layer thickness (δ) can be calculated from the Debye screening length (κ^{-1}). By definition, κ^{-1} is the distance from the droplet surface at which the surface potential decreased to 1/e of the original value. Some authors have reported that δ can be taken as equal to κ^{-1}, while others have proposed that δ is a function of κ^{-1} and the ratio of δ and κ^{-1} depended on the surface potential and the radius of the involved particles (Mondain-Monval et al., 1996; Weiss et al., 2000). Based on experimental measurement and calculations by Mondain-Monval et al. (1996), in the present case, the ratio of δ and κ^{-1} was taken as 2.4, meaning that the repulsive interactions between the droplets could still be significant at a distance 2.4 time κ^{-1} from the droplet surface.

A common way to calculate κ^{-1} is to use the equation given by Israelachvili for a 1:1 electrolyte at 25ºC (Israelachvili, 2011).

$$k^{-1} = 0.304/\sqrt{C} \qquad 4.1.1$$

where C is the concentration of the ions dispersed in water. Most of the researchers to date equated C to the concentration of ionic emulsifier (in this case SDS), C_e in emulsion as it was assumed that the molecules would be completely dissociated and the Na^+ counterions would be responsible for ion concentration in the continuous phase while the dodecyl sulfate ions would be either adsorbed at the droplet surface or formed micelles in the continuous phase (Weiss et al., 2000). However, large discrepancies in κ^{-1} calculated from eq 4.1.1 to a predicted κ^{-1} in case of repulsive nanoemulsions has been reported by Weiss et al. (2000). Others have also observed

that shear modulus of colloidal dispersions predicted using an empirical model involving κ^{-1}, deduced from eq 4.1.1, was 6 orders of magnitude less than the experimental value (Buscall et al., 1982). These discrepancies could be due to the binding of Na^+ ions to the dodecyl sulfate ions at the interface to reduce the lateral repulsion between the charged surfactant heads (Kralchevsky et al., 1999; Weiss et al., 2000). Therefore, only free Na^+ counterions participated in the screening of droplet charge. Consequently, the concentration term in eq 4.1.1 was multiplied by counterions dissociation factor (*f*) to reflect this behavior:

$$\kappa^{-1} = 0.304/\sqrt{f \cdot C_e} \qquad 4.1.2$$

Nespolo et al. (2001) calculated counterion dissociation factor ranging from 0.1 to 0.2 for a range of SDS concentration (0.1 mM to 1 mM) from the ratio of surface charge corresponding to the zeta potential of the charge for completely ionized SDS at the interface. Others have also reported similar values for SDS counterion dissociation factor (Kalinin et al., 1996). In the present thesis the counterions dissociation factor for SDS was taken as 0.1.

The increase in the concentration of SDS in the nanoemulsion results in the formation of micelles in the continuous phase. The values of κ^{-1} in the presence of micelles (starting from 5 CMC) can be calculated from eq 4.1.3 where it was assumed that the counter ions could be generated from three regions: i) from the monolayer of emulsifier molecules adsorbed on the droplet surface, ii) from the free emulsifiers in the continuous phase (equal to the CMC) and iii) and those dissociated from the micelles (Pashley et al., 1987; Mondain-Monval et al., 1996).

$$\kappa^{-1} = 0.304/\sqrt{f \cdot C_{monolayer} + CMC + q \cdot \left(C_e - C_{monolayer} - CMC\right)} \qquad 4.1.3$$

where $C_{monolayer}$ is the monolayer concentration of SDS adsorbed at the oil-water interface and q is the dissociation factor of counterions from the micelles, taken as 0.25 for SDS (Nespolo et al., 2001). The value of $C_{monolayer}$ can be calculated from surface load (Γ) and interfacial area ($A = 6\phi/d_{32}$):

$$C_{monolayer} = \Gamma.(6\phi/d_{32}) \qquad 4.1.4$$

The surface load for SDS and Tween 20 is taken as 1.90×10^{-6} and 2.96×10^{-6} moles/ m^2, respectively (Lu et al., 1995; Ghosh, 2009). It was found that for nanoemulsions with 0.5, 1 and 2 times CMC SDS concentration, no free emulsifier was present to form micelles in the

continuous phase. Therefore for these nanoemulsions eq 4.1.2 was used to calculate κ^{-1}. For all other nanoemulsions eq 4.1.3 was used.

The calculated values of δ ($\delta = 2.4\kappa^{-1}$) and ϕ_{eff} for all SDS nanoemulsions are shown in Table 4.1.1. For nonionic Tween 20 lack of charge on the droplets resulted in the absence of sufficient interfacial shell layer thickness leading to $\phi_{eff} \approx \phi_{core}$ (values not shown) and hence no repulsive gelation was observed. In contrast, ϕ_{eff} of 0.5, 1 and 2 CMC SDS nanoemulsions are well above the maximal random jamming limit (ϕ_{MRJ}=0.64) for monodisperse emulsions. However, only 2 CMC SDS nanoemulsion showed high yield stress and did not flow, while 0.5 and 1 CMC SDS nanoemulsions had low yield stress and flowed under gravity. The different behavior of 0.5 and 1 CMC nanoemulsions compared to 2 CMC nanoemulsion at approximately similar ϕ_{eff} (ranged from 0.71 to 0.75) can be explained by their polydispersity. A nanoemulsion with higher polydispersity would have greater ϕ_{MRJ}, hence its gel strength would be lower than a nanoemulsion with lower polydispersity but similar ϕ_{eff} (Groot et al., 2011).

In order to explain elasticity of repulsive nanoemulsion gels polydispersity of 0.5, 1 and 2 CMC SDS nanoemulsions was determined using a dynamic light scattering instrument (Zetasizer Nano-ZS90, Malvern Instruments, Montreal, QC, Canada). The average values of polydispersity were 0.23, 0.21 and 0.18 for the 0.5, 1 and 2 CMC nanoemulsions, respectively. Hence, ϕ_{MRJ} for 0.5 and 1 CMC nanoemulsions should be higher compared to 2 CMC nanoemulsions, therefore although their ϕ_{eff} is similar, they should have very different gel strength. In Figure 4.1.8A ϕ_{eff} is scaled by the polydispersity and plotted against the elastic moduli (G′) of these nanoemulsions. It can be seen that G′ progressively increased as a function of ϕ_{eff} / polydispersity, therefore, for electrostatically-stabilized nanoemulsions ϕ_{eff}'s proximity towards ϕ_{MRJ} governed their elasticity. It should be mentioned here that the counterion dissociation factor (*f*) of SDS could also have a significant effect on the estimated values of ϕ_{eff}. Here *f* was assumed as constant and equal to 0.1, however, with increase in emulsifier concentration, as the droplet surface become saturated, there would be a need for the counterions to be associated with the dodecyl sulfate anion at the droplet surface in order to reduce repulsion between the adsorbed molecules. A lower value of *f* would lead to higher ϕ_{eff} of 2 CMC SDS nanoemulsion compared to 0.5 and 1 CMC which could explain its high gel strength.

4.1.7 Calculation of depletion interactions

Considerably higher gel strength was observed for 5, 10 and 15 CMC SDS nanoemulsions compared to 0.5, 1 and 2 CMC nanoemulsions in spite of their lower estimated values of ϕ_{eff} (Table 4.1.1), which could be explained by the appearance of attractive depletion interactions among the nanodroplets by excess SDS micelles in the continuous phase. The long-range attractive interaction (despite short range repulsion due to interfacial SDS) formed a tenuous network of aggregated droplets which prevented the flow of water and increased the gel strength of the nanoemulsions. Datta et al. (2011) showed that attractive emulsions with $\phi_{eff} > \phi_{MRJ}$ have two peaks in strain-dependent G″ while those with $\phi_{eff} < \phi_{MRJ}$ have only one peak. In the present case 5, 10 and 15 CMC SDS nanoemulsions exhibited one peak in strain-dependent G″ curves (Figure 4.1.5), also indicating $\phi_{eff} < \phi_{MRJ}$ for these nanoemulsions.

The depletion effect of micelles on oil droplets has been shown by many researchers using both experimental and simulation work (Petsev et al., 1995; Mondain-Monval et al., 1996; Sharma et al., 1996). In order to interpret the viscoelastic behavior of the nanogels based on micelle-induced attraction, depletion interaction energy (W_D) was calculated using the equation given by Petsev et al. (1995).

$$W_D = -P_o \cdot V_E \qquad 4.1.5$$

where P_o is the osmotic pressure created by the presence of excess micelles in the continuous phase and V_E is the volume of the continuous phase confined between the two approaching droplets from which the micelles were squeezed out. P_o can be calculated using the following equations originally developed for non-ionic micelles (Carnahan et al., 1969; Petsev et al., 1995).

$$P_o = \xi C_M k_B T \qquad 4.1.6$$

$$\text{and, } \xi = (1 + \phi_m + \phi_m^2 - \phi_m^3)/(1 - \phi_m)^3 \qquad 4.1.7$$

where C_M, number density of micelles in the continuous phase; k_B, Boltzmann constant; T, temperature; and ϕ_m, the micelle volume fraction in the continuous phase. As this equation was originally developed for non-ionic species, a correction factor is needed for strong ionic emulsifier SDS, whose micelles would carry the counterion cloud around them, thus contributing

towards an increased effective micellar volume fraction ($\phi_{m\text{-}eff}$). Hence in the calculation of P_o, ϕ_m in eq 4.1.7 was replaced with $\phi_{m\text{-}eff}$ (Petsev et al., 1995).

Table 4.1.1 Interfacial shell layer thickness (δ, effective oil phase volume fraction (ϕ_{eff}), effective micelle volume fraction ($\phi_{m\text{-}eff}$) and depletion interaction energy (W_D/k_BT at h=δ) for SDS nanoemulsions calculated at counterion dissociation factor, f = 0.1. ϕ_m and W_D/k_BT (at h=δ) for Tween 20 nanoemulsions are shown. For SDS aqueous phase micelle appears at 41.4 mM concentration, while for Tween 20 it was at 16.6 mM.

Emulsifier concentration		SDS nanoemulsions					Tween 20 nanoemulsions	
mM	Multiples of SDS CMC	δ(=2.4 κ^{-1}) (nm)	ϕ_{eff}	ϕ_m	$\phi_{m\text{-}eff}$	W_D/ k_BT	ϕ_m	W_D/ k_BT
4.15	0.5 CMC	36.0	0.75	–	–	–	–	–
8.3	1 CMC	25.4	0.71	–	–	–	–	–
16.6	2 CMC	18.0	0.74	–	–	–	0.0009	-0.1
41.5	5 CMC	6.7	0.52	0.001	0.01	-0.2	0.02	-1.4
83.0	10 CMC	5.0	0.50	0.02	0.14	-6.8	0.06	-2.2
124.5	15 CMC	4.1	0.48	0.04	0.22	-17.8	0.12	-5.9
166.0	20 CMC	3.5	0.47	0.07	0.28	-32.6	0.19	-11.5
207.5	25 CMC	3.2	0.46	0.09	0.34	-53.5	0.25	-21.0
249.0	30 CMC	2.9	0.45	0.11	0.38	-81.2	0.32	-36.2

$$\phi_{m-eff} = \frac{4\pi}{3}\left(\frac{d_m}{2} + k^{-1}\right)^3 C_M \qquad 4.1.8$$

where d_m is the diameter of micelles (4.8 nm for SDS (Petsev et al., 1995) and 7.2 nm for Tween 20 (Basheva et al., 2007)). The value of C_M was calculated using the similar approach as in eq

4.1.3, by subtracting the amount of SDS adsorbed at the interface ($C_{monolayer}$) and free emulsifier present in the continuous phase (equal to CMC) from the total amount of emulsifier present in the system (C_e):

$$C_M = \left(C_e + C_{monolayer} - CMC\right) N_A / N_{agg} \qquad 4.1.9$$

where N_{agg} is micelle aggregation number (64 for SDS(Petsev et al., 1995) and 70 for Tween 20(Basheva et al., 2007)) and N_A is the Avogadro number (6.023×10^{23} mole^{-1}).

For the calculation of V_E, theequation developed by Richette and Kekicheff (Richetti et al., 1992) was used. It was assumed in their equation that the micelles with its charge cloud could not reach a separation from the droplet surface smaller than the interfacial shell layer thickness δ ($\delta = 2.4\ \kappa^{-1}$). This gives rise to micelle effective diameter $d_{m-eff} = (d_m + 2\delta)$. The micelles are also electrostatically repelled from the droplet surface leading to an increased excluded volume between the droplets compared to non-ionic micelles. When droplet diameter >> d_m, δ and κ^{-1}, V_E can be calculated from:

$$V_E = \pi \left(r_f^2 (d_m + 2\delta - h) + \frac{R}{2} (d_m + 2\delta - h)^2 \right) \qquad 4.1.9$$

where r_f is the radius of the film created by closely approached deformed droplets and is taken as 0.045 times the radius of the droplets (Petsev et al., 1995) and h is the distance between the droplets. Using equations 6 to 11 the values for depletion interaction energy for both SDS and Tween 20-stabilized nanoemulsions were calculated (Table 4.1.1).

From Table 4.1.1 it can be seen that increase in emulsifier concentration (and corresponding increased micelle volume fraction) led to stronger depletion attraction. For SDS, although the actual micelle volume fraction was quite low, the presence of charge cloud around them increased the effective micelle volume fraction to a great extent. The interfacial electrical double layer around the droplets also contributed towards increased excluded volume in the interdroplet region, which further increased depletion interaction. In contrast, Tween 20 micelles and the droplets stabilized with it did not have enough charge leading to a lower excluded volume and depletion attraction among the droplets. A similar effect of micelle charge on the depletion interaction has also been reported by Mondain Monval et al (Mondain-Monval et al., 1996).

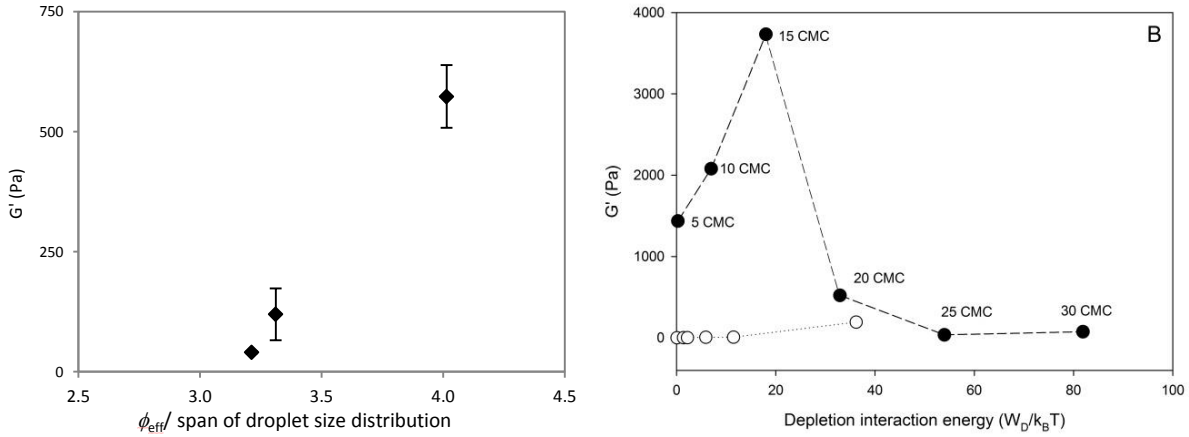

Figure 4.1.8 Storage modulus (G′) of SDS nanoemulsions in (A) repulsive and (B) attractive regimes expressed as a function of (A) ϕ_{eff} scaled by span of droplet size distribution and (B) depletion interaction energy. The G′ values were obtained from strain sweep measurements at 0.1% strain. In B data for Tween 20 nanoemulsions (○) were also plotted alongside SDS nanoemulsions (●). Lines are used to guide eyes. The difference in the scale of the y-axes between A and B is required for clarity.

An interesting observation of the present study was revealed when the elastic moduli (G′) of the resulting nanoemulsions were plotted as a function of the depletion interaction energy (Figure 4.1.8B). For SDS, from 5 CMC to 15 CMC SDS concentration, elastic moduli of nanoemulsions increased strongly with depletion attraction energy. However, starting from 20 CMC SDS a sudden drop in elastic moduli was observed where gel strength decreased with an increase in depletion interaction. In contrast, Tween 20 nanoemulsions showed very weak gelation behavior at all concentrations in-spite of their comparable depletion interaction energy. The progressive increase in gel strength from 5 to 15 CMC SDS with an increase in depletion interaction energy is expected (Jenkins et al., 1996). The increase in attractive interaction strengthens the bonds between the droplets in the aggregates that also immobilized continuous aqueous phase (Berli et al., 2003). This results in further increase of the effective droplet volume fraction, beyond what was obtained due to charge cloud on the droplet surface (ϕ_{eff} due to charge cloud ranged from 0.52 to 0.48 for 5 to 15 CMC SDS concentration, Table 4.1.1), leading to a stronger gel network. For non-ionic Tween 20, no such increase in ϕ_{eff} is expected, and the

depletion attraction generated by micelles alone is not enough to induce interdroplet aggregation and gelation. Nevertheless, at high emulsifier concentration, both SDS and Tween 20 nanoemulsions showed weak gel behavior which cannot be explained by depletion attraction as the interdroplet interaction falls into the oscillatory structural force (OSF) regime (Denkov et al., 1995; Basheva et al., 2007).

4.1.8 Calculation of oscillatory structural forces

In emulsions, oscillatory structural forces are observed when high concentration of nanoscale colloidal particles (e.g., nanoparticles, surfactant micelles, biopolymers) are confined between two approaching droplets (Richetti et al., 1992; Asnacios et al., 1997; Vesaratchanon et al., 2009). When the particles form layered structuring in the narrow interdroplet region such that at least one layer of the colloidal particles stays between the two approaching droplets, a repulsive structural barrier between them prevents the droplets from flocculation (Petsev et al., 1995; James et al., 2014a). As the droplets approach, layers of colloids are "squeezed out" leading to step-wise thinning of the interdroplet films. As a result, the osmotic pressure acting on the droplets fluctuates resulting in alternating repulsive and attractive forces operating on the droplets (James et al., 2014a). On the other hand, as the micelle concentration is decreased, the last layer of micelles could be squeezed out of the interdroplet region leading to depletion attraction among the droplets (as seen in 5, 10 and 15 CMC SDS nanoemulsions). OSF was experimentally determined with surface force apparatus (SFA) between two mica sheets by Richetti and Kekicheff; and with colloid probe atomic force microscopy (CP-AFM) between a silica hard sphere and a silica flat plate in a surfactant solution by James and Walz (James et al., 2014b). Tabor et al. (2011) and Stubenrauch et al. (2003) used AFM to measure OSF between two deformable oil droplets in SDS solutions and proposed that the role of OSF would be more significant in deformable systems due to difficulty in removing the last layer of micelles between the two approaching droplets as the force required for removing micelle layer is greater than the force required for droplet deformation. Recently, James et al. (2014b) showed that silica microparticle dispersion in SDS solution destabilized with extensive sedimentation due to depletion flocculation when SDS concentration was equal to 5 and 10 times CMC. However, at 20 CMC the dispersion remained stable due to depletion stabilization by OSF. In the present

case, the similar behavior of SDS micelles was observed. For 5 to 15 CMC SDS, extensive depletion flocculation led to droplet aggregation and gelation. However, beginning 20 CMC SDS, the interdroplet interaction was governed by OSF and the micelle layers between the droplets prevented them from flocculation. As a special case, in our system, prevention of flocculation led to the breakdown of interdroplet network essential for gelation and the strong attractive nanogels converted into weak gels.

A simple analytical expression for oscillatory interaction potential is not readily available due to complexity in the calculation and most of the modelling approach is based on the numerical solution of integral equations (Walz et al., 1994; Trokhymchuk et al., 2001). Denkov et al. (1995) developed a semiempirical formula for OSF between two solid surfaces in presence of hard spheres which were modified by Petsev et al. (1995) using Derjaguin's approximation for the interaction energy (W_{OSF}) between two deformed spheres (for any interdroplet distance $h >$ d_m):

$$W_{OSF}(h,r) = \pi r_f^2 P_0 \frac{d_m \exp(1-h/d_m)}{(4\pi^2+1)} \times \left[\cos\frac{2\pi h}{d_m} - 2\pi \sin\frac{2\pi h}{d_m}\right] - \pi R P_0 \frac{{d_m}^2 \exp(1-h/d_m)}{(4\pi^2+1)} \times \left[(4\pi^2+1)\cos\frac{2\pi h}{d_m} - 4\pi \sin\frac{2\pi h}{d_m}\right] \quad 4.1.11$$

By replacing micelle diameter, d_m with $d_{m\text{-}eff}$ (= $d_m+2\kappa^{-1}$) for SDS in eq 4.1.11 and calculating P_o from eq 4.1.8 W_{OSF} between the two approaching droplets was calculated as a function of interdroplet distance, h (Figure 4.1.9A). The calculations for Tween 20 were done with the original d_m in the absence of any charge cloud (Figure 4.1.9B).

From Figure 4.1.9 it can be seen that the interdroplet interaction oscillates between positive (repulsion) and negative (attraction) values as the droplets approach each other. The period of oscillation is equal to the $d_{m\text{-}eff}$ for SDS and d_m for Tween 20 nanoemulsions. As the layers of micelles are squeezed out from the interdroplet region, the structural force between the droplets reaches a maxima. When the interdroplet distance becomes equal to $d_{m\text{-}eff}$ or d_m repulsive interaction between the droplets prevents them from flocculation. From Figure 4.1.9 it can also be seen that the strength of the repulsive barrier increased with emulsifier concentration. At the lower limit, 5 CMC SDS nanoemulsion did not show any perceptible OSF acting between the droplets and the interdroplet interaction was governed by depletion attraction. For 10 and 15

CMC SDS concentration, a small increase in OSF can be seen from the Figure 4.1.9A, but the repulsive barrier must be insignificant compared to the depletion interaction. For, higher SDS concentrations (20, 25 and 30 CMC), although the value of W_D/ k_BT (Table 4.1.1) appeared to be higher than W_{OSF} (calculated from eq 4.1.11), presence of at least one layer of micelles between the droplets prevented them from flocculating leading to a drop in gel strength. It should be mentioned that the values for W_D and W_{OSF} might not be directly comparable as they signify two different scenarios. At present, there is no single analytical expression available which can combine both depletion and OSF.

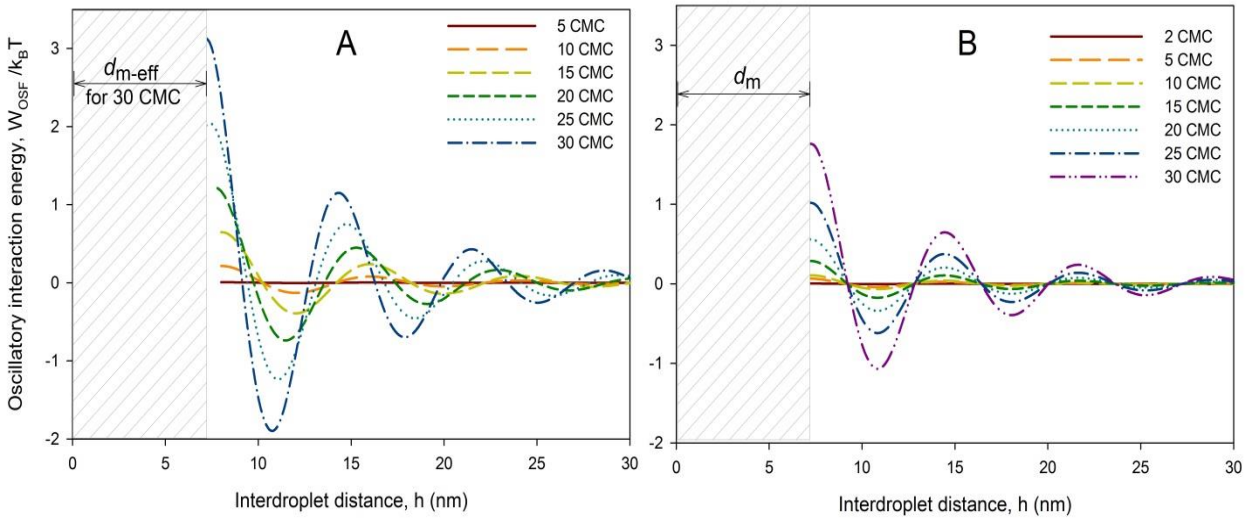

Figure 4.1.9 Calculated oscillatory interaction energy from eq 12 for 40 wt% O/W nanoemulsions stabilized with different concentration of (A) SDS and (B) Tween 20. The oscillating interaction potential is shown until the interdroplet distance equal to effective micelle diameter ($d_{m\text{-}eff}$) for SDS and original micelle diameter (d_m) for Tween 20. It was assumed that at high micelle concentrations (20 – 30 CMC) the shaded area will be inaccessible by the approaching droplet and will be filled with a layer of micelles. As $d_{m\text{-}eff}$ changes with micelle concentration for SDS, the curves begin at different distances.

In the case of Tween 20, the oscillatory interaction potential is weaker compared to SDS nanoemulsions mainly due to its lower ϕ_{eff} and ϕ_m. Weak OSF for Tween 20 was experimentally observed by Christov et al.(Christov et al., 2010). A more compelling evidence of action of OSF in Tween 20 nanoemulsions can be obtained from the stability diagram developed by Basheva et al. (Basheva et al., 2007) who showed that for a nonionic emulsifier, OSF arose when the ϕ_m > 0.12, which corresponds to 124.5 mM or an emulsifier concentration equivalent to 15 CMC SDS. Therefore, for Tween 20 nanoemulsions transition from attractive to OSF regime would occur at a lower emulsifier concentration compared to SDS.

4.1.9 Summary

In the present section, gelation in nanoemulsions was investigated as a function of emulsifier concentrations and types. 40 wt% O/W nanoemulsions were prepared by high pressure homogenizer in the presence of different concentration of either anionic SDS or nonionic Tween 20 emulsifiers. It was observed that liquid nanoemulsions transformed into viscoelastic gels at a specific concentration range of SDS while no gelation was observed for Tween 20. The apparent viscosity, yield stress and G′ of the nanogels increased with SDS concentration until 15 times CMC, thereafter decreased steadily as the gel broke down beginning 20 times CMC.

At low SDS concentration (0.5 – 2 CMC) the repulsive charge cloud acted as interfacial shell layer on the nanodroplets and significantly increased the effective droplet diameter ($d_{m\text{-}eff}$) and ϕ_{eff}. The ϕ_{eff} of these nanoemulsions reached the ϕ_{MRJ} and the random-jammed network of nanodroplets provided them elastic behavior (G′ > G″). As such this gels were named as repulsive elastic solids Wilking et al. (2007), in this thesis they are referred as repulsive nanogels. Nanoemulsions prepared with non-ionic Tween 20 showed weak elastic behavior and yield under gravity, as the lack of charge cloud led to no further increase in ϕ_{eff}.

As the SDS concentration increased to 5 – 15 CMC, more counter ions from SDS molecules screens the surface charge around the droplets leading to a drop in ϕ_{eff} compared to 0.5 – 2 CMC nanoemulsions (although it remained around 0.5). However, depletion attractions generated by micelles in the continuous phase further improved nanogels' storage moduli (G′ >> G″) indicating stronger gel formation. At a still higher concentration (≥ 20 CMC SDS), G′

suddenly dropped leading to the formation of very weak gels. Theory of depletion interaction and OSF were used to calculate the interaction energies among the nanaodroplets. It was shown that gel strength increased with an increase in depletion attraction followed by sudden drop due to the appearance of oscillatory structural forces (OSF) at higher SDS concentrations. Tween 20 nanoemulsions, on the other hand, showed weak depletion attraction and their OSF regime starts at a lower emulsifier concentration compared to SDS, leading to weak gelation behavior.

4.2 Influence of droplet size on nanoemulsion gelation

4.2.1 Average droplet size

The Sauter mean droplet diameter (d_{32}) of 2 and 15 CMC nanoemulsions as a function of homogenization passes are shown in Figure 4.2.1. For both nanoemulsions d_{32} initially decreased with an increase in the number of passes, however, reached a plateau towards saturated droplet diameter (d_s) beyond the sixth pass. In each pass d_{32} of 15 CMC nanoemulsions are smaller than 2 CMC nanoemulsions. Mason et al. (2006) used an empirical equation to model such decrease in droplet size as a function of homogenization passes:

$$d = d_s\left[1 + k\exp(-N/N_s)\right] \qquad 4.2.1$$

where N_s is the characteristics number of passes where the exponential factor become 1/e and k is a dimensionless number depicting the ratio of initial droplet diameter to d_s. The model is fitted to the experimental data (solid line in Figure 4.2.1) and excellent fits were obtained for both nanoemulsions with different emulsifier concentrations ($r^2 > 0.99$). Saturated droplet diameters (d_s) for 2 CMC and 15 CMC nanoemulsions were 156.5 and 131.5 nm, respectively. The smaller d_s for 15 CMC nanoemulsions were due to the high emulsifier concentrations which facilitate a further reduction in d_{32}. The values of N_s ranged from 1 to 2 and the dimensionless number k equals to 6.9 and 5.6 for 2 and 15 CMC nanoemulsions, respectively. The values of k signify that the initial drop in d_{32} would be higher for 2 CMC nanoemulsions compared to 15 CMC. This could be due to the limiting efficiency of the homogenizer in further decreasing the droplet size beyond a lower limit even in the presence of excess emulsifier. The empirical equation also predicts that further decrease in droplet radii would not be possible, as the saturated droplet size

was reached. In fact by increasing the emulsifier concentration from 2 times CMC to 15 times CMC, only 1.2 times drop in d_s was observed.

4.2.2 Influence of droplet size on nanoemulsion viscosity

Viscosities of the nanoemulsions were measured as a function of shear rate for both 2 and 15 CMC nanoemulsions. Both nanoemulsions showed shear thinning behavior where viscosity decreased with increase in shear rate (as shown in Figure 4.1.3). The shear stress ($\boldsymbol{\tau}$) and shear rate ($\dot{\gamma}$) data from these measurements after each pass of homogenization were fitted to a two parameter Hershel-Bulkley (HB) model (r^2 ranged from 0.85-0.93 for 2 CMC and 0.88-0.94 for 15 CMC nanoemulsions):

$$\tau = \tau_{HB} + K\,\dot{\gamma}^{\,n} \qquad 4.2.2$$

where n is the flow behavior index, K is the consistency coefficient, τ_{HB} is the Herschel-Bulkley yield stress. For some nanoemulsions values of yield stress were negligible and hence a simple power law model ($\tau = K\,\dot{\gamma}^{\,n}$) was used to fit the data (r^2 ranges from 0.76 to 0.89).

The viscosities of the nanoemulsions at a shear rate of 10 s^{-1} was calculated from the models and average viscosities were plotted in Figure 4.2.2 as a function of a range of droplet size at different homogenization passes. Viscosity increased with a decrease in droplet size for both nanoemulsions, however the nature of increase was very different. For 2 CMC nanoemulsions, the increase in viscosity was gradual while for 15 CMC nanoemulsions the increase is much more brisk and two distinct regimes can be observed. For the first three passes the viscosities increased from 0.004 and 0.06 Pa·s, while starting from fourth pass a rapid jump in viscosity can be observed which continues until eighth pass (increase from 0.44 to 23.3 Pa·s). This behaviour suggests that the underlying mechanisms of the increase in viscosity for these two systems are different.

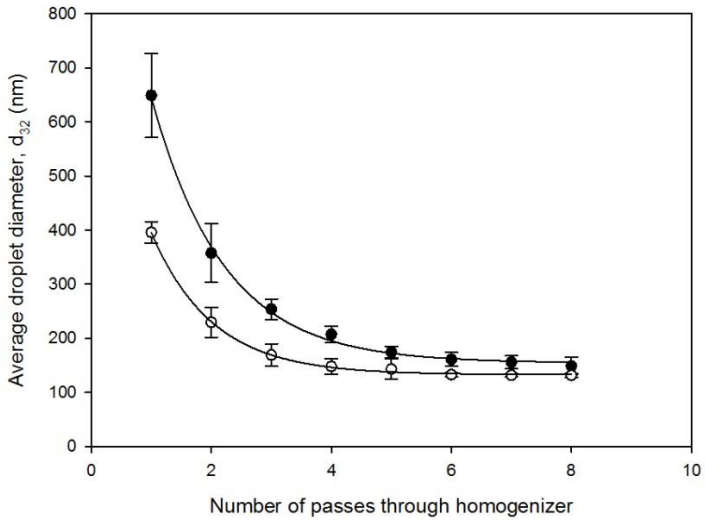

Figure 4.2.1 Effect of number of homogenization passes on the reduction in droplet size of 2 CMC (●) and 15 CMC (○) nanoemulsions. The lines represent the empirical model (eq 4.2.1) fit to the experimental data. Error bars represents ± one standard deviation (n=3).

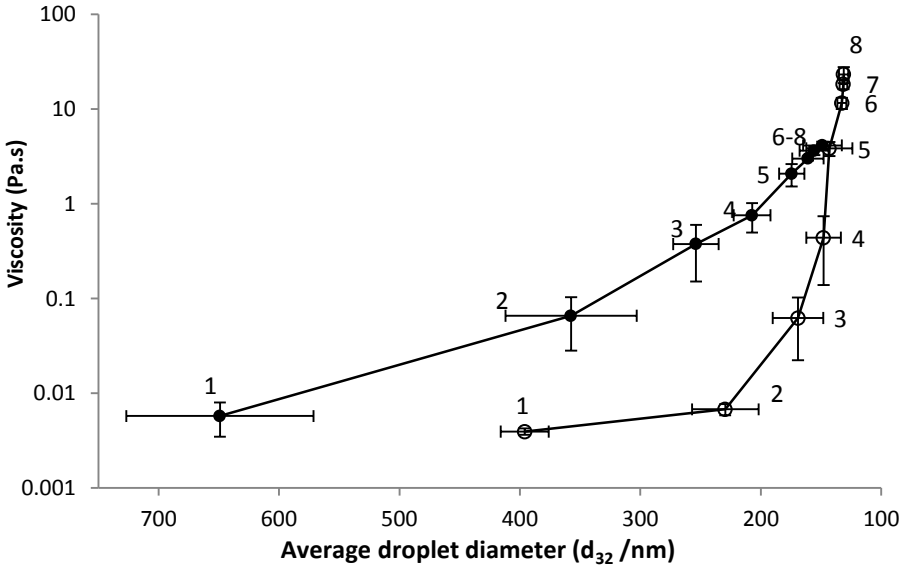

Figure 4.2.2 Change in viscosities of 2 CMC SDS (●) and 15 CMC SDS (○) nanoemulsions as a function of average droplet diameter (d_{32}) obtained after each pass through the homogenizer. Error bars represents ± one standard deviation (n=3). The horizontal error bars are because the average viscosity data were plotted at average d_{32} of the three replicates. The numbers in the graph represent the homogenization passes at each viscosity.

In order to understand whether the increase in viscosity of nanoemulsions resulted in restriction of flow behavior under their own weight, the yield stress (τ_{HB}) calculated from eq 4.2.2 was plotted as a function of number of homogenization passes (Figure 4.2.3). Until the fourth pass through the homogenizer, both emulsions had very low viscosities and did not show any yield stress. 2 CMC nanoemulsions showed observable yield stress starting from the fifth pass and the values increased from 10 Pa after fifth pass to 30 Pa after eighth pass. On the other hand, 15 CMC nanoemulsions showed measurable yield stress from the sixth pass where the values changes more rapidly from 30 Pa after sixth pass to 145 Pa after the end of eighth pass. Though the onset of yield stress for 15 CMC nanoemulsion appeared later than 2 CMC nanoemulsion the magnitude is comparable or even higher which can be comprehended by a swift change in the interactions between the nanodroplets in case of 15 CMC nanoemulsions (to be discussed later).

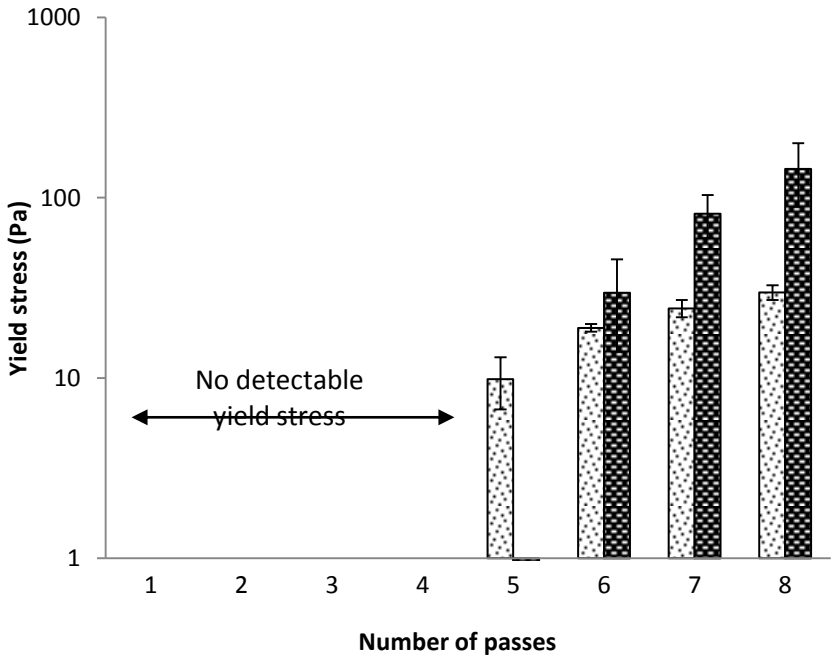

Figure 4.2.3 Yield stress values of 2 CMC (▒) and 15 CMC (▒) emulsions calculated from Hershel-Bulkley model as a function of a number of passes of homogenization. Error bars represents ± one standard deviation (n=3).

4.2.3 Influence of droplet size on nanoemulsion viscoelasticity

Storage and loss moduli (G′ and G″ respectively) of nanoemulsions at a constant frequency of 1 Hz were measured during strain sweep experiments (0.01 – 100% strain). Average data from each pass are shown in Figure 4.2.4. For 2 CMC nanoemulsions until third pass of homogenization, G″ is higher than G′ while after fourth pass G′ became greater than G″ although no sign of strong gelation was observed (no yield stress from Figure 4.2.3). Further homogenization transformed the nanoemulsions into nanogels which is evident from their large increase in G′ over G″ and appearance of yield stress. For 15 CMC nanoemulsions G′ became higher than G″ beginning fifth pass while the materials transformed into nanogel and showed yield stress beginning sixth pass. The linear viscoelastic region (LVR), where moduli are strain independent (below 2% strain), appeared from the fourth pass for 2CMC and fifth pass for 15 CMC nanoemulsions. For both nanoemulsions, at 5% strain, the linearity of G′ is ceased, and it is gradually dropped indicating yielding. At this strain, structural relaxation process occurs in the gel network which is manifested as a peak in the G″ values where it also crossed G′ (similar to the data reported in Figure 4.1.5). This crossover is termed as gel breakdown point. This type of behavior is ubiquitous for strong colloidal gels and has been observed by many researchers (Datta et al., 2011; Koumakis et al., 2011).

In order to compare how viscoelastic behaviour of nanoemulsions is influenced by their droplet size, G′ and G″ values at a constant strain (0.1 %) for all replicates were plotted against their average droplet diameter (d32) for both 2 and 15 CMC nanoemulsions. These values can be considered as plateau moduli, although for some earlier pass nanoemulsions plateau was not observed in the range of strain used. Similar to viscosity and yield stress viscoelastic behaviour of the nanoemulsions also evolved with a decrease in droplet size. In the case of 2 CMC nanoemulsions, G″ > G′ above 300 nm droplet size during the first two passes of homogenization. But with a decrease in droplet size the elastic nature superseded the viscous nature, and below 300 nm droplet diameter G′ became higher than G″ (Figure 4.2.5A). Similarly for 15 CMC nanoemulsions, G″ was initially higher than G′ at larger droplet sizes, however, below 150 nm (after around fourth pass) G′ dominated over G″ (Inset of Figure 4.2.5B). Similar to viscosity, elasticity of 2 CMC nanoemulsion gradually increased with reduction in droplet

size, however for 15 CMC nanoemulsions, elastic behaviour rapidly increased once the droplet size was below a critical level followed by a plateau in G' below 130 nm droplet size.

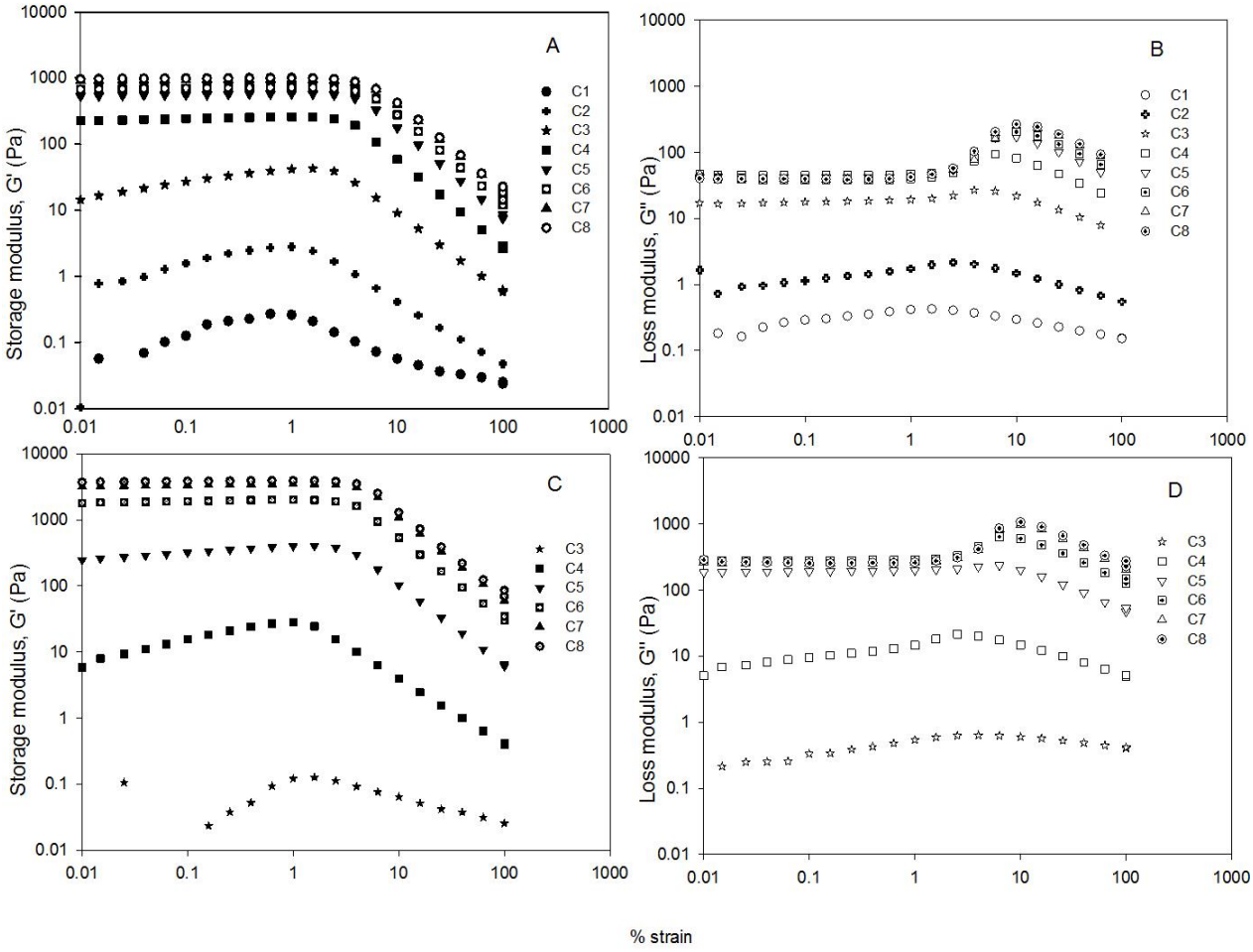

Figure 4.2.4 Average of oscillatory strain dependent storage (G′) and loss moduli (G″) of SDS nanoemulsions after different homogenization passes. (A) G′, (B) G″ of 2 CMC nanoemulsions; (C) G′ and (D) G″ of 15 CMC nanoemulsions. Note the difference in Y-axis scale between 2 and 15 CMC nanoemulsions. Standard deviations of the moduli are not shown for the same. For 15 CMC nanoemulsion data before the third pass (C3) are not shown, as the samples were too weak to show any gelation behaviour within the instrument limits.

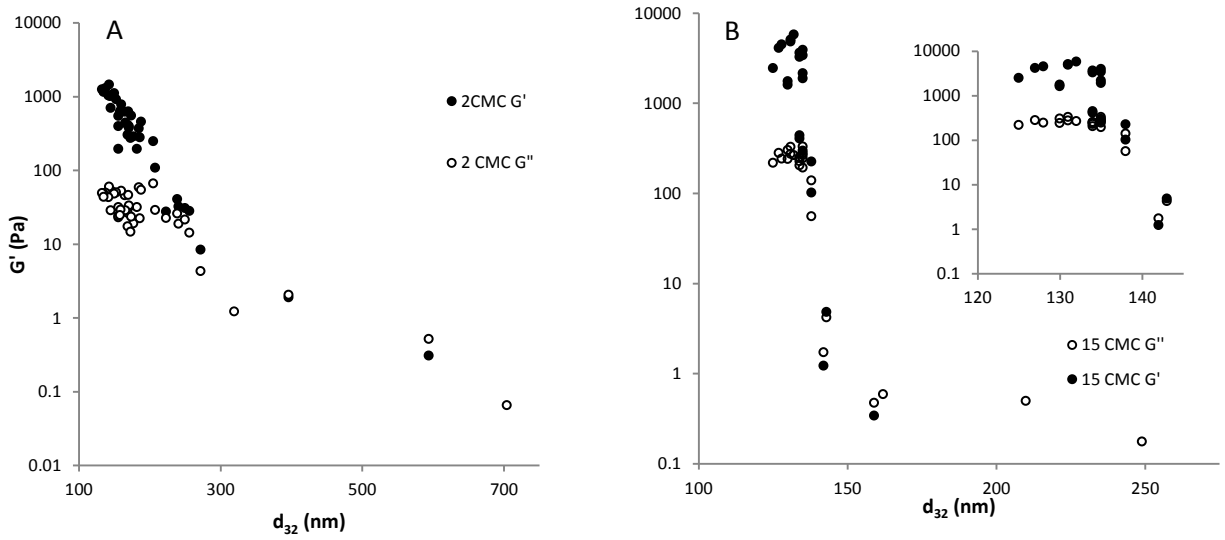

Figure 4.2.5 Characterization of the viscoelastic behavior of (A) 2 CMC and (B) 15 CMC nanoemulsions as a function of average droplet size (d_{32}). Values of storage (G′) (closed symbols) and loss (G″) (open symbols) moduli of emulsions (at a frequency of 6.28 rad/sec and 0.1% strain) were plotted from strain sweep measurements data. The inset shows a zoomed view of G′ and G″ of 15 CMC nanoemulsions from fifth to eighth passes. Note the difference in axis ranges for A and B.

4.2.4 Mechanism of gelation

The type of increase in gel strength as a function of droplet size was very different between the two different nanoemulsions discussed. In order to understand the mechanism of gelation, the effective droplet volume fractions for both nanoemulsions and the strength of the attractive interaction for 15 CMC nanoemulsions were calculated. Different regimes of gel transitions for both repulsive and attractive nanoemulsions were also predicted using the theories developed in the previous section.

4.2.4.1 Gelation in repulsive nanoemulsions

In repulsive 2 CMC SDS-stabilized nanoemulsions, gelation is effectively controlled by an effective dispersed phase volume fraction (ϕ_{eff}) which can be estimated from the interfacial shell layer thickness (δ).

The values for ϕ_{eff} were calculated from equations 2.3.5, 4.1.2 and 4.1.3 and plotted as a function of the number of homogenization pass in Figure 4.2.6. It can be seen that as the homogenization passes continue ϕ_{eff} increased. However the degree of increase for 2 CMC nanoemulsion (Figure 4.2.6A) is higher than 15 CMC nanoemulsions (Figure 4.2.6B). For 2 CMC nanoemulsions ϕ_{eff} increased from 0.46 to 0.78, whereas for 15 CMC nanoemulsions the maximum was 0.47. The lower ϕ_{eff} for 15 CMC nanoemulsions is due to the higher number of counterions influencing the debye screening length (δ). A plateau in the increase ϕ_{eff} was also observed in the case of 15 CMC nanoemulsions, this might be because of the plateau in a decrease of droplet size (see Figure 4.2.1). In order to understand how ϕ_{eff} influences G′ and G″, viscoelastic moduli of nanoemulsions from all replicates were re-plotted against ϕ_{eff} in Figure 4.2.7. In the case of 2 CMC SDS, both G′ and G″ gradually increased with ϕ_{eff}. A significant difference between G′ over G″ was observed when ϕ_{eff} is close to 0.60, indicating the development of viscoelastic behaviour in nanoemulsions. After that, as the ϕ_{eff} increased difference between G′ and G″ increased which led to improved gel strength.

It is well known that a repulsive emulsion transformed from a fluid into a viscoelastic gel as the volume fraction of droplets reached a critical value (ϕ_c) where the droplets become closely packed. However, if the viscoelastic behaviour of emulsions is followed as a function of dispersed phase volume fraction, two distinct transformations can be observed. An initial low volume fraction transition (at ϕ_{eff} = 0.55) when viscosity rapidly increased without any plateau in storage modulus. This is generally associated with glass transition (Mason et al., 1996). In this case the droplets simply are in a crowded state and form cage around each other without the need to deform as they do not touch each other. The volume fraction for this transition (ϕ_g) generally occurs at ϕ = 0.58 for monodispersed emulsions (Mason et al., 2014). In a colloidal glassy phase, each droplet can explore the free volume around them leading to an increase in the total entropy of the system. Any application of strain in this region would change the free volume thereby increasing the energy of the system that is stored as elastic modulus (Mason et al., 2014). Upon further increase in ϕ_{eff} the droplets' surface contact at a critical volume fraction (ϕ_c) above which the droplet become compressed leading to a dramatic increase in elasticity and appearance of yield stress (Ikeda et al., 2012). The droplet volume fraction at this transition from glassy to

jammed state are also known as critical volume fraction for maximal random jamming and is generally accepted as 0.64 for monodispersed emulsion droplets.

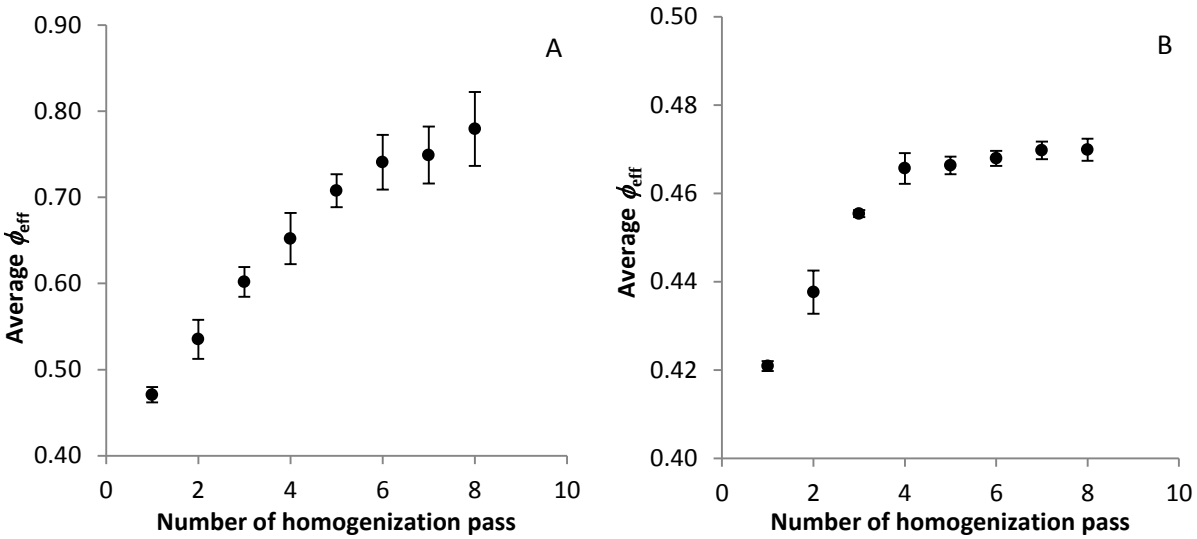

Figure 4.2.6 Average ϕ_{eff} as a function of the number of homogenization pass for (A) 2 CMC and (B) 15 CMC nanoemulsions. Note the scale difference on the y-axis between both A and B. Error bars represents ± one standard deviation (n=3).

From the strain sweep data in Figure 4.2.4A, it can be seen that plateau in G′ appeared at fourth pass, although the emulsion did not show any yield stress (Figure 4.2.3) in rotational shear experiments. This indicates that the nanoemulsions at fourth pass were not strictly in a jammed state, rather in a transition state from glassy to jammed state. Beyond fourth pass ϕ_{eff} reached a critical value (0.64) (Figure 4.2.6A) which led to jamming of droplets and the much wider difference between G′ and G″. Therefore, it can be said that the gelation in 2 CMC nanoemulsion is controlled by ϕ_{eff} that resulted in the fluid to glassy to jamming transition.

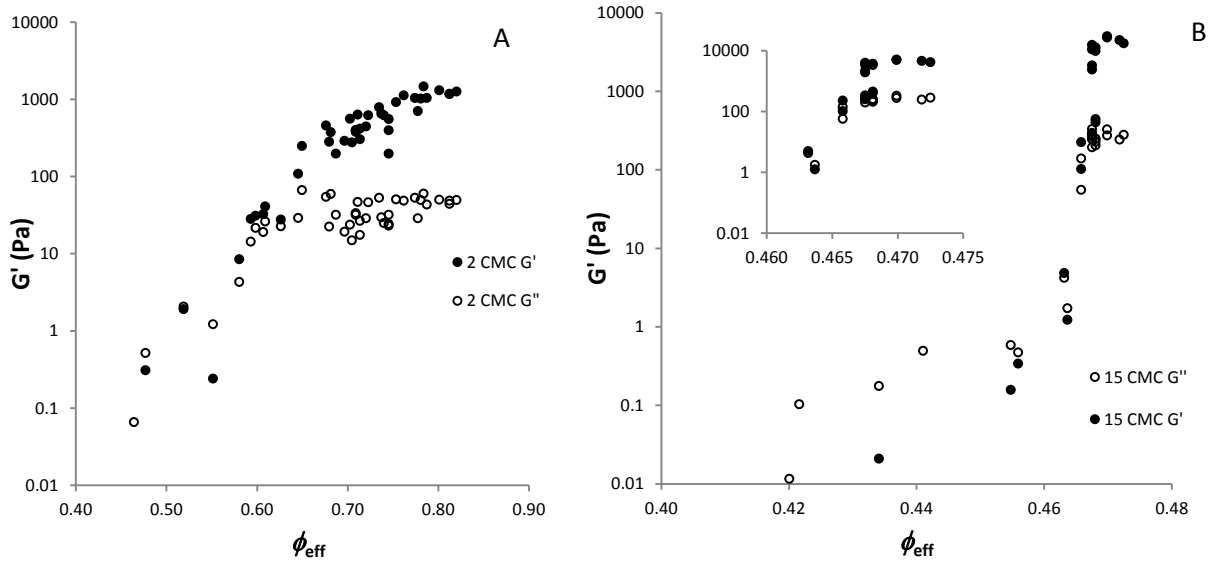

Figure 4.2.7 Characterization of the viscoelastic behavior of (A) 2 CMC and (B) 15 CMC emulsions as a function of ϕ_{eff}. Values of storage (G′) (closed symbols) and loss moduli (G″) (open symbols) of nanoemulsions (at a frequency of 6.28 rad/sec and 0.1% strain) were plotted from strain sweep measurements data against ϕ_{eff}. The inset shows a zoomed view of G′ and G″ of 15 CMC nanoemulsions from fifth to eighth passes. Note the difference in the x-axis for between both the graphs, which was needed to represent the data points more clearly and depict the differences in gelation mechanisms.

4.2.4.2 Gelation in attractive nanoemulsions

Unlike repulsive nanoemulsions, gelation in attractive 15 CMC SDS-stabilized nanoemulsions cannot be solely explained by ϕ_{eff}. For attractive nanoemulsion ϕ_{eff} increased from 0.42 to 0.47 from first through the eighth pass of homogenizer (Figure 4.2.6B) while the gel strength (G′) dramatically increased from 0.02 Pa to 5019 Pa (Figure 4.2.7B). For the first three passes, although ϕ_{eff} increased from 0.42 to 0.45, the nanoemulsions remain liquid with G″>G′. The crossover from liquid-like behaviour (G″>G′) to solid-like behaviour (G′>G″) was observed at ϕ_{eff} close to 0.465, much below than the ϕ_{eff} of 0.55 for repulsive nanoemulsions. Thereafter, a rapid increase in G′ was observed as the ϕ_{eff} increased from 0.46 to 0.47. In this case, excess micelles induced depletion attraction resulted in the formation of a tenuous network of aggregated droplets that prevented the flow of water thereby converting a liquid nanoemulsion

into a gelled system. Datta et al. (2011) observed that such attractive interactions can result in the elasticity in emulsions at much lower ϕ compared to repulsive emulsions where elasticity appears due to the close packing or cage formation of droplets at higher volume fraction (2 CMC nanoemulsion in the present case).

The depletion interaction energy (W_D) for 15 CMC SDS-stabilized nanoemulsions were calculated according to the theory developed by Petsev et al. (1995). Details of the calculations are shown in section 4.1. Figure 4.2.8 shows the calculated values of depletion interaction energy, expressed as W_D/k_BT, as a function of ϕ_{eff}. It can be seen that the depletion interaction energy drops with an increase in ϕ_{eff} or decrease in droplet size. With a decrease in the droplet size interfacial area is also increased which led to adsorption of emulsifiers from the continuous phase resulted in a drop in excess micelles. As the presence of excess micelles is directly proportional to the osmotic pressure (P_o) in the continuous phase, decrease in droplet size resulting in a continuous drop in depletion attraction energy (eq 4.1.5). However, the nature of the depletion attraction energy for the nanoemulsions raised two situations that must be discussed in order to understand attractive nanoemulsion gelation. First of all, if gelation in the nanoemulsions is due to attractive interactions among the nanodroplets, why samples from the first three passes of homogenization did not show any gelation behaviour where their attractive interactions were highest? Secondly, why is the drop in depletion attraction energy and droplet size accompanied by a rapid increase in elastic moduli of the nanoemulsions as shown in Figure 4.2.8?

To answer the first question we looked into how the of balance between the interdroplet interactions changes in presence of excess micelles. It is known that the presence of excess micelles in the interdroplet region would lead to depletion attraction. However, very high concentration of nanoscale particles or micelles in the interdroplet regions would form layered structure around the droplets where, depending on their concentration, at least one layer of micelles may always stay between the droplets (Basheva et al., 2007). As the droplet approach each other layers of micelles move out and the interdroplet interaction oscillates between positive (repulsion) and negative (attraction) values with the period of oscillation equal to the effective diameter of the micelles. When the approaching droplets face a layer of micelles, the interaction reaches repulsive maxima. On further approach, the layer of micelles is squeezed out

from the interdroplet region resulting in attractive minima as the droplets come closer to fill the area left void by the micelle layer. Finally, when the interdroplet distance becomes equal to one *micelle effective diameter*, a lot of energy is needed to remove the final layer (>>k_BT) and that layers stays in between the droplets as a final repulsive barrier (Basheva et al., 2007). This type of interactions known as oscillatory structural forces (OSF) are responsible for depletion stabilization resulting in a fluid-like behaviour (G″>G′) of the emulsions (section 4.1.9). Similar transformation from depletion flocculation to depletion stabilisation has also been observed in other studies (Richetti et al., 1992; Petsev et al., 1995; Christov et al., 2010; James et al., 2014a). In the present case, for the first three passes of homogenization droplet sizes are fairly large with lower interfacial area resulting in lot of free emulsifiers which led to an interdroplet interaction that stays in the structural force regime. After the fourth pass, as the droplet diameter dropped below 150 nm, more emulsifiers were adsorbed on the newly created interfacial area leading to a decrease in excess micelle concentration in the continuous phase. This transformed the net interdroplet interactions into depletion attraction resulting in droplet aggregation and gelation (G′>G″).

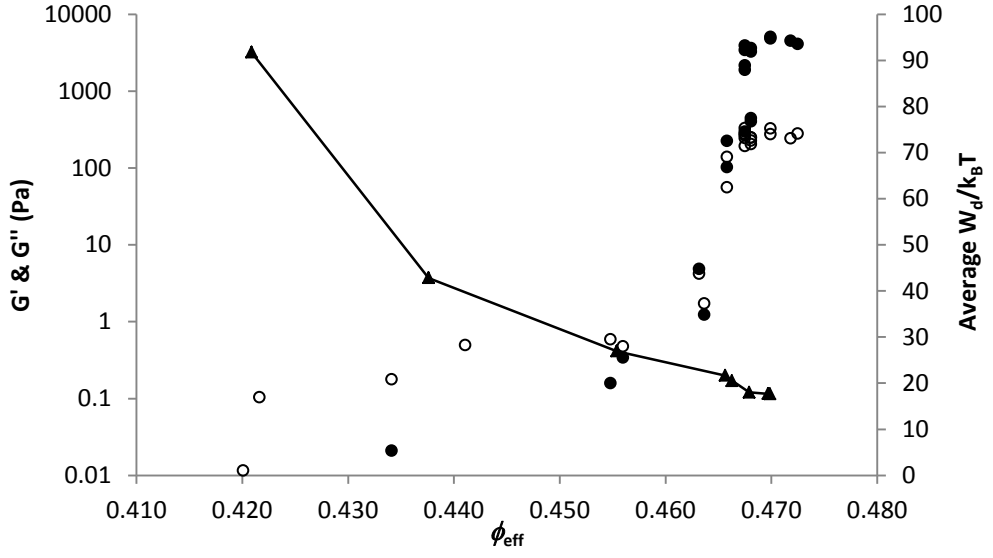

Figure 4.2.8 Storage (G′) (●) and loss moduli (G″) (○) of 15 CMC nanoemulsions as a function of ϕ_{eff}. Secondary axis has average W_d/k_BT values calculated for nanoemulsions after each homogenization pass.

Next, theory of the mechanism of gelation in attractive nanocolloids are used to understand the increase in gel strength with a decrease in droplet radius above ϕ_{eff} of 0.465. It has been proposed that when strong attraction is introduced (energies in the range of 10 – 20 times k_BT), gel transition in emulsion can occur at low volume fraction where the droplets stick to each other by diffusion limited cluster aggregation (DLCA) and form tenuous fractal cluster whose network connectivity fills space and provides elastic properties (Guo et al., 2011). Trappe et al. (2001) developed a generalized phase diagram for jamming transition in attractive hard spheres where a critical phase boundary (from fluid to gel) was observed at low volume fraction characterized by sharp rise in elasticity of the fractal network. For systems with weaker attraction, gelation requires higher volume fraction. Numerous theories have been proposed in order to explain the mechanism of gelation in these weakly attractive emulsions. Lu et al. (2008) proposed that in weakly attractive system (a few k_BT) gelation is induced by spinodal decomposition where thermodynamic instability driven phase separation led to spanning clusters that dynamically arrest to form gel. On the other hand, at a high volume fraction, crowding of droplets resulted in amorphous colloidal glasses even at the weak attraction. In this case, the droplets are said to be trapped in cages formed by nearest neighbours (Trappe et al., 2004). In both low volume fraction fractal gel or high volume fraction attractive glass, bonding between the droplets lead to higher constraints against particle movement and the elasticity of the attractive systems appears at lower volume fraction than that of maximal random jamming for repulsive emulsions (Datta et al., 2011; Koumakis et al., 2011). Experimentally this was observed by Dutta et al. (2011) for gelation in silicon oil-in-water emulsion stabilized by SDS where repulsive or attractive interactions were controlled by concentration of SDS (as in the case of the present study). Interestingly the authors observed two peaks in the loss modulus during yielding of attractive emulsions above close packing while those below yielded with one peak as in the case of repulsive emulsions (Datta et al., 2011). The two step yielding of attractive colloids were also studied in more details by Koumakis et al. (2011) who proposed that yielding of both close-packed attractive glass and fractal gel is a two-step process (two peaks in G″).The first yield strain (corresponding to the first peak in G″) was attributed to inter-cluster bond breaking while the second yield strain at higher value was due to breaking of clusters into individual particles (Koumakis et al., 2011; Shao et al., 2013). Nevertheless, only for high ϕ attractive glass the

second yielding and corresponding second peak in G″ would be visible before the crossover of G′ and G″ while for low ϕ attractive fractal gels fluid-like flow behaviour due to G′ < G″ cross over would supersede the second peak. In the present case, the two-step yielding of G″ was not observed for any nanoemulsions (Figure 4.2.4). Therefore it can be concluded that these elastic nanoemulsions fall within the category of fractal gels. The fact that ϕ_{eff} of the nanoemulsions with highest gel strength (0.473) is far below the limit of glass transition (0.58) and close packing (0.64), also support this hypothesis.

From Figure 4.2.8 it is also evident that a very small increase in ϕ_{eff} from 0.465 to 0.473 and corresponding decrease in W_d/k_BT from 21 to 17 has manifested a multitude of increase in the G′ from 223 to 4066 Pa. In order to understand this effect, droplet size and a corresponding increase in the number of droplets from fifth pass to eighth pass of homogenization were evaluated. The surface average mean droplet diameter (d_{32}) in this case decreased from 143 nm after fifth pass to 131 nm after eighth pass. Once again, this small decrease in mean droplets diameter does not explain such a large change in elasticity. It should be noted that the d_{32} values are sensitive towards smaller droplets while the effect of a few large droplets is neglected. If we consider volume-weighted mean droplet size (d_{43}) it can be seen that the average size decreased from 193 nm after fifth pass to 158 nm after the eighth pass (data not shown). This decrease is significant and is due to breaking a few large droplets into many small droplets. As the number of droplets increased there are more attractive bonds among them, which resulted in the larger fractal network that can occupy more space (Lu et al., 2013). Buscall et al. (1988) have shown that when aggregated networks of polystyrene spheres were subjected to compressive forces (e.g. in a centrifuge) the yield stress can be scaled with particle size (r) by $r^{-2.3}$. Therefore, the compactive strength of clusters, which is also proportional to elastic modulus (G′), is higher for smaller droplet sizes. Similar observation of effect of particle size on colloidal gelation was also observed by Bi et. al. (2014) during their study on effect of homogenization on the rheology and microstructure of acid induced soy protein isolate gels. It was reported that high shear homogenization decreased both the average particle size and their polydispersity index which resulted in a higher gel strength with reduced void space and more compact gel microstructure. Therefore it can be said that the rapid increase in gel strength of 15 CMC SDS-stabilized

nanoemulsions from fifth to eighth pass of homogenization could be due to stronger fractal network formation by decrease in droplet size and simultaneous increase in number of droplets.

4.2.5 Summary

In this section, the influence of droplet size on the gelation of both repulsive and attractive nanoemulsions was investigated. In repulsive emulsions, the counterion shell layer around the droplets had contributed to a significant increase in ϕ_{eff} with a decrease in droplet size. At higher droplet size (>250 nm), the emulsions existed as fluids where G′ < G″. As the droplet size decreased further below 200 nm, ϕ_{eff} of these emulsions got closer to the glass transition limit at which G′ > G″ and the liquid like nanoemulsions are transformed into weak gels with no yield stress. With further decrease in droplet size below 180 nm, the glassy nanoemulsion entered jamming transition where the droplets are jammed into cage formed by surrounding droplets. At this point, the G′ >> G″ and the liquid like emulsions are transformed into strong nanogels. The yield stress of these nanoemulsions also suggests the same.

In contrary, for attractive nanoemulsions decrease in droplet size manifested a different mechanism of gelation. An initial fluid-like emulsion (G′ < G″) transformed into nanogels below a critical droplet size where a rapid increase in gel strength was observed with a decrease in droplet size. The strength of the attractive interaction (W_d/k_BT) also decreased with a decrease in droplet size, which was attributed to drop in micelle concentration as more emulsifier molecules got adsorbed on the newly created interfacial area. It was proposed that despite higher W_d/k_BT, the fluid like behaviour of large droplet size nanoemulsions was due to structural forces generated by the presence of higher micelle concentrations (depletion stabilization). With a decrease in droplet size and a corresponding drop in micelle concentration, the interdroplet interaction transformed from structural force into depletion attraction. This led to gelation by the fractal network in nanodroplets. Although the rapid increase in G′ cannot alone be explained by W_d/k_BT, decrease in droplet size and corresponding increase in their number might have an integral impact on the fractal nature of the aggregates thus influencing gelation behaviour of the attractive nanoemulsions.

4.3 Effect of oil concentration on repulsive gelation

4.3.1 Average droplet size

Figure 4.3.1 represents the decrease in sauter mean diameter d_{32} of emulsions as a function of number of passes through the homogenizer for both LER and HER nanoemulsions. Depending on ϕ, some of the emulsions coming out of the homogenizer became thick gels before seventh pass and further homogenization could not be continued, hence droplet sizes for these nanoemulsions ($\phi = 0.45$, 0.50 and 0.60) are not shown for all passes. It is apparent from the figure that droplet size decreased with an increase in number of passes through the homogenizer and after about sixth pass it reached a plateau. The plateau droplet radii for HER nanoemulsions were slightly smaller than LER nanoemulsions. Also, at comparable ϕ between both the nanoemulsions, droplet size decreased with an increase in emulsifier concentrations.

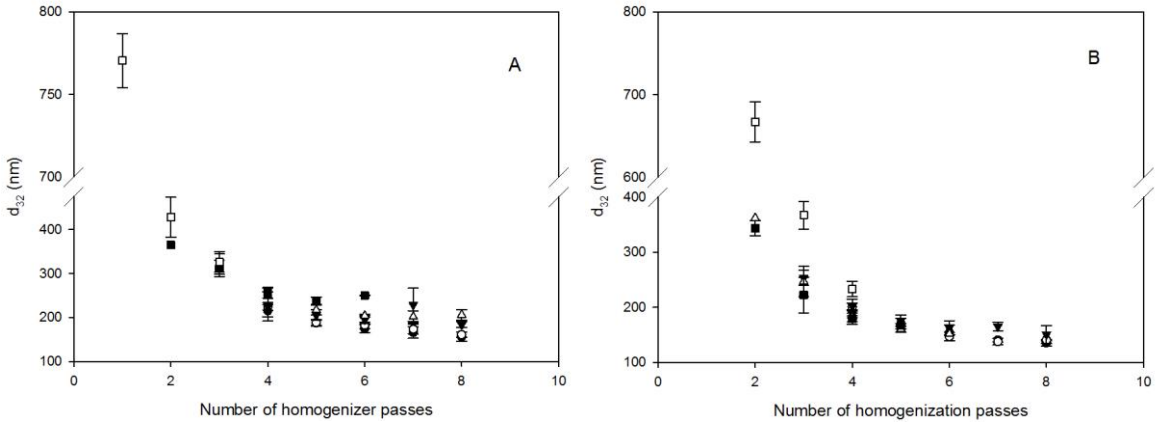

Figure 4.3.1 Average droplet diameter (d_{32}) as a function of number of homogenization passes for (A) LER and (B) HER nanoemulsions with dispersed oil phase volume fractions: 0.30(●), 0.35(○), 0.40(▼), 0.45 (Δ), 0.50(■), 0.60(□). Difference in the ranges omitted on y-axes to accommodate all the data points with clarity in the respective plots. Error bars represents ± one standard deviation (n=3).

4.3.2 Effect of ϕ on viscosity of repulsive nanogels

To understand the influence of oil concentration and droplet size on the bulk rheology of nanoemulsions, their viscosities after different homogenization passes were plotted as a function

of ϕ and droplet radius in a three dimensional graph in Figure 4.3.2. Overall viscosity increased with increase in oil volume fraction, however, at each oil volume fraction there is a range of viscosity that varies from low to high values depending on the droplet diameter. At a constant oil volume fraction viscosity increased with a decrease in droplet diameter. Therefore, it can be concluded that the rheology of repulsive emulsions cannot be explained by either droplet size or ϕ, rather a combined effect of both along with the interdroplet interactions would be necessary.

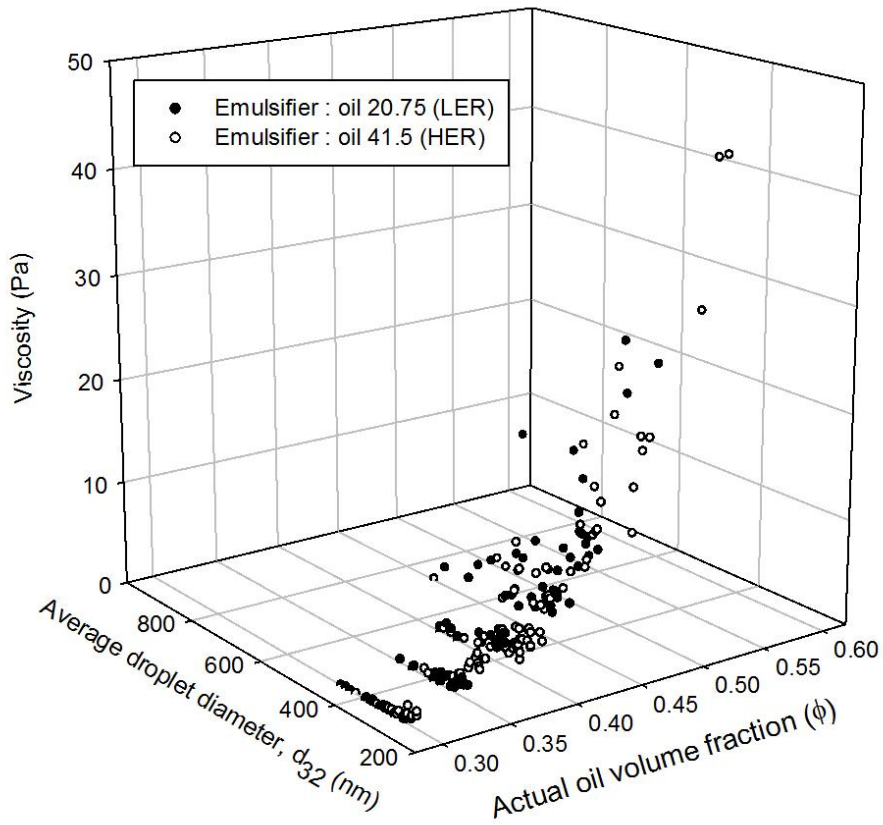

Figure 4.3.2 Apparent viscosities (at a shear rate of 10 s^{-1}) as a function of actual ϕ and average droplet diameter of repulsive SDS emulsions. Data for both LER (○) and HER (●) nanoemulsions are shown.

As explained in section 2.5.1.4 ionic emulsifiers at the droplet surface give rise to counterion charge cloud which acts like shell layer around them and increases the net ϕ of nanoemulsions by a volume equal to the volume of the combined electrical double layers of all

droplets. The effective oil phase volume fraction (actual plus the thickness of the electrical double layer), given by ϕ_{eff}, could be calculated using the theory described in section 4.1.7.

The calculated values of ϕ_{eff} for all emulsions at different ϕ was plotted as a function of droplet diameter in Figure 4.3.3. It can be seen that the decrease in droplet size as a function of homogenization pass at a constant ϕ propelled an increase in ϕ_{eff} for all emulsions. In fact, ϕ_{eff} increased to as much as 0.8 even at ϕ as low as 0.3 due to a reduction in droplet sizes to nanoscale and formation of charge cloud of comparable size around the droplets. At a comparable actual oil volume fraction, ϕ_{eff} is higher for LER nanoemulsions. This could be due to higher SDS concentration resulting in higher Na^+ counterions to screen the droplet charge thereby reducing effective electrical double layer around the droplets.

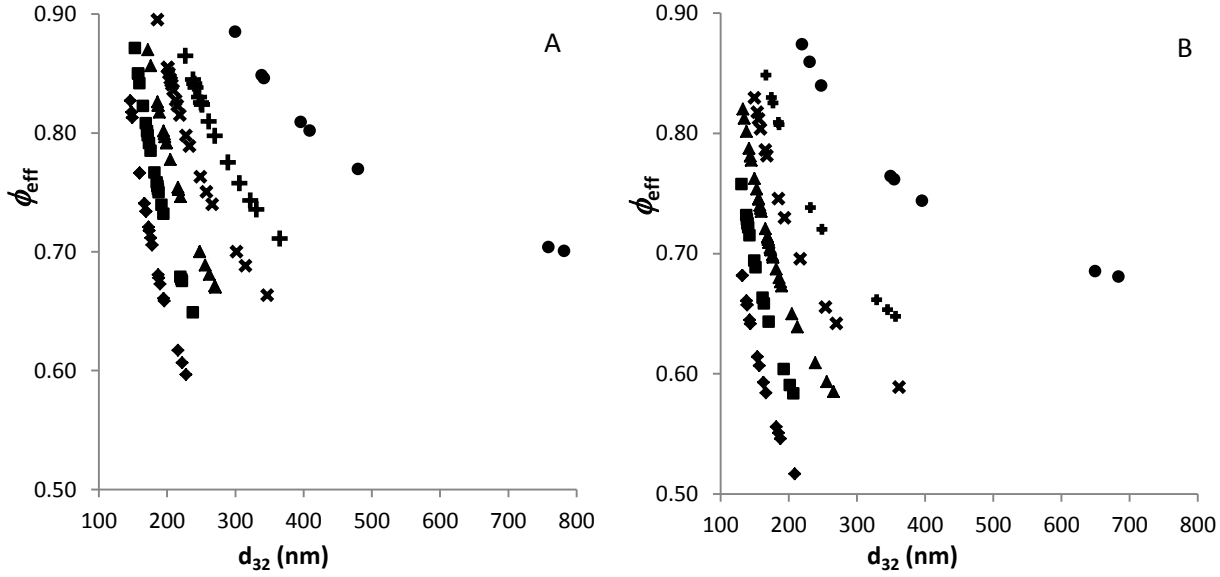

Figure 4.3.3 ϕ_{eff} as a function of average droplet diameter (d_{32}) at different dispersed phase oil concentrations: 0.3(♦), 0.35(■), 0.4(▲), 0.45 (x), 0.5(+), 0.6(●) at SDS emulsifier concentrations of (a) 1 CMC and (b) 2 CMC.

Next, viscosity data from Figure 4.3.2 and ϕ_{eff} data from Figure 4.3.3 were re-plotted in Figure 4.3.4. It is evident that the viscosity of the emulsions can be better described by the effective oil phase volume fraction (ϕ_{eff}) rather than their actual oil volume fraction alone. Initially viscosity of both emulsions increased gradually with an increase in ϕ_{eff}. However near a

critical value viscosity rapidly increased with just a small change in ϕ_{eff}. Similar behavior of viscosity was also observed by other researchers (McClements, 2005; Qian et al., 2011; Ikeda et al., 2012) and was explained by the appearance of a state where emulsion droplets along with its charge cloud approach each other with close proximity. When the droplets with their charge cloud overlap leading to close packing and deformation their viscosity increased sharply to a very high value. This situation is also referred to as maximal random jamming (Mason et al., 1995; Qian et al., 2011). The critical volume fraction (ϕ_c) for this jamming transition can be observed above 0.8 ϕ_{eff} for LER nanoemulsions, while for HER nanoemulsions it is just above 0.7 ϕ_{eff}. This could be due to emulsion polydispersity, which is higher for LER nanoemulsions (data not shown). In highly polydispersed emulsions numerous small droplets can be packed in the interstices of larger droplets, therefore the jamming transition is observed at a higher volume fraction (Groot et al., 2011). Moreover, the rapid rate of increase in viscosity for HER nanoemulsion (Fig 4.3.4B) was not observed for LER nanoemulsions (Fig 4.3.4A). This might be due to the critical ϕ_{eff} required for the rapid rise has not been approached by the LR nanoemulsions due to its higher polydispersity. .

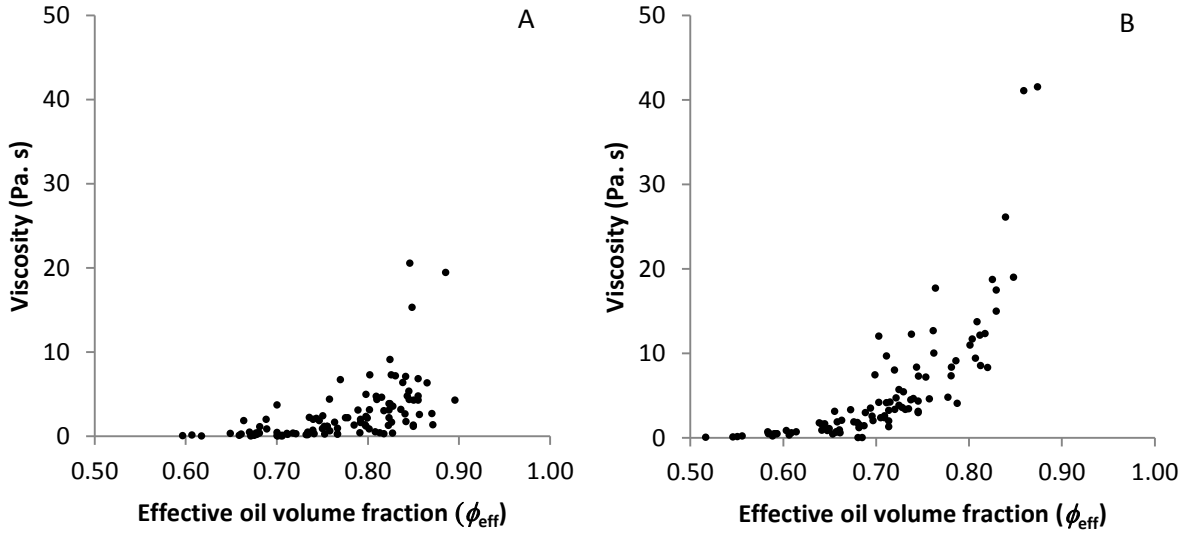

Figure 4.3.4 Viscosity as a function of effective oil phase volume fraction (ϕ_{eff}) of repulsive (A) LER and (B) HER nanoemulsions.

4.3.3 Viscoelastic properties of repulsive nanogels as influenced by ϕ

Figure 4.3.5 depicts the evolution of average storage (G′) and loss moduli (G″) as a function of % strain obtained from strain sweep measurements (at a constant frequency of 9.8 rad/sec) for all nanoemulsion gels after their final pass of homogenization. For all these nanoemulsions, G′ remains higher than G″ below a certain critical strain thereby confirming their gelled state. It is evident that with an increase in ϕ there is an increase in the magnitude of G′ and G″. Except for LER nanoemulsion at $\phi = 0.3$, the moduli are independent of strain below 2% resulting in a linear viscoelastic region (LVR). Beyond LVR, for all nanoemulsions G′ gradually dropped beginning 5% strain which marks the loss of gel strength. At the same time, a peak in G″ is observed due to the structural relaxation process in the gel (Figure 4.3.5 B and D). During this structural relaxation close-packed droplets start to rearrange before the emulsions begin to flow, a behavior manifested by the crossover of G″ over G′. This crossover point is usually termed as yield strain (Datta et al., 2011). Despite the increase in gel strength, the common behaviour of drop in G′ at a constant value of strain (yield strain) is intriguing and was also observed by Pham et al. (2008). However, the reason for this is not yet understood.

To understand the influence of ϕ_{eff} on the elastic properties of nanoemulsions in more detail, the plateau storage moduli (G'_p) of all individual emulsions at 0.1% strain (within the LVR region) obtained from strain sweep measurements were plotted in Figure 4.3.6 as a function of ϕ_{eff}. It can be seen that the initial rapid increase in G'_p values slow down at as ϕ_{eff} approach 0.9. Similar behavior of initial rapid increase (at ϕ_{eff} =0.64) followed by a slow increase of G'_p (at ϕ_{eff} =0.7) was observed by many researchers (Wilking et al., 2007; Graves et al., 2008; Scheffold et al., 2014). The G'_p values for LER nanoemulsions (filled symbols in Figure 4.3.6) are more scattered and shifted towards higher values of ϕ_{eff} similar to the viscosity results which was attributed to the higher polydispersity index of droplet size distribution for low emulsifier nanoemulsions.

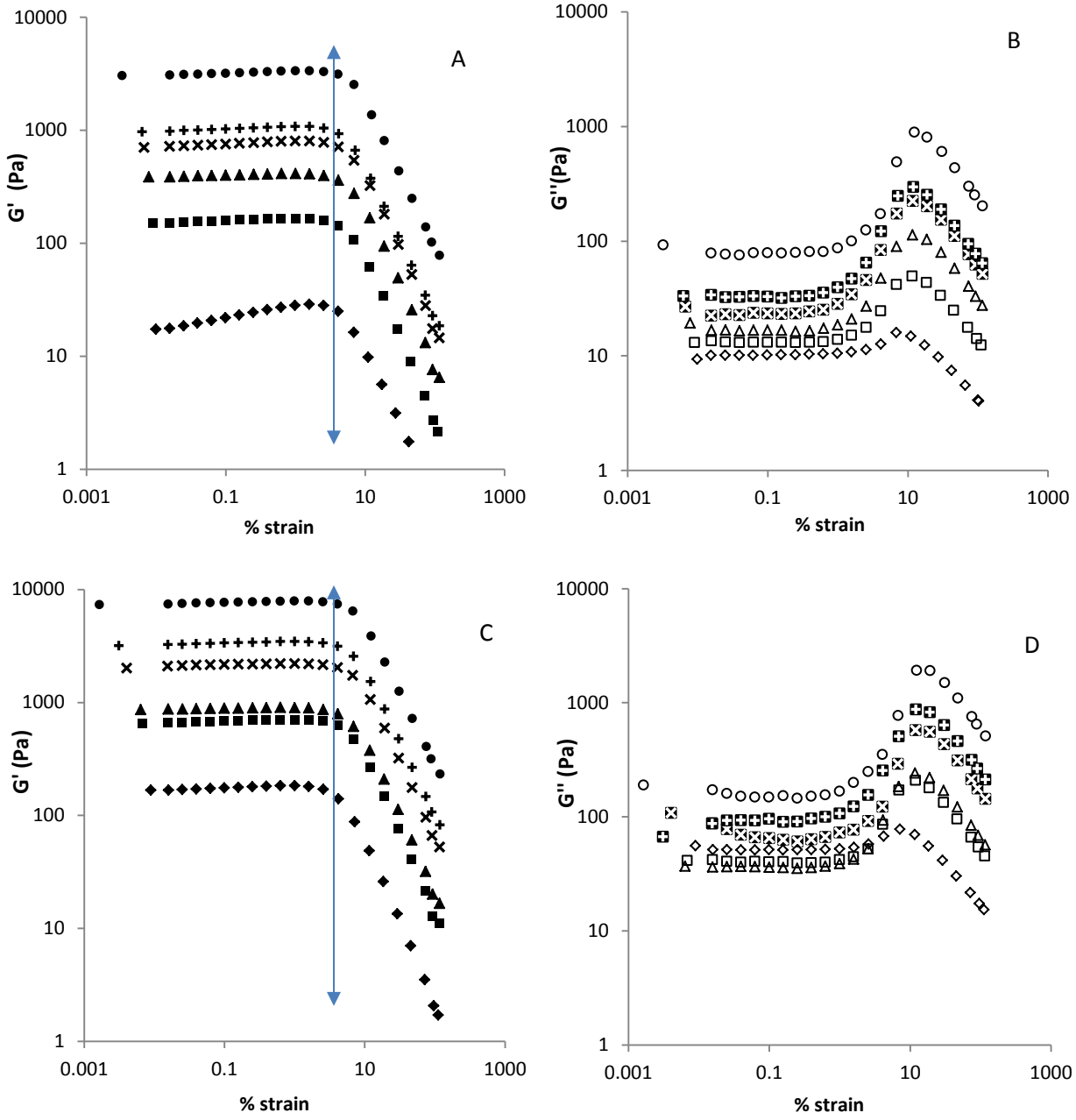

Figure 4.3.5 Storage (G′) (closed symbol) and loss moduli (G″) (open symbol) as a function of % strain obtained from strain sweep measurements at a constant frequency (1Hz) for LER (A and B) and HER (C and D) nanoemulsions at different dispersed phase oil concentrations: 0.3(♦), 0.35(■), 0.4(▲), 0.45 (x), 0.5(+), 0.6(●). The arrow indicates the deviation of G′ from LVR at similar % strain.

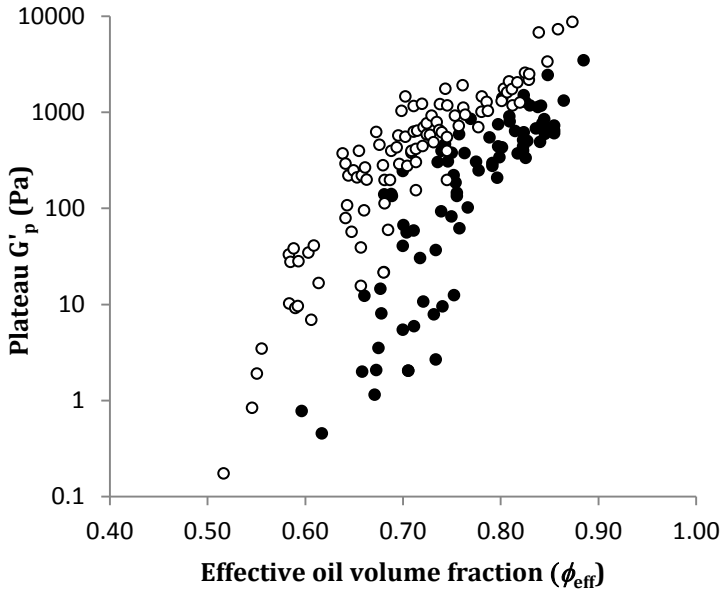

Figure 4.3.6 Plateau storage moduli (G'_p) of all individual nanoemulsions at 0.1% strain obtained from strain sweep measurements as a function of $\phi_{eff.}$ Filled symbols represent LER nanoemulsions while open symbols represent HER nanoemulsions.

4.3.4 Modelling the gel strength of repulsive nanogels

From Figure 4.3.6 it is apparent that close packing of droplets resulted in a rapid increase in G′ as ϕ_{eff} approached ϕ_c. Upon further increasing ϕ_{eff} above ϕ_c the droplets comes in contact and their surface get compressed. This compression results in the storage of additional energy leading to a dramatic increase in elasticity (G′). The energy scale that controls the deformation of droplets is their internal Laplace pressure given by γ/r, where γ is interfacial tension and r is the droplet radius. The ϕ_c at which droplet compression occurs is also denoted by jamming transition volume fraction (ϕ_j). Above the jamming transition when the droplets are close packed, shear elastic modulus is dependent on the droplet interaction potential and the connectivity of stress-bearing droplet network characterized by excess number of contacts between the droplets than that is at the jammed state ($\phi > \phi_j$). Using this concept Scheffold et al. (2013) developed an analytical expression for the elastic modulus of jammed emulsion as a function of droplet volume fraction. Their prediction also matched closely with the semi-empirical formula for elasticity of monodisperse nanoemulsions developed by Mason et al. (1995):

$$\frac{G_p'}{\gamma/R} = K\,\varphi\,(\varphi - \varphi_j) \qquad 4.3.1$$

where G'_p, the plateau elastic modulus of jammed emulsions is scaled by Laplace pressure (γ/R) and K is a constant which combines the dimensionless shear coupling parameter and the interfacial-entropic coupling parameter (Mason et al., 2014). Similar scaling expression for elastic modulus of jammed emulsions has also been used to fit experimental results before (Princen et al., 1986). These studies have shown that the critical volume fraction for maximal random jamming is 0.64 for monodispersed emulsion droplets. Here our aim was to determine the critical volume fraction needed for jamming transition in case of regular polydispersed nanoemulsions, so the above model was applied to the data with ϕ_j used as a fitting parameter (Figure 4.3.7). The fit of the model to our data gave r^2 values of 0.35 and 0.47 for LER and HER nanoemulsions, respectively. This is because the empirical model has been derived based on monodisperse emulsions, so it's fit to these emulsions with a wide range of polydispersity (span of droplet size distribution varying from 4.7 to 1.9) are not great. Span is a qualitative estimation of polydispersity and the values were obtained from the particle size distribution data using the formula $span = (d_{90} - d_{10}/d_{50})$, where the values indicated 10^{th}, 50^{th} and 90^{th} percentile droplet size. This also suggests that the decrease in polydispersity allows for a better fit to the model. The model predicts a ϕ_j of 0.69 and 0.71 for LER and HER nanoemulsions, respectively. The ϕ_j of both nanoemulsion systems is in agreement with polydisperse emulsions measured using the similar scaling law (Princen et al., 1986), which was also supported by other studies (Kraynik et al., 1991; Schaertl et al., 1994). For both the nanoemulsions the model predicts a steep increase in the G′ near ϕ_j, above after which it seems to attain a plateau. Simulation and experimental studies on monodisperse emulsions have shown that this scaling law holds well between the limit of $\phi_j \geq \phi_{eff} \leq 0.80$, where the jamming regime results in a weak deformation of droplets but not in the limit where there is a significant deformation ($\phi_{eff} \geq 0.80$) (Mason et al., 1995; Mason et al., 2014). However, in the present case of polydisperse emulsions this might occur at higher $\phi_{eff} \geq 0.9$

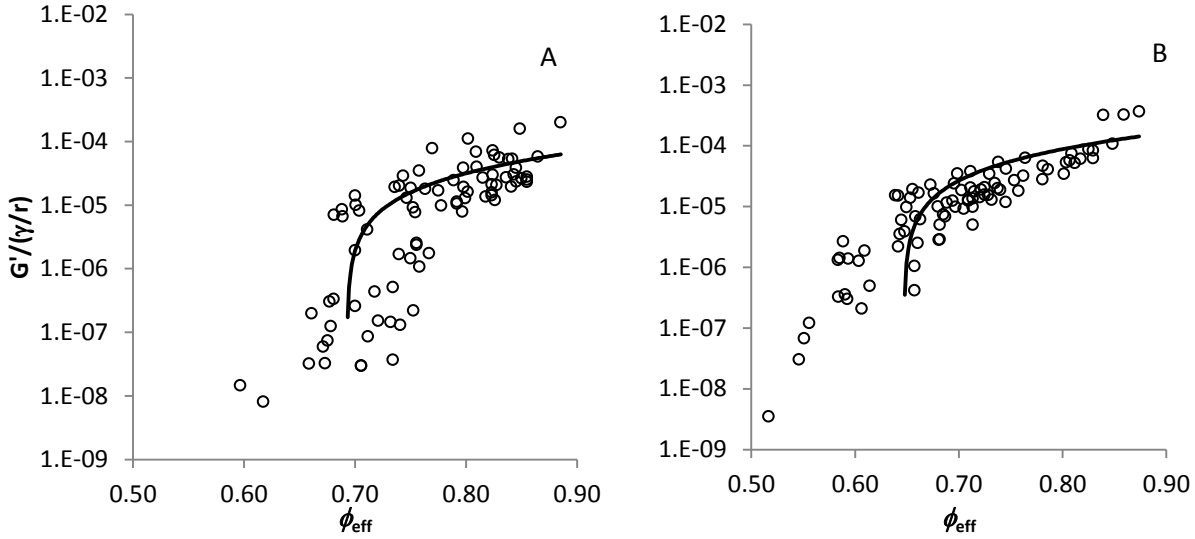

Figure 4.3.7 Elastic moduli (G′ from Figure 4.3.6) scaled with Laplace pressure as a function of ϕ_{eff} obtained from strain sweep measurements at different dispersed phase oil concentrations: 0.3(♦), 0.35(■), 0.4(▲), 0.45 (x), 0.5(+), 0.6(●) for (A) LER and (b) HER nanoemulsions. r^2 values are 0.35 and 0.47 for the LER and HER nanoemulsions respectively.

The jammed state model assumes that elasticity vanishes below ϕ_j, and it predicts a continuous drop in G′ at ϕ_j, which can be seen in Figure 4.3.6. However, in the actual case below random jamming the droplets remain in a crowded state and form cage around each other without the need to deform as they do not touch. This is termed as colloidal glassy phase (as shown in Figure 4.3.7) where the droplet movement is characterized by Brownian motion and each droplet can explore the free volume around it leading to an increase in total entropy of the system. Any applied strain in this region would change the available free volume thereby increasing the energy of the system which is stored as elastic modulus (Ikeda et al., 2012; Mason et al., 2014). The volume fraction (ϕ_g) for this transition generally occurs at ϕ = 0.58 for monodispersed emulsions (Clusel et al., 2009; Berthier et al., 2011; Lu et al., 2013). The entropically driven elastic modulus of glassy state should ideally be scaled with k_BT/R^3 and is distinguishable from that of jammed state; however in the present case there is insufficiency of data points in this region to ascertain this. Mason et al (2014) showed that for conventional emulsions the entropic contribution towards G′ is substantially below the jamming state when scaled by Laplace pressure, while for nanoemulsions entropic contribution become significant

towards overall magnitude of the G′ under jammed state and hence all the data can be scaled by Laplace pressure. Below the glass transition the crowding effect of droplets subsides and this results in liquid like response where G″> G′.

4.3.5 Summary

In this study influence of dispersed phase volume fraction on the jamming transition and resultant viscoelastic properties of the repulsive nanoemulsions has been investigated. Increase in average elastic modulus with oil volume fraction was seen in strain sweep measurements. Although the elastic moduli curves were similar, with only an increase in magnitude of moduli as a function of ϕ, modelling the G′ with empirical scaling law developed by Mason et al. resulted in two distinct transformations of elastic response. An initial regime where there is a gradual increase in G′ called glassy (ϕ_g ~ 0.58) which is entropically driven due to the crowding of droplets as a result of which they are caged between their neighbours. This is followed by a glassy to jamming transition that occurred at ϕ_j, the critical volume fraction for the transition. In this region the droplet surfaces are deformed and elasticity appears due to the work done against additional energy stored in the droplets due to the compression of their surface resulted by crowding of droplets. This resulted in a dramatic increase in elasticity (G′) at ϕ_j. The energy scale that controls the deformation of droplets is their internal Laplace pressure given by γ/r, where γ is interfacial tension and r is the droplet radius (as seen in section 4.1). The ϕ_j from the model are 0.69 and 0.71 for LER and HER nanoemulsions, respectively, which is in agreement with similar polydispersed emulsions reported before in the literature (Groot et al., 2011).

4.4 Long-term stability of nanogels

4.4.1 Coalescence and accelerated creaming stability of nanogels

Figure 4.4.1 shows the surface-volume mean diameter (d_{32}) of all nanogels as a function of storage time (until 90 days). It can be seen that the d_{32} of all the nanogels did not change significantly with time ($p > 0.3$ for all nanogels). This suggests that the nanodroplets are stable to coalescence within the experimental time period. However, d_{32} is only an average of droplet size and does not emphasize the whole droplet size distribution. Hence, droplet size distributions of

the nanogels were also compared. In Figures 4.4.2A and 4.4.2B two such distributions for the two extreme emulsifier concentrations (0.5 CMC and 15 CMC) are shown for day 1 and day 90. Not much change There was a small change in the droplet size distribution between day 1 and day 90, however, it is not much to signify droplet coalescence.

The creaming velocities of nanogels obtained at different relative centrifugal forces (RCF) using the photocentrifuge LUMiSizer are plotted in Figure 4.4.3. As the SDS concentration increased the creaming velocity at any RCF decreased. This could be due to the reduction in droplet size, which is inverse proportional to creaming velocity, and also increase in gel strength, which prevents the droplets from moving under centrifugal force. In other words, as the gel strength increased the creaming velocity of the droplets decreased. From Figure 4.4.3 it can also be seen that the nanogels did not even cream until a critical RCF and thereafter increased steadily as a function of RCF. The minimum RCF at which droplet creaming started can be regarded as the yield point of the interdroplet network responsible for gelation. As expected, the minimum RCF required for creaming of nanodroplets also increased with an increase in gel strength.

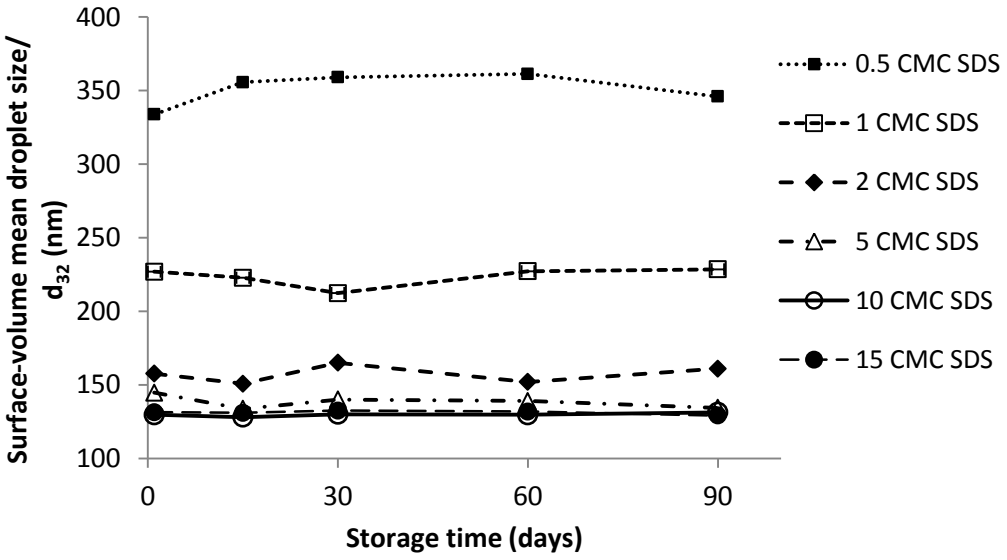

Figure 4.4.1 Sauter mean of droplet diameter (d_{32}) for all six nanogels as a function of storage time in days. Standard deviation is not shown for clarity.

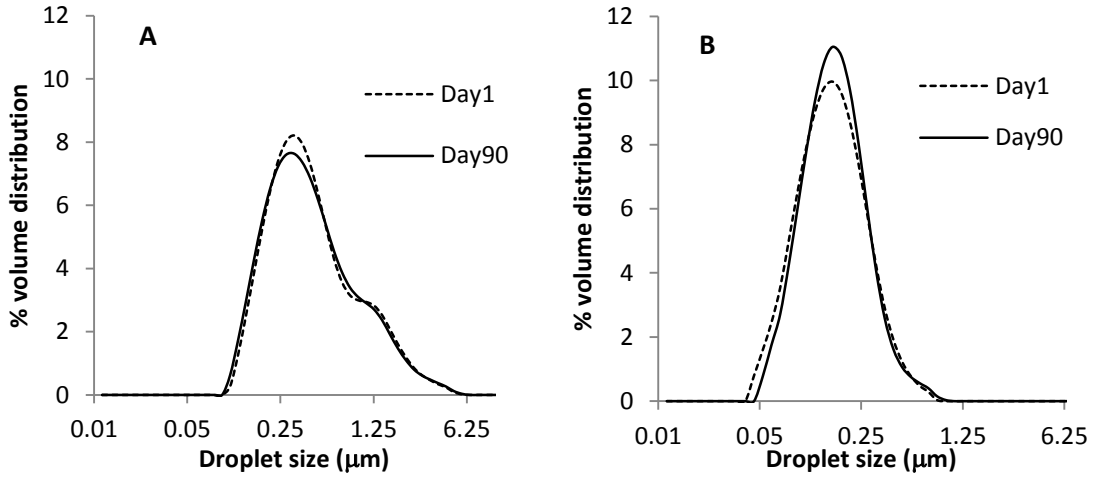

Figure 4.4.2 Average volume distribution of droplets as a funtion of droplet size for (A) 0.5 CMC and (B) 15 CMC SDS nanogel.

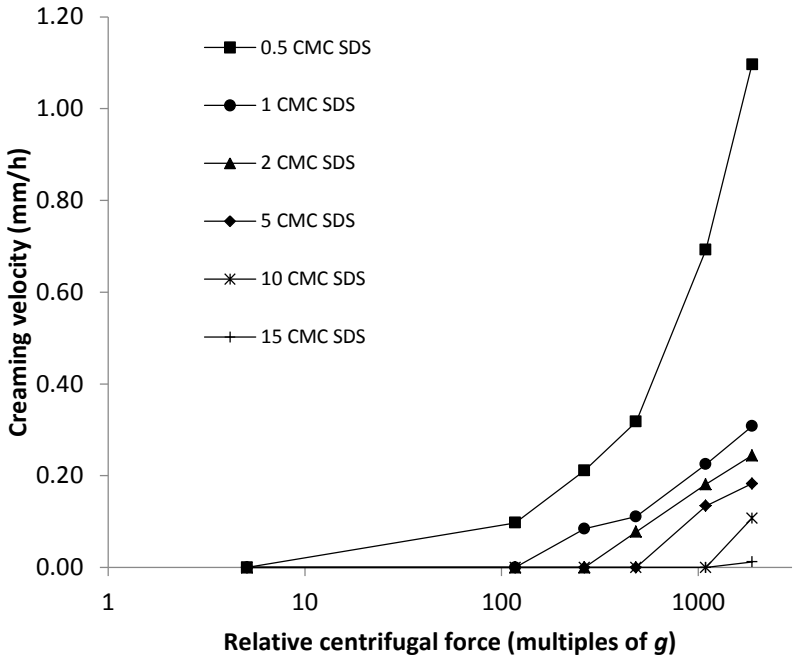

Figure 4.4.3 Creaming velocities of nanogels at different RCFs obtained from accelerated shelf-life study using the LUMiSizer.

Creaming rates of highly stable nanoemulsions at earth's gravity are hard to measure by visual observation. Hence by using this type of accelerated shelf-life study, the creaming velocities of the nanoemulsions at earth's gravity can be estimated by extrapolating the curves in Figure 4.4.3 to RCF = 1. From the figure 4.4.3 it can be seen that at earth's gravity the droplets in nanogels would not cream at all as they already reached zero creaming velocity at a higher RCF. This extreme stability against creaming could be the result of two factors. First, the network of droplets forming the gel structure hinders any movement of droplets. Second, the extreme stability of nanogels to creaming can also be a direct result of very small droplet size of the nanoemulsions. As given by Stokes equation (eq 2.1.2 in section 2.1.) the creaming velocity of emulsion droplets is inversely proportional to the square of their radius. In order to understand which of these two factors dominates, the same experiment (as reported in Figure 4.4.3) has been repeated with 5 and 10 CMC emulsions after 200 days of storage. Due to limitation in the availability of samples at this time this experiment could not be performed with other nanoemulsions.

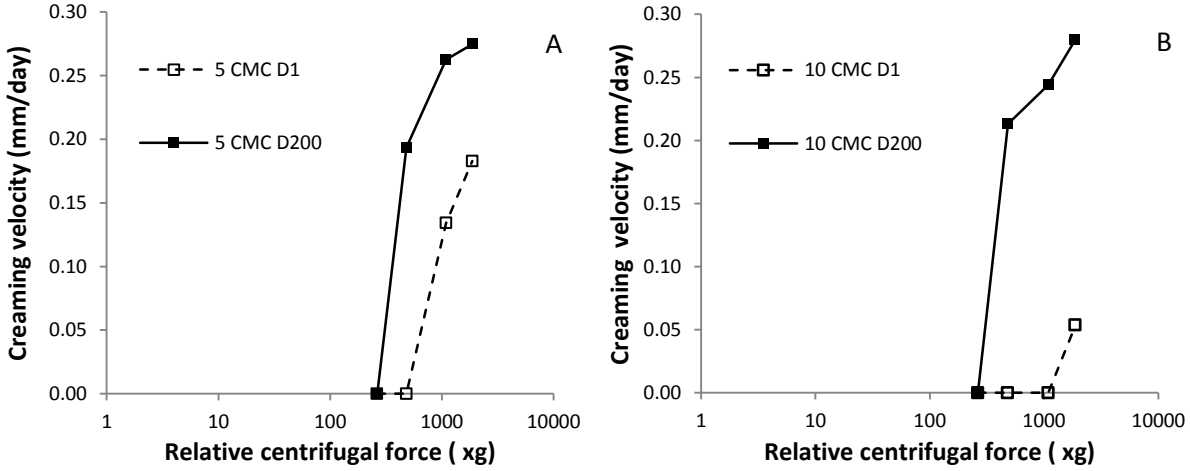

Figure 4.4.4 Creaming velocities as a function of time (on day 1 and day 200) of (A) 5 CMC and (B) 10 CMC nanogels at different RCFs obtained from accelerated shelf-life study using LUMiSizer.

Figure 4.4.4 shows the creaming velocity of 5 and 10 CMC nanoemulsions on day 1 and day 200 at different relative centrifugal forces. It can be seen that the critical centrifugal force for

the first observation of droplet creaming (yield point) is observed at a lower value for aged nanoemulsions. Thereafter, creaming velocity of aged nanoemulsions remained higher at comparable relative centrifugal forces. It should also be noted that the droplet size of the nanoemulsions did not change significantly until 200 days (data not shown). Therefore, it must be the interdroplet network structure that was responsible for this drop in critical RCF required for creaming and it was investigated using subsequent rheological experiments (reported below). However, despite increase in creaming velocities at higher relative centrifugal force, the extrapolated creaming velocity at earth's gravity remained zero for the aged nanoemulsions, meaning that the droplet size of the nanoemulsions were small enough to prevent creaming at earth's gravity by themselves.

4.4.2 Rheology study as a function of time

Figure 4.4.5 and 4.4.6 shows evolution of storage (G′) and loss (G″) moduli of the nanogels obtained from strain sweep experiments (at a constant frequency of 9.8 rad/sec) using the rheometer on day 1 and day 90 of storage periods. For all nanoemulsions on day 1, G′ and G″ were independent of strain below 2%, showing the existence of linear viscoelastic region (LVR). Within the LVR G′ is significantly greater than G″ for these nanoemulsions, reflecting their dominant elastic nature. With the increase in strain beyond a critical value G′ tends to decrease, and G″ tend to dominate G′ resulting in gel breakdown and liquid like behavior of nanogels at higher % strains. It can be seen that for repulsive nanogels (0.5, 1 and 2 CMC SDS nanogels) in Figure 2.4.5, the magnitude of G′ decreased remarkably with time from day 1 to day 90 and the LVR is lost, whereas for attractive nanogels shown in Figure 2.4.6 (5, 10 and 15 CMC SDS nanogels) the decrease in G′ with time is much less. These results suggest that the gel strength of the nanogels was significantly influenced by storage time, and this effect is decreased with an increase in emulsifier concentration and gel strength.

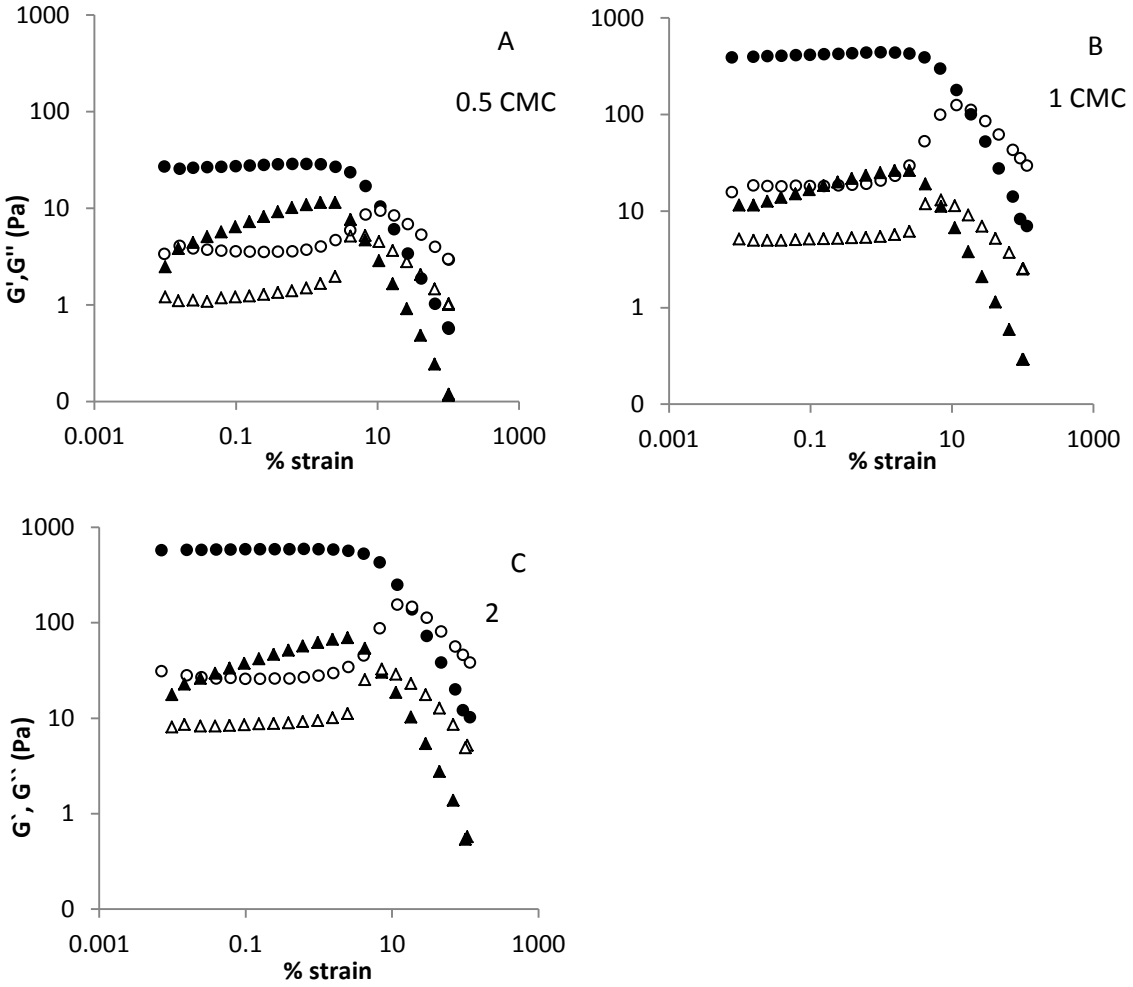

Figure 4.4.5 Storage (G′, filled symbol) and loss (G″, open symbol) moduli of repulsive (A) 0.5 CMC (B) 1 and (C) 2 CMC SDS nanogels obtained from strain sweep measurements (at a frequency of 9.8 rad/sec) on day 1 (●) and day 90 (▲) of their storage period.

In order to understand how gel strength evolved with time for different nanogels, the plateau G′ from the LVR at 0.1% strain is plotted as a function of storage time in Figure 4.4.7. It can be observed that for repulsive nanogels (0.5, 1 and 2 CMC SDS) there is a significant decrease in G′ with time until 90 days ($p < 0.05$). Attractive nanogels (5, 10 and 15 CMC SDS) also showed a significant decrease ($p < 0.05$) in G′, but the magnitude of decrease is not much compared to repulsive nanogels. This suggests that gel strength of attractive nanogels remain more stable than repulsive nanogels during the 90days storage period.

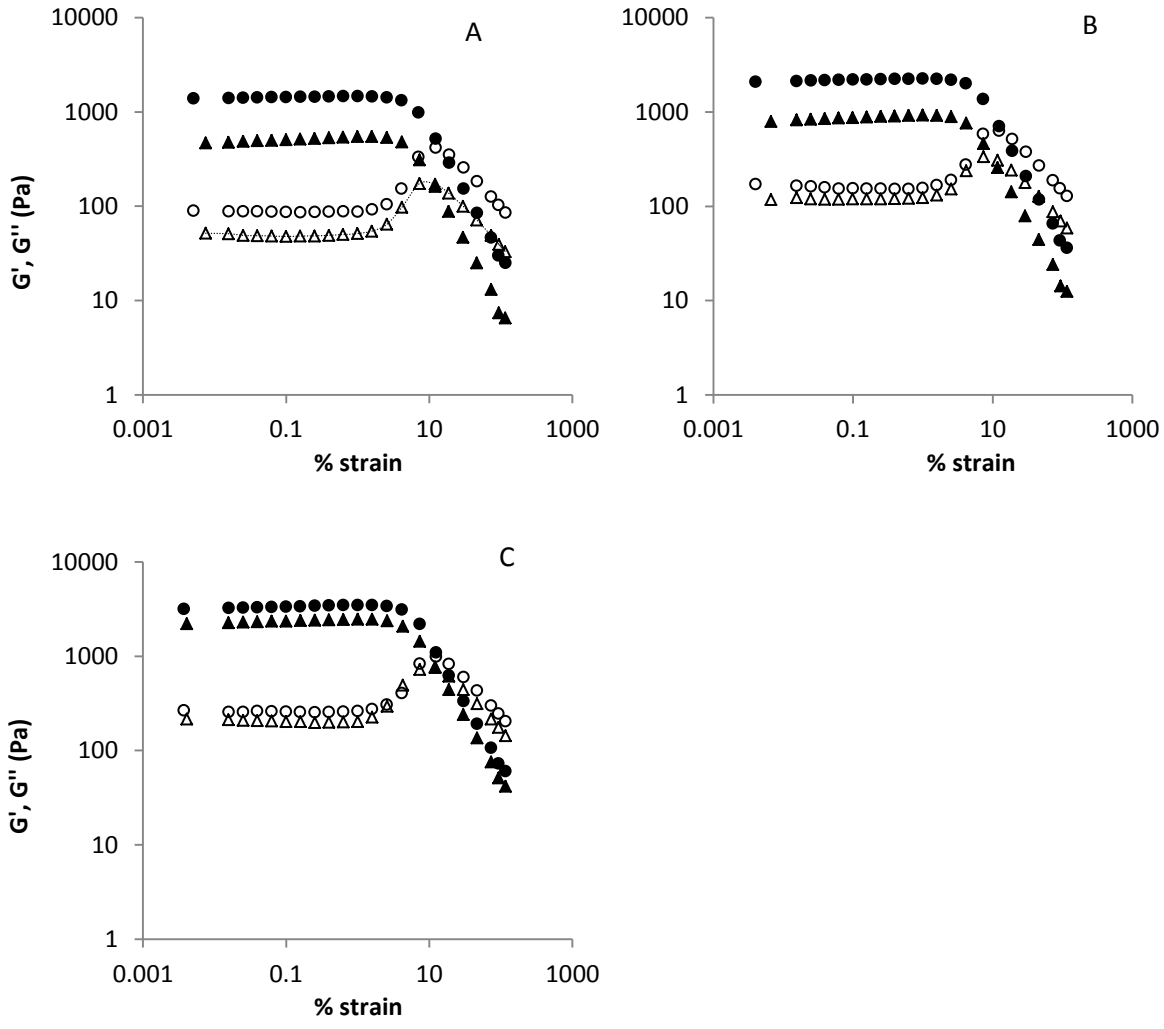

Figure 4.4.6 G′ (filled symbol) and G″ (open symbol) of attractive (A) 5 CMC (B) 10 CMC and (C) 15 CMC SDS nanogels obtained from strain sweep measurements (at a constant frequency of 9.8 rad/sec) on day 1 (●) and day 90 (▲) of their storage period.

Visual observation of the nanogels was also recorded as a function of the storage period. The vials containing nanogels were tilted at an angle and waited for 30 seconds to see if the nanogels flow, after which the photos were taken with a digital camera. Figure 4.4.8 shows the pictures of tilted vials on day 1 and day 90. Repulsive nanogels (0.5 and 1 CMC SDS) flowed

under gravity on day 1 and day 90, as the yield stress is low to support the nanogel. Starting from 2 CMC SDS, nanogels did not flow under gravity on day 1 as they had high yield stress. However, on day 90 when the vials were tilted 2, 5 and 10 CMC SDS nanogels flowed indicating week gelation behaviour. However, 15 CMC SDS nanogel did not flow even on day 90 demonstrating stable gel that can support its weight against gravity.

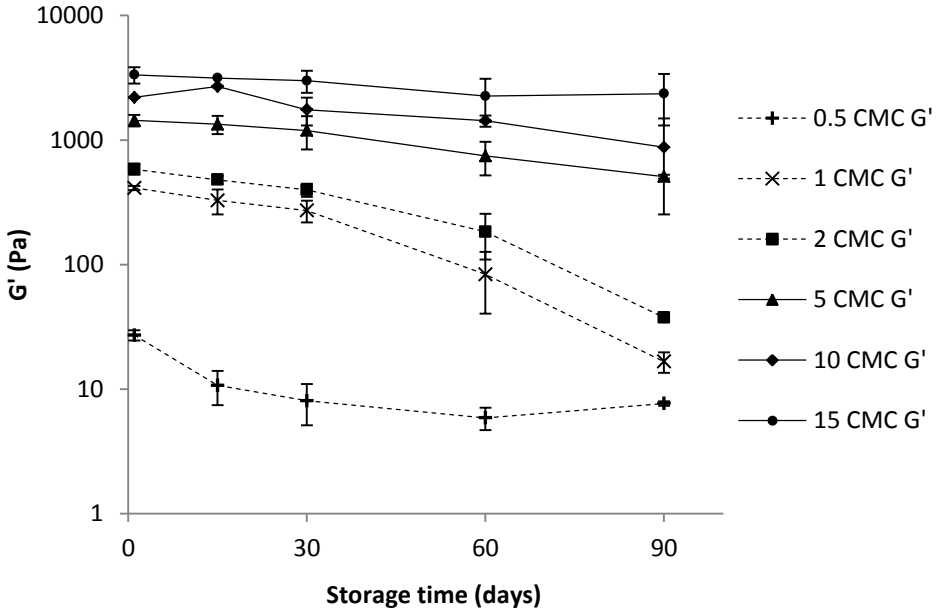

Figure 4.4.7 Plateau G′ at 0.1% strain of repulsive (0.5, 1 and 2 CMC SDS) and attractive nanogels (5, 10 and 15 CMC SDS) obtained from strain sweep measurements (at a constant frequency of 9.8 rad/sec) plotted against storage time in days. Error bars represents ± one standard deviation (n=3).

The yielding behavior of the nanogels is quantified in Figure 4.4.9 where the yield stresses were calculated using the Hershel-Bulkley model from the viscosity data (not shown). It can be seen that the yield stress of all the nanogels except 15 CMC decreased ($p < 0.05$) with time, which resulted in the flowing of nanogels during the visual observation experiment. For 15 CMC SDS nanogel yield stress did not change significantly ($p > 0.05$) as a function of time because of which it did not flow even on day 90.

SDS concentrations	Day 1	Day 90
0.5 CMC SDS		
1 CMC SDS		
2 CMC SDS	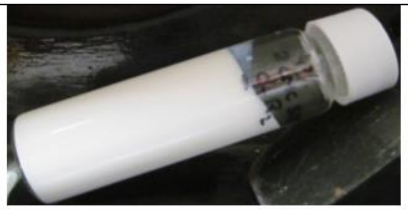	
5 CMC SDS		
10 CMC SDS		
15 CMC SDS		

Figure 4.4.8 Visual observation experiment of SDS nanogels. Vials containing nanogels were tilted at a certain angle to record their flow behavior and waited for 30 seconds after which the pictures were taken. This was done on day 1 and day 90 of their storage period.

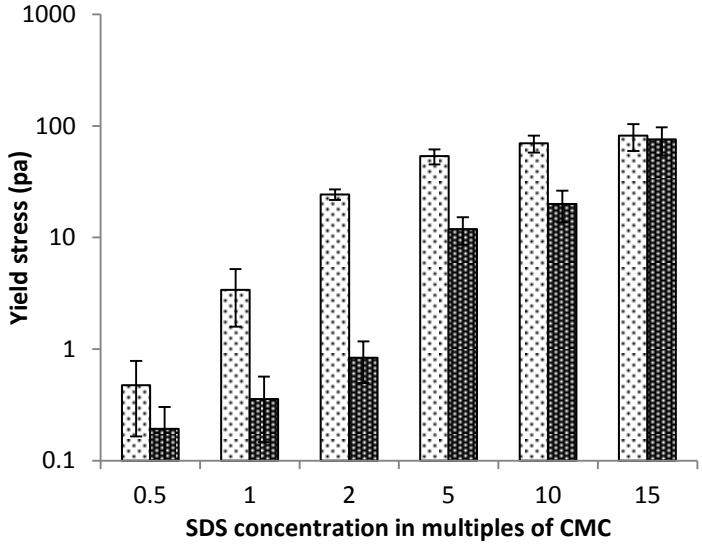

Figure 4.4.9 Yield stress values of nanogels on day 1 (▒) and day 90 (▓) calculated from the Hershel-Bulkley model as a function of emulsifier concentration. The viscosity data used for the model was obtained from rotational rheology experiments. Error bars represents ± one standard deviation (n=3).

The above experiments demonstrated that the gel strength of nanogels decreased with time, and it is common for both repulsive and attractive nanogels. However, attractive gel showed higher stability to change in gel strength compared to repulsive nanogels, with 15 CMC SDS nanogel showing the insignificant change in gel strength and yield stress.

4.4.3 Effect of aging on nanogels' strength

Properties of out-of-equilibrium colloids such as repulsively jammed and attractive nanogels are known to evolve slowly towards equilibrium with time; a behavior known as aging (Cipelletti et al., 2003). In other words, they exhibit-ultra slow relaxation during which the correlation or response functions such as structure factor measured by dynamic light scattering, or viscoelasticity evolve (Jabbari-Farouji et al., 2012). The effect of aging mechanism on the viscoelasticity of glasses and gels has been studied by few researchers (Struik, 1978; Derec et al., 2000). However, most of the studies investigated the aging on the time scale of minutes to hours if not days (Cipelletti et al., 2003). In the current study aging resulted in a decrease in the gel strength of nanogels over a period of 90 days. For repulsive nanogels, gelation happens due to

increase in ϕ_{eff} above a critical value where the droplets randomly jammed thereby preventing flow. As discussed in section 4.1 this increase in ϕ_{eff} was due to the formation of charge cloud (electric double layer) around anionic SDS-stabilized nanodroplets which acted as an additional shell layer that prevented close approach. In section 4.1 it was shown that an initial 40 wt% emulsions with 0.5, 1 and 2 CMC SDS concentrations would give rise to ϕ_{eff} equivalent to 0.74. Any drop in charge cloud around the nanodroplets and the thickness of electrical double layer (EDL) would negatively impact ϕ_{eff} and ultimately reduce gel strength. An estimation of charge on the EDL can be obtained by zeta potential (ζ). In order to confirm whether this phenomenon is responsible for loss of gel strength, ζ of the nanodroplets were measured using a Zeta potential Analyzer (Nano-ZS90, Malvern Instruments, Montreal, QC, Canada). Over a period of 90 days, 0.5 CMC nanogels showed a decrease in ζ from -58.7 mV to -53. 3mV, 1 CMC nanogels did not show any change averaging at -61 mV, while 2 CMC nanogels showed an increase in ζ from -58.0 mV to -61.0 mV. The drop in ζ for 0.5 CMC nanogels could result in the reduction of EDL and ϕ_{eff} and corresponding loss of gel strength. In this case there were insufficient emulsifier molecules to cover the droplet interface (and negligible among of free emulsifier in the aqueous phase), therefore the desorption of interfacial emulsifier into the aqueous phase may lead to a faster drop in surface charge, EDL and gel strength as seen in Figure 4.4.7. For 1 and 2 CMC nanogels the interface was mostly saturated and free emulsifiers were also present in the aqueous phase leading to a dynamic exchange of emulsifiers between these two phases (Chien et al. 1994). The dynamic equilibrium between adsorbed and unabsorbed emulsifiers (timescale of microseconds) may prevent any of loss of surface charge. Therefore, loss of gelation in 1 and 2 CMC nanogels could not be explained by this hypothesis. It is also not clear why ζ would increase in case of 2 CMC nanogels.

In a recent published patent on nanoemulsion gelation Graves et al. (2008) showed that G'_p of 40 wt% Polydimethylsiloxane (PDMS) silicone oil nanoemulsions stabilized with 116 mM SDS (equivalent to 14 CMC) did not change significantly over a period of 461 days. This observation directly contradicts our results that showed a notable drop in G'_p within 90 days for all nanogels except 15 CMC SDS. Although, visual observation of 15 CMC SDS nanogel showed liquid-like behavior after a storage period of more than 180 days (data not shown). The only different between Graves and co-workers' nanogel and our nanogel is in the types of oil

used. While silicone oil is an organic polymer which does not undergo chemical reactions such as oxidation, triacylglycerol (canola oil) used in our work is susceptible to lipid oxidation and hydrolysis reactions. The nanogels in the present work were stored at room temperature (RT), which also promoted oxidation. Also, the extremely small droplet size of nanoemulsions means a higher amount of interfacial area and hence, a greater chance of oxidation. In fact, after 90 days of storage at RT rancid smell was obtained from all nanogels indicating extensive lipid oxidation. It has been proposed that lipid oxidation in emulsion may induce changes in interfacial composition as the hydroperoxides (primary oxidation products) and broken down aldehyde and ketones (secondary oxidation products) are surface active (Abousalham et al., 2000; Nuchi et al., 2002). As lipid undergoes oxidation in droplets, these oxidized products move toward the interface and may also get desorbed from the interface into the aqueous phase leading to reorganization and even desorption of some emulsifier from the oil droplet interface (Berton-Carabin et al., 2014). Desorbed emulsifiers may also help solubilization of oxidation products by forming micelles in the aqueous phase (Berton-Carabin et al., 2012; Berton-Carabin et al., 2013). We propose that these changes in interfacial dynamics may lead to a reduction in charge cloud (EDL) around the droplets which would negatively impact effective oil phase volume fraction and hence gelation in repulsive nanogels. The changes in charge cloud due to lipid oxidation may not be enough to be detected by zeta potential analyzer; hence we were unable to prove this using direct measurement.

However, in order to support this hypothesis, the extent of lipid oxidation using peroxide value (PV) and *p*-anisidine value (AV) of the oil phase of the nanogels was determined. The PV gives an estimation of primary oxidation products while the AV measures presence of secondary oxidation products in the oil. Both methods were performed according to the Official Methods of American Oil Chemists' Society (Cd 8-53 for PV and Cd 18-90 for AV). A total estimation of oil oxidation was obtained from TOTOX value where TOTOX = 2PV + AV (Frankel, 1980). The oils were separated from the nanogels using repeated freeze/thaw passes which completely destabilized the nanoemulsions, although this approach neglected the oxidized products present in the aqueous phase. Three to four fold increase in TOTOX values were found in the oil phase of the repulsive nanogels compared to a fresh oil (TOTOX = 8 units in bulk oil purchased from grocery store, while TOTOX = 24 - 34 in oils separated from the repulsive nanogels after 180

days of storage at RT. This result indicates that changes in EDL around the nanodroplets are possible due to presence and transfer of surface active oxidized products which negatively impacts ϕ_{eff} necessary for random jamming and gelation in repulsive nanogels.

In the case of attractive nanogels, gelation was due to attractive depletion interactions between the droplets caused by SDS micelles (Section 4.1). Studies have shown that depletion attraction between the emulsion droplets resulted in diffusion limited cluster aggregation (DLCA), in which the droplets diffuse and form aggregated clusters by sticking with each other due to shear rigid bonds between them (Trappe et al., 2001; Shah et al., 2003). This results in the formation of fractal colloidal gels (Ramakrishnan et al., 2004; Katsuyoshi, 2009). Cipelletti et al. (2000) observed restructuring of the network in fractal colloidal gels, formed by the salt induced aggregation and syneresis of polystyrene spheres, due to aging. Dynamic light scattering studies done by them have shown breaking of intercluster bonds with aging which weakened the network structure. However, the authors did not study the viscoelastic response of the network restructuring. Seager et al. (2007) have shown that depletion attraction between liquid droplets of emulsions resulted in slippery bonds (Seager et al., 2007; Babu et al., 2008). It was proposed that slippery bonds do not break, yet they allow rotational diffusion of each droplet in the cluster. It also permits translational diffusion of droplets on the surface of another to find the most stable configuration leading to the compactness of the network. With compaction, the fractal network of nanodroplets failed to cover a large volume required for gelation. We hypothesized that the slippery bonds among the nanodroplets led to a gradual change in fractal nature which led to a decrease in gel strength with time. Nevertheless, for 15 CMC nanogels no significant loss in gel strength was observed in the experimental time frame. This could be explained by very strong attractive interactions among the nanodroplets (section 4.1), which prevented the slippery diffusion of the droplets around each other. However, it is possible that given enough time, this nanogel would also loose its gel strength. In fact, observation after a long storage time of more than180 days showed that 15 CMC nanogels also transformed into liquid nanoemulsions (data not shown).

The lipid oxidation hypothesis proposed to explain loss of gelation in repulsive nanogels may also be applied to attractive nanogels. In this case presence of excess micelles in the continuous phase of the nanoemulsions would facilitate removal of surface active oxidation

products from the droplets (Berton-Carabin et al., 2013). Micelles are highly dynamic system and the time scale of molecule exchanges among interfacial emulsifier, free emulsifier in the aqueous phase and micelles are in the range of micro to milliseconds (Patist et al., 2002). Therefore diffusion of oxidized products into micelles and their and distribution would be much faster compared to the rate of lipid oxidation (Romsted et al., 2013). It may also promote the transfer of hydroperoxides from one droplet to another by micelles leading to enhanced lipid oxidation in droplets (Nuchi et al., 2002). In fact, evidence of higher lipid oxidation in attractive nanogels (TOTOX = 30-38 in oils separated from the attractive nanogels after 180 days of storage at RT) was seen. The EDL around the droplets and corresponding ϕ_{eff} of attractive nanogels may also be affected by diffusion of oxidation products through droplet interface, however, in this case their effect would not be as significant as gelation in these nanogels were due to attractive interactions among the nanodroplets leading to the formation of fractal gels. Nevertheless, changes in micelle dynamics due to the uptake of lipid oxidation products may also alter their charge and size leading to a change in attractive depletion interactions as a function of time. We propose that this could also be partially responsible for loss of gel strength in attractive nanogels.

4.4.4 Summary

In this objective, the storage stability of the nanogels developed in the first objective was investigated as a function of time. It has been shown that the nanodroplets sere stable to coalescence and creaming over a period of 90 days. However, the elastic storage moduli (G′) of the nanogels decreased with time during storage. For repulsive nanogels (0.5, 1 and 2 CMC SDS) a significant decrease in G′ was observed converting the gels into a flowable liquid. For attractive nanogels (5, 10 and 15 CMC SDS) decrease in G′ was much less, although given enough time they also showed liquid-like behaviour.

It was proposed that dynamic equilibrium between interfacial (adsorbed) and aqueous phase (unadsorbed) emulsifiers could lead to change in charge cloud around the droplets leading to a reduction in ϕ_{eff} and loss of gel strength. However, using zeta potential measurement, drop in droplet charge could only be detected for 0.5 CMC nanogels as the equilibrium is shifted towards desorption. It was also proposed that generation of surface active components due to

extensive lipid oxidation may alter the interfacial composition and ultimately reduce the thickness of EDL leading to a reduction in gel strength. In attractive nanogels, the presence of excess micelles in the continuous phase may have facilitated the transfer of surface active lipid oxidation products from droplets towards micelles or other droplets leading to a change in EDL and attractive depletion interactions. However, in fractal gels formed by attractive interactions, the slippery nature of the bonds among liquid nanodroplets could permit rotational and translational diffusion of droplets on the surface of another in order to find the most stable configuration leading to compactness of the network. It was proposed that the slippery bonds among the nanodroplets led to a gradual change in fractal nature which led to a decrease in gel strength with time.

5. OVERALL CONCLUSION

Traditionally, structure formation in lipid-rich foods (e.g., spreads, chocolate etc.) come from the microscopic fat crystal network made of saturated and trans fats which holds liquid oil immobile, providing shape and form to the product. However, the epidemic of obesity and cardiovascular disease forced us to limit saturated and trans fat in our diet. In this research, a novel approach to providing structure to lipid-rich foods by developing nanogels from low oil containing liquid nanoemulsions was used. The overall goal of this research was to investigate the elastic properties of nanogels developed using ionic-emulsifier which resulted in repulsive and attractive gelation. It was divided into four distinct but related objectives. In the first two, the influence of emulsifier concentration and droplet size on nanoemulsion gelation was investigated. It was followed by an investigation on the influence of oil volume fraction on gelation of a low emulsifier containing nanoemulsions. In the last part, long-term stability and gelation behaviour of the nanoemulsions was studied in order to understand whether their gel strength varied with time.

In the first part, the aim was to optimize and understand the influence of emulsifier concentration on the elasticity and flow behavior of the nanoemulsions. It was observed that liquid nanoemulsions transformed into viscoelastic gels at a specific concentration range of anaionic SDS emulsifier while no gelation was observed for nonionic Tween 20. The apparent viscosity, yield stress and storage moduli (G′) of the nanogels increased with SDS concentration until 15 times its CMC, thereafter decreased steadily as the gel broke down beginning 20 times CMC. At low SDS concentration (0.5 – 2 CMC) the repulsive charge cloud acted as interfacial shell layer on the nanodroplets and significantly increased the effective droplet diameter ($d_{\text{m-eff}}$) and effective oil phase volume fraction (ϕ_{eff}). When ϕ_{eff} of these nanoemulsions reached the volume fraction for random jamming of nanodroplets (ϕ_{MRJ}) elastic behavior (G′ > G″) appeared. These gels were named as repulsive nanogel due to inherent repulsive interactions among the nanodroplets. Nanoemulsions prepared with non-ionic Tween 20 showed weak elastic behavior and flowed under gravity, as the lack of charge cloud led to no further increase in ϕ_{eff}.

With increase in SDS concentration to 5 – 15 CMC, excess SDS moleculs formed micelles in the continuous phase which created depletion attractions among the nanodroplets and led to their aggregation resulting in nanogels with high gel strength ($G' >> G''$). These gels were termed attractive nanogels. At a still higher concentration (≥ 20 CMC SDS), G' suddenly dropped leading to the formation of very weak gels. It was psoposed that excess micelles in continuous phase led to depeltion stabilization between nanodroplets leading to loss of attractive interactions and gel strength. The theory of depletion interaction and oscillatory structural force (OSF) were used to calculate the interaction energies among the nanaodroplets which showed that gel strength increased with increase in depletion attraction followed by sudden drop due to the appearance of OSF at higher SDS concentrations.

Next, the effect of droplet size as a function of homogenization passes on both repulsive and attractive nanogels was investigated. At higher droplet diameter (>250nm), the emulsions existed as fluids where $G' < G''$. As the droplet diameter decreased to 160 nm the liquid like repulsive nanoemulsions gradually transformed into strong nanogels where $G' >> G''$. It was proposed that the jamming transition caused by an increase in ϕ_{eff} due to a reduction in droplet size was responsible for this behaviour. On the contrary, for attractive nanoemulsions decrease in droplet size manifested a different mechanism of gelation. An initial fluid-like emulsion ($G' < G''$) transformed into nanogels below a critical droplet diameter of 160 nm, where a rapid increase in gel strength was observed. However, it was also found that the strength of the attractive interaction (W_d/k_BT) also decreased with decrease in droplet size, which was attributed to the drop in micelle concentration as more emulsifier molecules got adsorbed on the newly created interfacial area. It was proposed that despite higher W_d/k_BT, the fluid like the behaviour of large droplet size nanoemulsions was due to structural forces generated by the presence of higher micelle concentrations (depletion stabilization). With a decrease in droplet size and a corresponding drop in micelle concentration, the interdroplet interaction transformed into depletion attraction and led to gelation by fractal network among the nanodroplets. Moreover, decrease in droplet size and a corresponding increase in their number were also hypothesized to have an integral impact on the fractal nature of the aggregates contributing to the gelation behaviour of the attractive nanoemulsions.

Attractive nanogels require high emulsifier concentration in the continuous phase to induce depletion interactions. Moreover, it is uncommon in food emulsions to use such high emulsifier concentrations. Hence, the influence of ϕ on the jamming transition and resulting viscoelastic properties was investigated for repulsive nanoemulsions with low emulsifier concentrations. The repulsive nanogels were prepared at different ϕ (0.30. 0.35, 0.40, 0.45, 0.50 and 0.60) and two different emulsifier concentration (mM) to oil volume fraction (ϕ) ratio. The average elastic modulus from strain sweep measurements increased with oil volume fraction. Modelling the G′ with empirical scaling law developed by Mason et al. (1995) resulted in two distinct transformations of elastic response with an increase in ϕ. An initial regime where there was a gradual increase in G′ called glassy transition ($\phi_g \sim 0.58$) which is entropically driven due to the crowding of droplets as a result of which they are caged between their neighbours. This was followed by a glassy to jamming transition that occurred at ϕ_j, the critical volume fraction for the transition, where a dramatic increase in elasticity (G′) was observed. The model predicted ϕ_j of 0.69 and 0.71 for nanoemulsions with low and high emulsifier concentrations, respectively, which is in agreement with previous studies that dealt with similar polydispersed emulsions (Clusel et al., 2009; Groot et al., 2011).

The long-term storage stability of nanogels would dictate their potential applications. It was seen that the nanodroplets were stable to coalescence and creaming over a period of 90 days. However, for repulsive nanogels (0.5, 1 and 2 CMC SDS) significant decrease in G′ was observed during storage converting the gels into the flowable liquid. For attractive nanogels (5, 10 and 15 CMC SDS) decrease in G′ was much less, although given enough time they also transformed from strong to weak gels. It was proposed that for repulsive nanogels dynamic equilibrium between interfacial (adsorbed) and aqueous phase (unadsorbed) emulsifiers could lead to change in charge cloud around the droplets leading to reduction in ϕ_{eff} and loss of gel strength. However, using zeta potential measurement, drop in droplet charge could only be detected for 0.5 CMC nanogels as the equilibrium was shifted towards desorption. It was also proposed that generation of surface active components due to extensive lipid oxidation may alter the interfacial composition. These two mechanisms might have reduced the thickness of electrical double layer leading to decrease in gel strength. In attractive nanogels, presence of excess micelles in the continuous phase may have facilitated transfer of surface active lipid

oxidation products from droplets towards micelles or other droplets leading to a change in electric double layer and attractive depletion interactions. However, in fractal gels formed by attractive interactions, the slippery nature of the bonds among the liquid nanodroplets could also permit rotational and translational diffusion of the nanodroplets on the surface of each other in order to find the most stable configuration leading to compactness of the network and decrease in gel strength with time. In conclusion, more research is needed in order to fully understand the aging effect of the nanogels. The nanogels with extremely small droplet size and low oil volume fraction possess great potential for use in low-fat foods and related soft materials.

6. FUTURE STUDIES

The nanogels discussed in this thesis behaved as thick gels even at low concentrations of the dispersed phase oil volume fraction (ϕ). They have the potential for applications in food, pharmaceuticals, and cosmetics. In this research, nanogels were prepared using anionic SDS emulsifier which is not food-grade. There is a need to develop such nanogels using food grade emulsifiers to be able to use it in novel food applications. However, in order to achieve this, the emulsifiers need to satisfy these conditions: 1) they should be able to achieve extremely smaller droplet size required for these nanoemulsions (McClements et al., 2011) and 2) they should have charge (anionic or cationic) on them which is required for the presence of electrical double layer and repulsive gelation (Scheffold et al., 2014). This makes it challenging to find appropriate emulsifiers. Most of the available ionic food grade emulsifiers are anionic (e.g. mono-diglycerides derivatives (DATEM, CITREM), Sodium Stearoyl Lactylate (SSL) and so on) and at least one cationic emulsifier can be found in literature (e.g. lauric arginate) (McClements et al., 2011). CITREM and SSL were used for preparation of nanoemulsions in few studies and they achieved the required sub-micron droplet size (Wooster et al., 2009; Kaasgaard et al., 2010; Speranza et al., 2013). However, the charge on such emulsifiers and their potential in forming electrical double layer enough to form nanogel is yet to be known. On the other hand globular proteins (such as sodium caseinate and β-lactoglobulin) were shown to induce depletion attraction between oil droplets in O/W emulsions leading to their gelation (Dickinson et al., 1997). But, it is also known that proteins are not effective in achieving extremely small droplet sizes of nanoemulsions compared to small molecule emulsifiers (McClements et al., 2011). Therefore, use of solvent evaporation technique would be needed for the development of nanoemulsions (Lee et al., 2010). In this method, oil is mixed with an organic solvent in which it is soluble and homogenization is done to prepare emulsions. The oil-solvent droplets are stabilized by biopolymer emulsifiers. In the second step, the solvent is evaporated making the oil droplets to shrink and form nanodroplets (McClements et al., 2011). Lee et al. (2010) developed corn oil nanoemulsions stabilized by WPI using solvent evaporation technique (ethyl acetate was

used as solvent). Thus finding the food-grade emulsifiers and appropriate emulsification method is necessary for applications of these nanogels in foods.

The repulsive nanogels in the section 4.3 showed two transitions, the first one being glass transition in which liquid emulsions (G″ > G′) transform into the glassy state (G′ > G″). It was followed by the jamming transition in which glassy emulsions evolved towards a jammed state where each droplet is caged between the neighbouring droplets (where G′ >> G″). The empirical model in the study covered only the jamming transition and obtained the critical concentration ϕ_c required for jamming. However, a self-consistent model that covers both the glass and jamming transitions is needed to understand the behavior of repulsive gelation better. Mason et al. (2014) developed an empirical model for monodisperse emulsions that covers both the glassy and jamming regions. However, the applicability of the model for polydisperse nanogels as in this thesis should be verified in future studies.

Microscopic images of the nanogels would also help us to visually determine the glass and jamming transitions of emulsions. Confocal microscopy was tried, but was unable to resolve the large number of extremely small droplets of the nanogels. Transmission Electron Microscopy (TEM) of the nanogels did not yield the required results as the nanogels got destabilized during the air drying technique. An ideal microscopy needs supercritical drying of nanogels using CO_2 before characterizing the images. The nanogels can also be evaluated by Freeze-Fracture Scanning Electron Microscopy (FF-SEM). As discussed in section 4.4 the loss of gel strength of nanogels with aging was not fully understood. SEM images might shed some information on the changes in gel structure with aging. Image analysis of SEM micrographs can also be used to measure the fractal dimension (D_f) of the network structures (Krohn et al., 1986; Risović et al., 2008; Lobato-Calleros et al., 2009). SEM micrographs paired with the fractal dimension can help us analyze the changes in microstructure and may show subtle differences responsible for loss of gel strength with time. The hypothesis of slippery bonds between the nanodroplets resulting in restructuring and loss of gel strength (section 4.4) can be tested by measuring the fractal dimensions as a function time. If the slippery nature resulted in compaction of network structure, the fractal dimension should increase with time.

Graves et al. (2008) in their patent work prepared elastic repulsive nanoemulsions using silicone oil as dispersed phase. These gels bear structural similarities with the nanogels discussed

in this thesis but were stable for more than a year. In this thesis, nanogels prepared with canola oil showed a loss of gel strength during an aging time of 90 days. It was hypothesized that (see section 4.4) generation of surface active oxidized products due to oxidation of canola oil droplets might lead to the destabilization of nanogels. This hypothesis can be tested by preparing nanogels with silicone oil or mineral oil which is not susceptible to oxidation or by adding antioxidants to oil phase that prevent oxidative destabilization of the nanogels and compare their aging behaviour with the present nanogels.

The nanogels in this thesis are non-Newtonian fluids, and viscosity of such material depend on the magnitude of shear as well as the length of time the fluid is subjected to flow (Triantafillopoulos, 1948). In other words, the viscosity of thixotropic material will decrease with time when subjected to constant shear, which imply a progressive breakdown of structure (Abu-Jdayil, 2003). A preliminary study showed that the nanogels instantly recovered their elastic modulus when the applied stress was removed. However, more investigation is needed in order to fully understand this behaviour. There is also a need for creep compliance and recovery tests for these nanogels. This will give information on the extent of recovery of the nanogel structure after a constant stress is applied and then removed. This will help in understanding the performance of these nanogels under processing conditions typically encountered in foods. Therefore, time-dependent rheology, creep and recovery compliance tests would be important to know the unique features of these nanogels which are still in the early stages of development.

7. REFERENCES

Abousalham, A., Fotiadu, F., Buono, G., & Verger, R. (2000). Surface properties of unsaturated non-oxidized and oxidized free fatty acids spread as monomolecular films at an argon/water interface. *Chemistry and Physics of Lipids, 104*(1), 93-99.

Abu-Jdayil, B. (2003). Modelling the time-dependent rheological behavior of semisolid foodstuffs. *Journal of Food Engineering, 57*(1), 97-102.

Alleoni, A. C. C. (2006). Albumen protein and functional properties of gelation and foaming. *Scientia Agricola, 63*(3), 291-298.

Arltoft, D., Ipsen, R., Madsen, F., & de Vries, J. (2007). Interactions between carrageenans and milk proteins: A microstructural and rheological study. *Biomacromolecules, 8*(2), 729-736.

Asakura, S., & Oosawa, F. (1954). On interaction between 2 bodies immpersed in a solution of macromolecules. *Journal of Chemical Physics, 22*(7), 1255-1256.

Asnacios, A., Espert, A., Colin, A., & Langevin, D. (1997). Structural Forces in Thin Films Made from Polyelectrolyte Solutions. *Physical Review Letters, 78*(26), 4974-4977.

Babu, S., Gimel, J. C., & Nicolai, T. (2008). Diffusion limited cluster aggregation with irreversible slippery bonds. *European Physical Journal E, 27*(3), 297-308.

Banerjee, S., & Bhattacharya, S. (2012). Food Gels: Gelling Process and New Applications. *Critical Reviews in Food Science and Nutrition, 52*(4), 334-346.

Barnes, H. A., Hutton, J. F., & Walters, K. (1989). *An introduction to rheology*. Amsterdam; New York: Elsevier : Distributors for the U.S. and Canada, Elsevier Science Pub. Co.

Basheva, E. S., Kralchevsky, P. A., Danov, K. D., Ananthapadmanabhan, K. P., & Lips, A. (2007). The colloid structural forces as a tool for particle characterization and control of dispersion stability. *Physical Chemistry Chemical Physics, 9*(38), 5183-5198.

Batchelor, G. K., & Green, J. T. (1972). The determination of the bulk stress in a suspension of spherical particles to order c^2. *Journal of Fluid Mechanics, 56*(3), 401-427.

Bergeron, V., & Radke, C. J. (1992). Equilibrium measurements of oscillatory disjoining pressures in aqueous foam films. *Langmuir, 8*(12), 3020-3026.

Berli, C. L. A., Quemada, D., & Parker, A. (2002). Modelling the viscosity of depletion flocculated emulsions. *Colloids and Surfaces A: Physicochemical and Engineering Aspects, 203*(1-3), 11-20.

Berli, C. L. A., Quemada, D., & Parker, A. (2003). Gel transition of depletion flocculated emulsions. *Colloids and Surfaces A: Physicochemical and Engineering Aspects, 215*(1-3), 201-204.

Bernal, J. D., & Mason, J. (1960). Packing of Spheres: Co-ordination of Randomly Packed Spheres. *Nature, 188*(4754), 910-911.

Berryman, J. G. (1983). Random close packing of hard-spheres and disks. *Physical Review A, 27*(2), 1053-1061.

Berthier, L., Jacquin, H., & Zamponi, F. (2011). Microscopic theory of the jamming transition of harmonic spheres. *Physical Review E, 84*(5).

Berton-Carabin, C. C., Coupland, J. N., Qian, C., McClements, D. J., & Elias, R. J. (2012). Reactivity of a lipophilic ingredient solubilized in anionic or cationic surfactant micelles. *Colloids and Surfaces a-Physicochemical and Engineering Aspects, 412*, 135-142.

Berton-Carabin, C. C., Elias, R. J., & Coupland, J. N. (2013). Reactivity of a model lipophilic ingredient in surfactant-stabilized emulsions: Effect of droplet surface charge and ingredient location. *Colloids and Surfaces a-Physicochemical and Engineering Aspects, 418*, 68-75.

Berton-Carabin, C. C., Ropers, M.-H., & Genot, C. (2014). Lipid Oxidation in Oil-in-Water Emulsions: Involvement of the Interfacial Layer. *Comprehensive Reviews in Food Science and Food Safety, 13*(5), 945-977.

Bibette, J., Mason, T. G., Gang, H., Weitz, D. A., & Poulin, P. (1993). Structure of adhesive emulsions. *Langmuir, 9*(12), 3352-3356.

Bibette, J., Roux, D., & Nallet, F. (1990). Depletion interactions and fluid-solid equilibrium in emulsions. *Physical Review Letters, 65*(19), 2470-2473.

Bibette, J., Roux, D., & Pouligny, B. (1992). Creaming of emulsions -The role of depletion forces induced by surfactant. *Journal De Physique II, 2*(3), 401-424.

Bijsterbosch, B. H., Bos, M. T. A., Dickinson, E., vanOpheusden, J. H. J., & Walstra, P. (1995). Brownian dynamics simulation of particle gel formation: From argon to yoghurt. *Faraday Discussions, 101*, 51-64.

Bremer, L. G. B., Bijsterbosch, B. H., Walstra, P., & van Vliet, T. (1993). Formation, properties and fractal structure of particle gels. *Advances in Colloid and Interface Science, 46*, 117-128.

Broide, M. L., & Cohen, R. J. (1992). Measurements of cluster-size distributions arising in salt-induced aggregation of polystyrene microspheres. *Journal of Colloid and Interface Science, 153*(2), 493-508.

Buscall, R., Goodwin, J. W., Hawkins, M. W., & Ottewill, R. H. (1982). Viscoelastic properties of concentrated latices. 2. Theoretical analysis. *Journal of the Chemical Society-Faraday Transactions I, 78*, 2889-2899.

Buscall, R., Mills, P. D. A., Goodwin, J. W., & Lawson, D. W. (1988). Scaling behavior of the rheology of aggregate networks formed from colloidal particles. *Journal of the Chemical Society-Faraday Transactions I, 84*, 4249-4260.

Butt, H. J., Cappella, B., & Kappl, M. (2005). Force measurements with the atomic force microscope: Technique, interpretation and applications. *Surface Science Reports, 59*(1–6), 1-152.

Carnahan, N. F., & Starling, K. E. (1969). Equation of state for nonattracting rigid spheres. *Journal of Chemical Physics, 51*(2), 635-636.

Chang, Y. H., McLandsborough, L., & McClements, D. J. (2012). Physical Properties and Antimicrobial Efficacy of Thyme Oil Nanoemulsions: Influence of Ripening Inhibitors. *Journal of Agricultural and Food Chemistry, 60*(48), 12056-12063.

Chen, J., Dickinson, E., & Lee, W. P. (2001). Protein-based emulsion gels: effects of interfacial properties and temperature. In E. Dickinson & R. Miller (Eds.), *Food colloids: Fundamentls and formulation* (pp. 384 - 391). Cambridge, UK: Royal Society of Chemistry.

Christov, N. C., Danov, K. D., Zeng, Y., Kralchevsky, P. A., & von Klitzing, R. (2010). Oscillatory Structural Forces Due to Nonionic Surfactant Micelles: Data by Colloidal-Probe AFM vs Theory. *Langmuir, 26*(2), 915-923.

Cipelletti, L., Manley, S., Ball, R. C., & Weitz, D. A. (2000). Universal aging features in the restructuring of fractal colloidal gels. *Physical Review Letters, 84*(10), 2275-2278.

Cipelletti, L., Ramos, L., Manley, S., Pitard, E., Weitz, D. A., Pashkovski, E. E., & Johansson, M. (2003). Universal non-diffusive slow dynamics in aging soft matter. *Faraday Discussions, 123*, 237-251.

Clusel, M., Corwin, E. I., Siemens, A. O. N., & Brujic, J. (2009). A 'granocentric' model for random packing of jammed emulsions. *Nature, 460*(7255), 611-615.

Co, E. D., & Marangoni, A. G. (2012). Organogels: An Alternative Edible Oil-Structuring Method. *Journal of the American Oil Chemists Society, 89*(5), 749-780.

Courtney, T. H. (1990). *Mechanical behavior of materials*. New York: McGraw-Hill.

Danov, K. D., Denkov, N. D., Petsev, D. N., Ivanov, I. B., & Borwankar, R. (1993). Coalescence dynamics of deformable brownian emulsion droplets. *Langmuir, 9*(7), 1731-1740.

Datta, S. S., Gerrard, D. D., Rhodes, T. S., Mason, T. G., & Weitz, D. A. (2011). Rheology of attractive emulsions. *Physical Review E, 84*(4), 041404.

Denkov, N. D., Petsev, D. N., & Danov, K. D. (1995). Flocculation of deformable emulsion droplets: I. Droplet shape and line tension effects. *Journal of Colloid and Interface Science, 176*(1), 189-200.

Derec, C., Ajdari, A., Ducouret, G., & Lequeux, F. (2000). Rheological characterization of aging in a concentrated colloidal suspension. *Comptes Rendus De L Academie Des Sciences Serie Iv Physique Astrophysique, 1*(8), 1115-1119.

Derjaguin, B., & Landau, L. (1993). Theory of the stability of strongly charged lyophobic sols and of the adhesion of strongly charged particles in solutions of electrolytes. *Progress in Surface Science, 43*(1), 30-59.

Desrumaux, A., & Marcand, J. (2002). Formation of sunflower oil emulsions stabilized by whey proteins with high-pressure homogenization (up to 350 MPa): effect of pressure on emulsion characteristics. *International Journal of Food Science and Technology, 37*(3), 263-269.

Dickinson, E. (1982). *Colloids in food* (G. Stainsby Ed.). London: Elsevier Applied Science.

Dickinson, E. (1992). Interfacial interactions and the stability of oil-in-water emulsions. *Pure and Applied Chemistry, 64*(11), 1721-1724.

Dickinson, E. (2000). Structure and Rheology of Simulated Gels Formed from Aggregated Colloidal Particles. *Journal of Colloid and Interface Science, 225*(1), 2-15.

Dickinson, E. (2010). Food emulsions and foams: Stabilization by particles. *Current Opinion in Colloid & Interface Science, 15*(1-2), 40-49.

Dickinson, E. (2012). Emulsion gels: The structuring of soft solids with protein-stabilized oil droplets. *Food Hydrocolloids, 28*, 17.

Dickinson, E. (2013a). Stabilising emulsion-based colloidal structures with mixed food ingredients. *Journal of the Science of Food and Agriculture, 93*(4), 710.

Dickinson, E. (2013b). Structure and rheology of colloidal particle gels: Insight from computer simulation. *Advances in Colloid and Interface Science, 199-200*, 114-127.

Dickinson, E., & Chen, J. (1999). Heat-set whey protein emulsion gels: Role of active and inactive filler particles. *Journal of Dispersion Science and Technology, 20*(1-2), 197-213.

Dickinson, E., & Golding, M. (1997). Depletion flocculation of emulsions containing unadsorbed sodium caseinate. *Food Hydrocolloids, 11*(1), 13-18.
Dickinson, E., Murray, B. S., & Stainsby, G. (1988). Coalescence stability of emulsion-sized droplets at a planar oil-water interface and the relationship to protein film surface rheology. *Journal of the Chemical Society-Faraday Transactions I, 84*, 871-883.
Djabourov, M. K. N., & Simon, B. R.-M. (2013). *Physical Gels from Biological and Synthetic Polymers*. New York, NY: Cambridge University Press.
Doublier, J. L. (1992). Viscoelastic properties of food gels. In M. A. Rao (Ed.), *Viscoelastic properties of foods*. New York, USA: Elsevier applied science.
Færgemand, M., Murray, B. S., & Dickinson, E. (1997). Cross-Linking of Milk Proteins with Transglutaminase at the Oil−Water Interface. *Journal of Agricultural and Food Chemistry, 45*(7), 2514-2519.
Findley, W. N. (1989). *Creep and relaxation of nonlinear viscoelastic materials : with an introduction to linear viscoelasticity*. New York: Dover.
Fischer, P., & Windhab, E. J. (2011). Rheology of food materials. *Current Opinion in Colloid & Interface Science, 16*(1), 36-40.
Florian, M. W., William, H. H., & Richard, B. W. (2005). Food Gums *Handbook of Food Science, Technology, and Engineering - 4 Volume Set*: CRC Press.
Flory, P. J. (1941). Molecular Size Distribution in Three Dimensional Polymers. I. Gelation1. *Journal of the American Chemical Society, 63*(11), 3083-3090.
Floury, J., Desrumaux, A., Axelos, M. A. V., & Legrand, J. (2003). Effect of high pressure homogenisation on methylcellulose as food emulsifier. *Journal of Food Engineering, 58*(3), 227-238.
Floury, J., Desrumaux, A., & Legrand, J. (2002). Effect of ultra-high-pressure homogenization on structure and on rheological properties of soy protein-stabilized emulsions. *Journal of Food Science, 67*(9), 3388-3395.
Frankel, E. N. (1980). Lipid oxidation. *Progress in Lipid Research, 19*(1), 1-22.
Friberg, S. E., Lochhead, R. V., Blute, I., & Warnheim, T. (2004). Hydrotropes - Performance chemicals. *Journal of Dispersion Science and Technology, 25*(3), 243-251.
Fryd, M. M., & Mason, T. G. (2012). Advanced Nanoemulsions. In M. A. Johnson & T. J. Martinez (Eds.), *Annual Review of Physical Chemistry, Vol 63* (Vol. 63, pp. 493-518).
Furusawa, K., Sato, A., Shirai, J., & Nashima, T. (2002). Depletion flocculation of latex dispersion in ionic micellar systems. *Journal of Colloid and Interface Science, 253*(2), 273-278.
Garcia-Gonzalez, C. A., Alnaief, M., & Smirnova, I. (2011). Polysaccharide-based aerogelsâ€"Promising biodegradable carriers for drug delivery systems. *Carbohydrate Polymers, 86*(4), 1425-1438.
Ghosh, P. (2009). *Colloid and interface science*. New Delhi, India: PHI Learning Pvt. Ltd.
Ghosh, S., Cramp, G. L., & Coupland, J. N. (2006). Effect of aqueous composition on the freeze-thaw stability of emulsions. *Colloids and Surfaces A: Physicochemical and Engineering Aspects, 272*(1–2), 82-88.
Ghosh, S., & Rousseau, D. (2010). Emulsion breakdown in foods and beverages. In L. H. Skibsted, J. Risbo & M. L. Andersen (Eds.), *Chemical deterioration and physical instability of food and beverages*. Cambridge, U.K.: Woodhead Publishing Limited.

Graves, S. M., Mason, T. G., Meleson, K., & Wilking, J. N. (2008). Elastic vitrification of emulsions by droplet rupturing. US Patent No. Google Patents: U. S. P. a. T. Office.
Groot, R. D., & Stoyanov, S. D. (2011). Close packing density and fracture strength of adsorbed polydisperse particle layers. *Soft Matter, 7*(10), 4750-4761.
Guo, H., Ramakrishnan, S., Harden, J. L., & Leheny, R. L. (2011). Gel formation and aging in weakly attractive nanocolloid suspensions at intermediate concentrations. *The Journal of Chemical Physics, 135*(15), 154903.
Gutierrez, J. M., Gonzalez, C., Maestro, A., Sole, I., Pey, C. M., & Nolla, J. (2008). Nano-emulsions: New applications and optimization of their preparation. *Current Opinion in Colloid & Interface Science, 13*(4), 245-251.
Hatanaka, J., Chikamori, H., Sato, H., Uchida, S., Debari, K., Onoue, S., & Yamada, S. (2010). Physicochemical and pharmacological characterization of alpha-tocopherol-loaded nano-emulsion system. *International Journal of Pharmaceutics, 396*(1-2), 188-193.
Hecke, M. v. (2010). Jamming of soft particles: geometry, mechanics, scaling and isostaticity. *Journal of Physics: Condensed Matter, 22*(3), 033101.
Hoffmann, M. A. M., & van Mil, P. J. J. M. (1997). Heat-Induced Aggregation of Î²-Lactoglobulin:â€‰ Role of the Free Thiol Group and Disulfide Bonds. *Journal of Agricultural and Food Chemistry, 45*(8), 2942-2948.
Holmberg, K., Jönsson, B., Kronberg, B., & Lindman, B. (2003). *Surfactants and Polymers in Aqueous Solution* (2nd ed.). West Sussex, England: John Wiley & Sons, Ltd.
Horst, P. D. B., Helfried, H., & Henker, P. (2012). Xerogels with homogeneously embedded food additives comprising food dye, food preservative and/or flavor enhancer, which are embedded into a silicate-containing xerogel matrix, useful as powdery products/granules in e.g. cosmetic products. US Patent No. Google patents: U. S. P. a. T. Office.
Hrubesh, L. W. (1998). Aerogel applications. *Journal of Non-Crystalline Solids, 225*(1-3), 335-342.
Huang, Q. R., Yu, H. L., & Ru, Q. M. (2010). Bioavailability and Delivery of Nutraceuticals Using Nanotechnology. *Journal of Food Science, 75*(1), R50-R57.
Hui, Y. H. (2006). *Handbook of food science, technology, and engineering*. Boca Raton: Boca Raton : Taylor & Francis.
Ikeda, A., Berthier, L., & Sollich, P. (2012). Unified study of glass and jamming rheology in soft particle systems. *Physical Review Letters, 109*(1), 018301.
Israelachivili, J. N. (2011). *Intermolecular and Surface Forces* (3rd ed.). Boston, MA, USA Elsevier Inc.
Israelachvili, J. N. (2011). *Intermolecular and surface forces*. London: Academic Press.
Ivanov, I. B., Danov, K. D., & Kralchevsky, P. A. (1999). Flocculation and coalescence of micron-size emulsion droplets. *Colloids and Surfaces A: Physicochemical and Engineering Aspects, 152*(1-2), 161-182.
Jabbari-Farouji, S., Zargar, R., Wegdam, G. H., & Bonn, D. (2012). Dynamical heterogeneity in aging colloidal glasses of Laponite. *Soft Matter, 8*(20), 5507-5512.
Jafari, S. M., Assadpoor, E., He, Y. H., & Bhandari, B. (2008). Re-coalescence of emulsion droplets during high-energy emulsification. *Food Hydrocolloids, 22*(7), 1191-1202.
James, G. K., & Walz, J. Y. (2014a). Experimental and theoretical investigation of the depletion and structural forces produced by ionic micelles. *Colloids and Surfaces A: Physicochemical and Engineering Aspects, 441*, 406-419.

James, G. K., & Walz, J. Y. (2014b). Experimental investigation of the effects of ionic micelles on colloidal stability. *Journal of Colloid and Interface Science, 418*(0), 283-291.
Jenkins, P., & Snowden, M. (1996). Depletion flocculation in colloidal dispersions. *Advances in Colloid and Interface Science, 68*, 57-96.
Jorjadze, I., Pontani, L. L., Newhall, K. A., & Brujic, J. (2011). Attractive emulsion droplets probe the phase diagram of jammed granular matter. *Proceedings of the National Academy of Sciences of the United States of America, 108*(11), 4286-4291.
Jost, R. (1993). Functional characteristics of dairy proteins. *Trends in Food Science & Technology, 4*(9), 283-288.
Jullien, R., & Kolb, M. (1984). Hierarchial model for chemically limited cluster cluster aggregations. *Journal of Physics a-Mathematical and General, 17*(12), L639-L643.
Kaasgaard, T., & Keller, D. (2010). Chitosan coating improves retention and redispersibility of freeze-dried flavor oil emulsions. *Journal of Agricultural and Food Chemistry, 58*(4), 2446.
Kabalnov, A. (2001). Ostwald ripening and related phenomena. *Journal of Dispersion Science and Technology, 22*(1), 1-12.
Kalinin, V. V., & Radke, C. J. (1996). An ion-binding model for ionic surfactant adsorption at aqueous-fluid interfaces. *Colloids and Surfaces A: Physicochemical and Engineering Aspects, 114*, 337-350.
Katsuyoshi, N. (2009). Some thoughts on the definition of a gel. In T. Masayuki & N. Katsuyoshi (Eds.), *Progress in colloida and polymer science* (Vol. 136, pp. 87-94): Springer Science & Business Media.
Kawada, H., Kume, T., Matsunaga, T., Iwai, H., Sano, T., & Shibayama, M. (2010). Structure and Rheology of a Self-Standing Nanoemulsion. *Langmuir, 26*(4), 2430-2437.
Kekicheff, P., & Richetti, P. (1992). Effect of electrolyte on the depletion and structural forces in a micellar system. *Progress in Colloid and Polymer Science, 88*, 8-17.
Kikoin, K. A., & Maksimov, L. A. (1973). Anisotropy of brownian motion in emulsions in an external electric-field. *Zhurnal Fizicheskoi Khimii, 47*(3), 711-712.
Knowlton, E. D., Pine, D. J., & Cipelletti, L. (2014). A microscopic view of the yielding transition in concentrated emulsions. *Soft Matter, 10*(36), 6931-6940.
Koumakis, N., & Petekidis, G. (2011). Two step yielding in attractive colloids: transition from gels to attractive glasses. *Soft Matter, 7*(6), 2456-2470.
Kralchevsky, P. A., Danov, K. D., Broze, G., & Mehreteab, A. (1999). Thermodynamics of ionic surfactant adsorption with account for the counterion binding: Effect of salts of various valency. *Langmuir, 15*(7), 2351-2365.
Kraynik, A. M., Reinelt, D. A., & Princen, H. M. (1991). The nonlinear elastic behavior of polydisperse hexagonal foams and concentrated emulsions. *Journal of Rheology, 35*(6), 1235-1253.
Krohn, C. E., & Thompson, A. H. (1986). Fractal sandstone pores: Automated measurements using scanning-electron-microscope images. *Physical Review B, 33*(9), 6366-6374.
Lee, L., & Norton, I. T. (2013). Comparing droplet breakup for a high-pressure valve homogeniser and a Microfluidizer for the potential production of food-grade nanoemulsions. *Journal of Food Engineering, 114*(2), 158-163.

Lee, S. J., & McClements, D. J. (2010). Fabrication of protein-stabilized nanoemulsions using a combined homogenization and amphiphilic solvent dissolution/evaporation approach. *Food Hydrocolloids, 24*(6-7), 560-569.
Lekkerkerker, H. W., & Tuinier, R. (2011). Depletion Interaction *Colloids and the Depletion Interaction* (Vol. 833, pp. 57-108): Springer Netherlands.
Line, V. L. S., Remondetto, G. E., & Subirade, M. (2005). Cold gelation of beta-lactoglobulin oil-in-water emulsions. *Food Hydrocolloids, 19*(2), 269-278.
Liu, A. J., & Nagel, S. R. (1998). Nonlinear dynamics: Jamming is not just cool any more. *Nature, 396*(6706), 21-22.
Liu, A. J., & Nagel, S. R. (2010). The Jamming Transition and the Marginally Jammed Solid. *Annual Review of Condensed Matter Physics, 1*, 347.
Liu, J. W., & Luijten, E. (2004). Rejection-free geometric cluster algorithm for complex fluids. *Physical Review Letters, 92*(3).
Lobato-Calleros, C., Recillas-Mota, M. T., Espinosa-Solares, T., Alvarez-Ramirez, J., & Vernon-Carter, E. J. (2009). Microstructural and rheological properties of low-fat stirred yoghurts made with skim milk and skim mil and multiple emulsions. *Journal of Texture Studies, 40*(6), 657-675.
Lu, J. R., Purcell, I. P., Lee, E. M., Simister, E. A., Thomas, R. K., Rennie, A. R., & Penfold, J. (1995). The Composition and Structure of Sodium Dodecyl Sulfate-Dodecanol Mixtures Adsorbed at the Air-Water Interface: A Neutron Reflection Study. *Journal of Colloid and Interface Science, 174*(2), 441-455.
Lu, P. J., & Weitz, D. A. (2013). Colloidal Particles: Crystals, Glasses, and Gels. *Annual Review of Condensed Matter Physics, 4*, 217-233.
Lu, P. J., Zaccarelli, E., Ciulla, F., Schofield, A. B., Sciortino, F., & Weitz, D. A. (2008). Gelation of particles with short-range attraction. *Nature, 453*(7194), 499-503.
Maali, A., & Mosavian, M. T. H. (2013). Preparation and Application of Nanoemulsions in the Last Decade (2000-2010). *Journal of Dispersion Science and Technology, 34*(1), 92-105.
Macosko, C. W., & Knovel. (1994). *Rheology principles, measurements, and applications*.
Malone, M. E., Appelqvist, I. A. M., & Norton, I. T. (2003). Oral behaviour of food hydrocolloids and emulsions. Part 2. Taste and aroma release. *Food Hydrocolloids, 17*(6), 775-784.
Maltais, A., Remondetto, G. E., Gonzalez, R., & Subirade, M. (2005). Formation of soy protein isolate cold-set gels: Protein and salt effects. *Journal of Food Science, 70*(1), C67-C73.
Mangione, M. R., Giacomazza, D., Bulone, D., Martorana, V., & San Biagio, P. L. (2003). Thermoreversible gelation of kappa-Carrageenan: relation between conformational transition and aggregation. *Biophysical Chemistry, 104*(1), 95-105.
Marangoni, A. G., Barbut, S., McGauley, S. E., Marcone, M., & Narine, S. S. (2000). On the structure of particulate gels - the case of salt-induced cold gelation of heat-denatured whey protein isolate. *Food Hydrocolloids, 14*(1), 61-74.
Masalova, I., & Malkin, A. Y. (2007). Rheology of highly concentrated emulsions - Concentration and droplet size dependencies. *Applied Rheology, 17*(4).
Mason, T. G., Bibette, J., & Weitz, D. A. (1995). Elasticity of compressed emulsions. *Physical Review Letters, 75*(10), 2051-2054.
Mason, T. G., Bibette, J., & Weitz, D. A. (1996). Yielding and Flow of Monodisperse Emulsions. *Journal of Colloid and Interface Science, 179*(2), 439-448.

Mason, T. G., Graves, S. M., Wilking, J. N., & Lin, M. Y. (2006). Extreme emulsification: formation and structure of nanoemulsions. *Condensed Matter Physics, Vol 9, Iss 1, Pp 193-199 (2006)*.

Mason, T. G., Lacasse, M. D., Grest, G. S., Levine, D., Bibette, J., & Weitz, D. A. (1997). Osmotic pressure and viscoelastic shear moduli of concentrated emulsions. *Physical Review E, 56*(3), 3150-3166.

Mason, T. G., & Scheffold, F. (2014). Crossover between entropic and interfacial elasticity and osmotic pressure in uniform disordered emulsions. *Soft Matter, 10*(36), 7109-7116.

Mason, T. G., Wilking, J. N., Meleson, K., Chang, C. B., & Graves, S. M. (2007). Nanoemulsions: formation, structure, and physical properties. *Journal of Physics-Condensed Matter, 19*(7).

Masuelli, M. A. (2012). Hydrodynamic Properties of Gelatin - Studies from Intrinsic Viscosity Measurements. In C. J. R. Verbeek (Ed.), *Products and Applications* (pp. 85 - 116): InTech.

Matsushita, M. (1994). Experiments on Aggregations In R. Takaki (Ed.), *Research of pattern formation* (pp. 169 - 175). Tokyo, Japan: KTK Scientific publishers.

Maxwell, J. C. (1866). The Bakerian Lecture: On the Viscosity or Internal Friction of Air and Other Gases. *Philosophical Transactions of the Royal Society of London (1776-1886), 156*(-1), 249-268.

McClements, D. J. (2000). Comments on viscosity enhancement and depletion flocculation by polysaccharides. *Food Hydrocolloids, 14*(2), 173-177.

McClements, D. J. (2005). *Food emulsions: principles, practices, and techniques* (2nd ed. Vol. 1). Boca Raton: CRC Press.

McClements, D. J. (2007). Critical review of techniques and methodologies for characterization of emulsion stability. *Critical Reviews in Food Science and Nutrition, 47*(7), 611-649.

McClements, D. J. (2011). Edible nanoemulsions: fabrication, properties, and functional performance. *Soft Matter, 7*(6), 2297-2316.

McClements, D. J. (2012). Nanoemulsions versus microemulsions: terminology, differences, and similarities. *Soft Matter, 8*(6), 1719-1729.

McClements, D. J., Decker, E. A., & Weiss, J. (2007). Emulsion-based delivery systems for lipophilic bioactive components. *Journal of Food Science, 72*(8), R109.

McClements, D. J., & Rao, J. (2011). Food-Grade Nanoemulsions: Formulation, Fabrication, Properties, Performance, Biological Fate, and Potential Toxicity. *Critical Reviews in Food Science and Nutrition, 51*(4), 285-330.

Meleson, K., Graves, S., & Mason, T. G. (2004). Formation of concentrated nanoemulsions by extreme shear. *Soft Materials, 2*(2-3), 109-123.

Mewis, J. (2012). *Colloidal suspension rheology*. Cambridge: Cambridge University Press.

Meyers, M. A. (2009). *Mechanical behavior of materials* (2nd ed.. ed.). Cambridge: Cambridge University Press.

Mihranyan, A., Ferraz, N., & Stromme, M. (2012). Current status and future prospects of nanotechnology in cosmetics. *Progress in Materials Science, 57*(5), 875-910.

Mikkonen, K. S., Parikka, K., Ghafar, A., & Tenkanen, M. (2013). Prospects of polysaccharide aerogels as modern advanced food materials. *Trends in Food Science & Technology, 34*(2), 124-136.

Mondain-Monval, O., Leal-Calderon, F., & Bibette, J. (1996). Forces Between Emulsion Droplets: Role of Surface Charges and Excess Surfactant. *Journal de Physique II 6*(9), 1313-1329.

Mondain-Monval, O., Leal-Calderon, F., Phillip, J., & Bibette, J. (1995). Depletion forces in the presence of electrostatic double-layer repulsion. *Physical Review Letters, 75*(18), 3364-3367.

Morrison, F. A. (2001). *Understanding rheology*. London: Oxford University Press.

Muschiolik, G. (2007). Multiple emulsions for food use. *Current Opinion in Colloid & Interface Science, 12*(4-5), 213-220.

Narine, S. S., & Marangoni, A. G. (1999). Mechanical and structural model of fractal networks of fat crystals at low deformations. *Physical Review E, 60*(6), 6991-7000.

Nespolo, S. A., Bevan, M. A., Chan, D. Y. C., Grieser, F., & Stevens, G. W. (2001). Hydrodynamic and electrokinetic properties of decane droplets in aqueous sodium dodecyl sulfate solutions. *Langmuir, 17*(23), 7210-7218.

Nishinari, K. (2009). Some Thoughts on The Definition of a Gel *Gels: Structures, Properties, and Functions: Fundamentals and Applications* (Vol. 136, pp. 87-94).

Nuchi, C. D., Hernandez, P., McClements, D. J., & Decker, E. A. (2002). Ability of lipid hydroperoxides to partition into surfactant micelles and alter lipid oxidation rates in emulsions. *Journal of Agricultural and Food Chemistry, 50*(19), 5445-5449.

Oakenfull, D., & Scott, A. (1984). Hydrophobic interaction in the gelation of high methoxyl pectins. *Journal of Food Science, 49*(4), 1093-1098.

Oakenfull, D. G. P., R. J.; Burley, R. W. (1997). Protein Gelation. In S. Damodaran (Ed.), *Food proteins and their applications* (Vol. 4, pp. 111 - 142). New York: Marcel Dekker.

Ochowiak, M., Broniarz-Press, L., & Rozanski, J. (2012). Rheology and Structure of Emulsions and Suspensions. *Journal of Dispersion Science and Technology, 33*(1-3), 177-184.

Olson, D. W., White, C. H., & Richter, R. L. (2004). Effect of pressure and fat content on particle sizes in microfluidized milk. *Journal of Dairy Science, 87*(10), 3217-3223.

Otte, J., Ju, Z. Y., FÆRgemand, M., Lomholt, S. B., & Qvist, K. B. (1996). Protease-Induced Aggregation and Gelation of Whey Proteins. *Journal of Food Science, 61*(5), 911-916.

Pal, R. (1996a). Effect of droplet size on the rheology of emulsions. *Aiche Journal, 42*(11), 3181-3190.

Pal, R. (1996b). Rheology of emulsions containing polymeric liquids. In P. Becher (Ed.), *Encyclopedia of Emulsion Technology* (Vol. 4). New York, NY: Marcel Dekker.

Pal, R., Yan, Y., & Masliyah, J. (1992). Rheology of emulsions. *Advances in Chemistry Series*(231), 131-170.

Pashley, R. M., & Ninham, B. W. (1987). Double-layer forces in ionic micellar solutions. *Journal of Physical Chemistry, 91*(11), 2902-2904.

Patist, A., Kanicky, J. R., Shukla, P. K., & Shah, D. O. (2002). Importance of micellar kinetics in relation to technological processes. *Journal of Colloid and Interface Science, 245*(1), 1-15.

Petsev, D. N., Denkov, N. D., & Kralchevsky, P. A. (1995). Flocculation of deformable emulsion droplets: II. Interaction energy. *Journal of Colloid and Interface Science, 176*(1), 201-213.

Pettitt, D. J., Wayne, J. E. B., Nantz, J. J. R., & Shoemaker, C. F. (1995). Rheological propoerties of solutions and emulsions stabilized with xanthan gum and propylene-glycol alginate. *Journal of Food Science, 60*(3), 528-&.

Pham, K. N., Petekidis, G., Vlassopoulos, D., Egelhaaf, S. U., Poon, W. C. K., & Pusey, P. N. (2008). Yielding behavior of repulsion- and attraction-dominated colloidal glasses. *Journal of Rheology, 52*(2), 649-676.

Princen, H. M., & Kiss, A. D. (1986). Rheology of foams and highly concentrated emulsions. III. Static shear modulus. *Journal of Colloid and Interface Science, 112*(2), 427-437.

Qian, C., & McClements, D. J. (2011). Formation of nanoemulsions stabilized by model food-grade emulsifiers using high-pressure homogenization: Factors affecting particle size. *Food Hydrocolloids, 25*(5), 1000-1008.

Rahalkar, R. R. (1992). Viscoelastic properties of oil-water emulsions. In M. A. Rao (Ed.), *Viscoelastic properties of foods*. New York, USA: Elsevier science publishers.

Ramakrishnan, S., Chen, Y. L., Schweizer, K. S., & Zukoski, C. F. (2004). Elasticity and clustering in concentrated depletion gels. *Physical Review E, 70*(4).

Rao, J., & McClements, D. J. (2012). Food-grade microemulsions and nanoemulsions: Role of oil phase composition on formation and stability. *Food Hydrocolloids, 29*(2), 326-334.

Rao, M. A. (2005). Rheological Properties of Fluid Foods *Engineering Properties of Foods, Third Edition*: CRC Press.

Rao, M. A. (2007). *Rheology of Fluid and Semisolid Foods Principles and Applications* (Second Edition.. ed.). Boston, MA: Boston, MA : Springer-Verlag US.

Richardson, P. H., Willmer, J., & Foster, T. J. (1998). Dilute solution properties of guar and locust bean gum in sucrose solutions. *Food Hydrocolloids, 12*(3), 339-348.

Richetti, P., & Kekicheff, P. (1992). Direct measurement of depeltion and structural forces in a micellar system. *Physical Review Letters, 68*(12), 1951-1954.

Risović, D., Poljaček, S. M., Furić, K., & Gojo, M. (2008). Inferring fractal dimension of rough/porous surfaces—A comparison of SEM image analysis and electrochemical impedance spectroscopy methods. *Applied Surface Science, 255*(5, Part 2), 3063-3070.

Romsted, L. S., & Bravo-Diaz, C. (2013). Modeling chemical reactivity in emulsions. *Current Opinion in Colloid & Interface Science, 18*(1), 3-14.

Rosa, P., Sala, G., Van Vliet, T., & Van De Velde, F. (2006). Cold gelation of whey protein emulsions. *Journal of Texture Studies, 37*(5), 516-537.

Sala, G. (2007). *Food Gels Filled with Emulsion Droplets: Linking Large Deformation Properties to Sensory Perception*: Wageningen Universiteit.

Sala, G., Van Aken, G. A., Stuart, M. A. C., & Van de Velde, F. (2007). Effect of droplet-matrix interaction on large deformation properties of emulsion-filled gels. *Journal of Texture Studies, 38*(4), 24.

Sapir, L., & Harries, D. (2015). Is the depletion force entropic? Molecular crowding beyond steric interactions. *Current Opinion in Colloid & Interface Science, 20*(1), 3-10.

Schaertl, W., & Sillescu, H. (1994). Brownian dynamics of polydisperse colloidal hard-spheres - equilibrium structures and random close packings. *Journal of Statistical Physics, 77*(5-6), 1007-1025.

Scheffold, F., Cardinaux, F., & Mason, T. G. (2013). Linear and nonlinear rheology of dense emulsions across the glass and the jamming regimes. *Journal of Physics: Condensed Matter, 25*(50), 502101.

Scheffold, F., Wilking, J. N., Haberko, J., Cardinaux, F., & Mason, T. G. (2014). The jamming elasticity of emulsions stabilized by ionic surfactants. *Soft Matter, 10*(28), 5040-5044.
Schowalter, W. R. (1978). *Mechanics of non-Newtonian fluids*. London, UK: Pergamon Press.
Seager, C. R., & Mason, T. G. (2007). Slippery diffusion-limited aggregation. *Physical Review E, 75*(1).
Shah, S. A., Chen, Y.-L., Schweizer, K. S., & Zukoski, C. F. (2003). Viscoelasticity and rheology of depletion flocculated gels and fluids. *The Journal of Chemical Physics, 119*(16), 8747-8760.
Shao, Z., Negi, A. S., & Osuji, C. O. (2013). Role of interparticle attraction in the yielding response of microgel suspensions. *Soft Matter, 9*(22), 5492-5500.
Sharma, A., & Walz, J. Y. (1996). Direct measurement of the depletion interaction in a charged colloidal dispersion. *Journal of the Chemical Society-Faraday Transactions, 92*(24), 4997-5004.
Sherman, P. (1968). *Emulsion science*. London: Academic Press.
Silva, H. D., Cerqueira, M. A., & Vicente, A. A. (2012). Nanoemulsions for Food Applications: Development and Characterization. *Food and Bioprocess Technology, 5*(3), 854-867.
Solans, C., & Sole, I. (2012). Nano-emulsions: Formation by low-energy methods. *Current Opinion in Colloid & Interface Science, 17*(5), 246-254.
Sorensen, C. M. (2001). Light Scattering by Fractal Aggregates: A Review. *Aerosol Science and Technology, 35*(2), 648-687.
Speranza, A., Corradini, M. G., Hartman, T. G., Ribnicky, D., Oren, A., & Rogers, M. A. (2013). Influence of Emulsifier Structure on Lipid Bioaccessibility in Oil–Water Nanoemulsions. *Journal of Agricultural and Food Chemistry, 61*(26), 6505-6515.
Steffe, J. F. (1992). *Rheological methods in food process engineering*. East Lansing, Mich. USA: East Lansing, Mich. USA : Freeman Press.
Struik, L. C. E. (1978). *Physical Aging in Amorphous Polymers and Other Materials*: Elsevier Scientific Publishing Company.
Stubenrauch, C., & Klitzing, R. v. (2003). Disjoining pressure in thin liquid foam and emulsion films-new concepts and perspectives. *Journal of Physics: Condensed Matter, 15*(27), R1197.
Sun, A., & Gunasekaran, S. (2009a). Yield Stress in Foods: Measurements and Applications. *International Journal of Food Properties, 12*(1), 70-101.
Sun, C., & Gunasekaran, S. (2009b). Effects of protein concentration and oil-phase volume fraction on the stability and rheology of menhaden oil-in-water emulsions stabilized by whey protein isolate with xanthan gum. *Food Hydrocolloids, 23*(1), 165-174.
Tabor, R. F., Chan, D. Y. C., Grieser, F., & Dagastine, R. R. (2011). Structural Forces in Soft Matter Systems. *Journal of Physical Chemistry Letters, 2*(5), 434-437.
Tadros, T., Izquierdo, R., Esquena, J., & Solans, C. (2004). Formation and stability of nano-emulsions. *Advances in Colloid and Interface Science, 108*, 303-318.
Tadros, T. F. (1994). Fundatmental principles of emulsion rheology and their applications. *Colloids and Surfaces a-Physicochemical and Engineering Aspects, 91*, 39-55.
Tanaka, T. (1981). Gels. *Scientific American, 244*(1), 124-138.
Trappe, V., Prasad, V., Cipelletti, L., Segre, P. N., & Weitz, D. A. (2001). Jamming phase diagram for attractive particles. *Nature, 411*(6839), 772-775.

Trappe, V., & Sandkuhler, P. (2004). Colloidal gels - low-density disordered solid-like states. *Current Opinion in Colloid & Interface Science, 8*(6), 494-500.

Triantafillopoulos, N. (1948). *Measurement of fluid rheology and interpretation of rheograms*

Trokhymchuk, A., Henderson, D., Nikolov, A., & Wasan, D. T. (2001). A simple calculation of structural and depletion forces for fluids/suspensions confined in a film. *Langmuir, 17*(16), 4940-4947.

Truskett, T. M., Torquato, S., & Debenedetti, P. G. (2000). Towards a quantification of disorder in materials: Distinguishing equilibrium and glassy sphere packings. *Physical Review E, 62*(1), 993.

Tuinier, R., Dhont, J. K. G., & De Kruif, C. G. (2000). Depletion-Induced Phase Separation of Aggregated Whey Protein Colloids by an Exocellular Polysaccharide. *Langmuir, 16*(4), 1497-1507.

Vesaratchanon, J. S., Nikolov, A., Wasan, D., & Henderson, D. (2009). The Importance of Oscillatory Structural Forces in the Sedimentation of a Binary Hard-Sphere Colloidal Suspension. *Industrial & Engineering Chemistry Research, 48*(14), 6641-6651.

Walstra, P. (1993). Principles of emulsion formation. *Chemical Engineering Science, 48*(2), 333-349.

Walstra, P. (2003). *Physical Chemistry of Foods* (Vol. 1). New York, NY: Marcel Dekker.

Walz, J. Y., & Sharma, A. (1994). Effect of Long Range Interactions on the Depletion Force between Colloidal Particles. *Journal of Colloid and Interface Science, 168*(2), 485-496.

Weiss, J., & McClements, D. J. (2000). Influence of Ostwald ripening on rheology of oil-in-water emulsions containing electrostatically stabilized droplets. *Langmuir, 16*(5), 2145-2150.

Weitz, D. A., Huang, J. S., Lin, M. Y., & Sung, J. (1985). Limits of the fractal dimension for irrversible kinetic aggregation of gold colloids. *Physical Review Letters, 54*(13), 1416-1419.

Whitmer, J. K., & Luijten, E. (2011). Sedimentation of aggregating colloids. *The Journal of Chemical Physics, 134*(3), 034510.

Wilking, J. N., Graves, S. M., Chang, C. B., Meleson, K., Lin, M. Y., & Mason, T. G. (2006). Dense Cluster Formation during Aggregation and Gelation of Attractive Slippery Nanoemulsion Droplets. *Physical Review Letters, 96*(1), 015501.

Wilking, J. N., & Mason, T. G. (2007). Irreversible shear-induced vitrification of droplets into elastic nanoemulsions by extreme rupturing. *Physical Review E, 75*(4).

Winter, H. H., & Chambon, F. (1986). Analysis of linear viscoelasticity of a crosslinking polymer at the gel point. *Journal of Rheology (1978-present), 30*(2), 367-382.

Wooster, T. J., Andrews, H. F., & Sanguansri, P. (2009). Nanoemulsions.

Yamamoto, Y., & Dickinson, E. (1997). Rheology of protein gels and protein stabilized emulsion gels cross-linked with transglutaminase. In E. Dickinson & B. Bergenståhl (Eds.), *Food colloids: Proteins, lipids and polysaccharides* (pp. 326 - 334). Cambridge, UK: Royal Society of Chemistry.

Zha, J., & Roggendorf, H. (1991). Sol–gel science, the physics and chemistry of sol–gel processing, Ed. by C. J. Brinker and G. W. Scherer, Academic Press, Boston 1990, xiv, 908 pp., bound—ISBN 0-12-134970-5. *Advanced Materials, 3*(10), 522-522.